2016

Design and Development of a High-Temperature High-Pressure Rolling Ball Viscometer/Densimeter and Evaluation of Star Polymer-Solvent Mixtures

Matthew Stanton Newkirk
Virginia Commonwealth University

Design and Development of a High-Temperature High-Pressure Rolling Ball Viscometer/Densimeter and Evaluation of Star Polymer-Solvent Mixtures

A dissertation submitted in partial fulfillment of requirements for the Degree of Doctor of Philosophy at Virginia Commonwealth University

by

Matthew Stanton Newkirk
Doctor of Philosophy, Virginia Commonwealth University, 2016

Dissertation Director: Dr. Mark A. McHugh,
Professor Emeritus, Department of Chemical and Life Science Engineering
Dissertation Director: Dr. B. Frank Gupton,
Professor and Chair, Department of Chemical and Life Science Engineering

Virginia Commonwealth University
Richmond, Virginia
December 2016

Acknowledgement

I dedicate this work and thesis to my family. To my wife, Julie: from the day I first saw you peeking down from above, I knew that I had found my life's only true love. You are the reason I wake up in the morning, and look forward to being home every day. To my son, Jeffrey, and daughter, Sarah: never stop dreaming and learning. Know how tremendously proud I am to be your father. You make me truly proud to watch you work hard, achieve your goals, and show compassion for others. I am sure that you will have the profound impact on others that you have on me.

I would like to acknowledge and expresses my most sincere and deep gratitude to Dr. Mark McHugh. You are a friend and an eminently respected mentor. I have learned so much from you, and would never have been successful in this endeavor without your dedication, commitment, hard work, and support.

I am also extremely grateful and wish to thank Dr. B. Frank Gupton for his friendship, guidance, and support that he provided as a valued advisor and Chemical and Life Science Engineering Chair throughout my time at Virginia Commonwealth University. I look forward to many more years working together.

Finally, I wish to acknowledge and thank Dr. Reddy Mallapaly, Dr. Yue Wu, and Dr. Babatunde Bambgbade, Mr. Aaron Rowane, and Mr. Sean Dudek for their tremendous support of my and assistance with this research. I absolutely could not have achieved this without you all.

Table of Contents

List of Tables

List of Figures

List of Abbreviations

±	plus or minus
~	approximately
AAD	Average Absolute Deviation
°C	degrees centigrade
cm	centimeters
CAFE	Corporate Average Fuel Economy
D	internal diameter of the RBVD
d	diameter of the ball
D_{max}	maximum deviation
EGDMA	ethylene glycol dimethacrylate
emf	electromotive force
f	friction factor
ft-lb	foot-pounds
g	acceleration of gravity
HTHP	High-Temperature High-Pressure
ID	Inside Diameter
k	RBVD constant
K	RBVD constant, k/l
K	absolute temperature in Kelvin
l	fixed distance ball rolls (length) in RBVD
LMA	lauryl methacrylate
LMA-MMA	poly(lauryl methacrylate-*co*-methyl methacrylate)
LVDT	Linear Variable Differential Transducer
MMA	methyl methacrylate
MPa	mega pascal
Mw	weight averaged molecular weight
N	Number of data points
NIST	National Institute of Standards and Technology
OD	Outside diameter
p	pressure
p_0	atmospheric pressure
PDI	Polydispersity Index
psia	pounds per square inch absolute
PS	polystyrene
Re	Reynolds number
s	seconds
SAE	Society of Automotive Engineers
SD	Standard Deviation
s-PS	star polystyrene
T	Temperature
t	time

$U_c(\eta)$	expanded uncertainty calculated for viscosity
wt%	percent by weight/mass
$x_{i,cal}$	calculated of literature data value
$x_{i,exp}$	value of an experimental data point

Greek Letter as Symbols

η	viscosity
η_o	reference viscosity
ρ_b	ball density
ρ_{fl}	fluid density
ρ_{exp}	experimentally measured density
ρ_{NIST}	density from NIST database
θ	angle of the viscometer or angle of inclination
v	terminal velocity of the rolling ball
$\overline{\gamma}$	average shear rate
π	pie, ratio of circle circumference to diameter, 3.14159

Abstract

DESIGN AND DEVELOPMENT OF A HIGH-TEMPERATURE HIGH-PRESSURE ROLLING BALL VISCOMETER/DENSIMETER AND EVALUATION OF POLYMER-SOLVENT MIXTURES

By Matthew Stanton Newkirk, Ph.D.

A dissertation submitted in partial fulfillment of requirements for the Degree of Doctor of Philosophy at Virginia Commonwealth University.

Virginia Commonwealth University, 2016.

Major Director: Dr. Mark A. McHugh, Professor Emeritus, Department of Chemical and Life Science Engineering
Major Director: Dr. B. Frank Gupton, Professor and Chair, Department of Chemical and Life Science Engineering

Modern automotive applications such as transmission clutch plates, combustion chambers, diesel fuel injector tips, and axle gears and friction plates operate at temperatures that can exceed 250°C and pressures of 40,000 psia. Industrial practice is to add homopolymers and copolymers to base oils to modify bulk fluid viscosity and frictional properties for these demanding applications. However, designing polymeric additives for lubricants and predicting their performance is limited by the lack of available high-temperature high-pressure (HTHP) viscosity and density data needed to test contemporary lubricity models. Thus, a major objective of this thesis is the design, development, and commissioning of a rolling ball viscometer/densitometer

(RBVD) capable of simultaneously determining fluid densities and viscosities at temperatures in excess of 250°C and pressures of 40,000 psia. Resulting data may then be generated to directly address the fundamental need for lubricant property data at these HTHP conditions. The design and development of the RBVD is described in detail to highlight the design iterations and modifications utilized to ensure robust operation at extreme conditions. Three significant and novel features of this RBVD apparatus that distinguish and differentiate it from other apparatus of this type are: (1) specially designed metal-to-metal and sapphire-to-metal seated surfaces capable of eliminating temperature- and chemically-sensitive elastomeric seals; (2) use of a bellows piston to eliminate significant temperature and operational constraints; and (3) incorporation of a linear variable differential transducer (LVDT) to simultaneously permit determination of solution density and viscosity. A detailed analysis of initial accumulated uncertainty for the experimental viscosity and density techniques revealed the need for key RBVD modifications. Final data are presented showing that the RBVD is capable of measuring viscosities with an accuracy of ± 2 to 3 percent and densities to ± 0.7 percent, including at the extreme operating conditions targeted.

A second objective of this thesis is the measurement of HTHP viscosities of star polymer-solvent mixtures to determine the impact of star polymer architecture on solution viscosity at extreme conditions similar to those that might be experienced in automotive applications. This objective is motivated by current challenges facing industry to identify polymeric additives that can be added to base oils to improve fuel economy and allow for the implementation of novel hardware technology that relies on enhanced lubricant properties. Relative to linear polymers, the unique architecture of star polymers enhances polymer solubility in base oils while having a more favorable impact on viscosity and density properties over a wide range of temperatures and

pressures. Data are presented for an industrially-relevant star polymer in octane to assess the impact of the star configuration on solvent viscosity at extreme conditions. The star polymer used in this instance consists of an ethylene glycol dimethacrylate (EGDMA) core with poly(lauryl methacrylate-*co*-methyl methacrylate) (LMA-MMA) arms. The star polymer has a total weight averaged molecular weight (Mw) and Mw of each arm of 575,000, and 45,000, respectively. The copolymer arms of the star polymer have an LMA-to-MMA mole ratio of 0.6.

The results of further viscosity studies are presented for a model system of well-characterized commercially available narrow polydispersity index (PDI) star polystyrenes (PS) in toluene. Each PS is evaluated at a two percent by weight concentration in toluene to evaluate the effect of arm molecular weigh on viscosity. Each three-arm star polymer has arm and total molecular weights ([arm Mw] total star Mw) of ([15,400] 41,200), ([36,000] 97,600), and ([108,000] 305,000). In this instance, the viscosity of toluene increased by more than a factor of three for the star with the highest Mw arms.

The information generated with both the PS and LMA-MMA star polymers can be used to test contemporary viscosity models. This research will also provide direction toward future development of novel polymer additives capable of optimally extending the performance of lubricants to extreme temperature and pressure regimes.

Chapter 1. Introduction

Viscosity, density, and solubility, as fundamental thermodynamic properties, are important in the production, manufacture, and purification of specialty chemicals, lubricant additives, crude oil, polymers, pharmaceuticals, and a variety of other chemically-based products. Although these properties can be readily obtained at ambient conditions, applied product development in many fields requires accurate viscosity and density data at extreme temperatures and pressures. However, in order to accurately make these measurements appropriate equipment capable of operating effectively and generating accurate and repeatable data at these extreme temperatures and pressures must first be designed, constructed, optimized, implemented, and validated. Therefore, the primary objective of this Ph.D. study is the design, development, and commissioning of a novel, HTHP rolling ball viscometer/densitometer capable of producing viscosity and density data for solutions at extreme operating conditions. A secondary objective of this Ph.D. study is to determine the impact of star polymer architecture on viscosity/density at extreme operating conditions using well-characterized polystyrene (PS) star and linear polymers.

1.1 Background and Context

This impetus for studying this topic and the driver for the three major objectives of this thesis are derived from the potential of using star polymers as petroleum additives. In order to do so, critical solution properties of density and viscosity need to first be developed at the relevant extreme temperatures and pressures common to applications in the automotive industry. Polymer additives, including star polymers, have an important role in lubricants since they can impact fuel economy, lubrication, friction, wear protection, contaminant dispersion, and other critical properties. However, improved vehicle fuel efficiency has become a critical focus and market driver for vehicle and engine manufacturers worldwide due to significant mandated reductions in carbon dioxide emissions by the United States Environmental Protection Agency and other government agencies around the globe. For example, at a recent Baltimore, Maryland, Society of Automotive Engineering (SAE) conference in October 2016, a panel discussion consisting of key automotive, oil, and supplier industry executives along with top ranking federal and state regulators focused solely on the enormous task of balancing regulatory requirements, including mandated vehicle fuel economy improvements, with consumer expectations like performance and cost [1]. Throughout the main sessions of this conference, the vast majority of the presentations and papers primarily emphasized mechanical and hardware design approaches. Although hardware approaches can be effective, lubricant contribution is also critical since eight to nine percent of overall vehicle efficiency improvements still remain that can be impacted by fuel and lubricant additives.

Figure 1 presents an illustration showing the two main areas where automotive energy losses can be reduced with effective additives. It is important to recognize that according to recent fuel economy regulations promulgated worldwide, the impact of a one percent improvement in fuel economy toward meeting future Corporate Average Fuel Economy (CAFE) standards in the U.S. alone amounts to more than $300 million annual savings to the automobile manufacturers in non-compliance penalties [2]. As illustrated in Figure 1, the fuel and lubricant additive industry estimates that of the nine percent vehicle efficiency that can be affected by specialty polymer additives, five percent is currently lost to internal engine friction, and four percent is consumed by driveline friction [3].

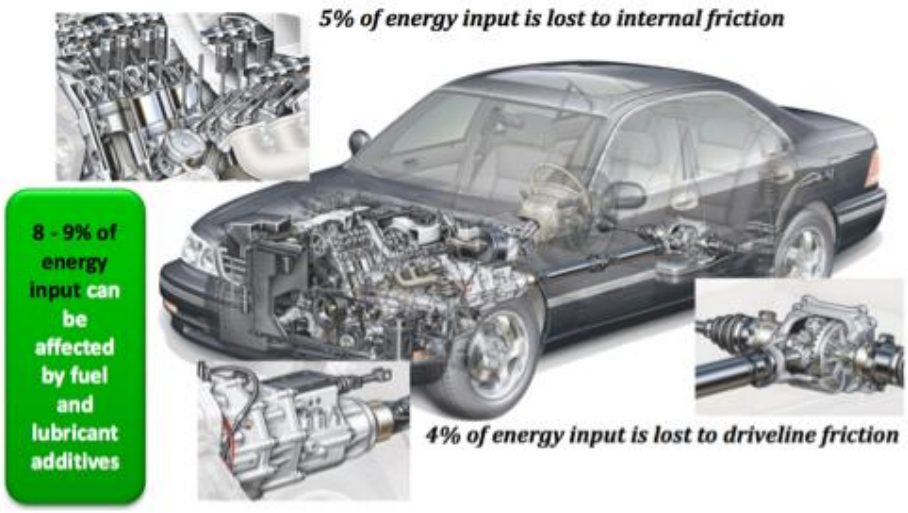

Figure 1. Energy loss map within a vehicle that can be affected by fuels and lubricants [3].

New regulations for the year 2025 that increase fuel economy standards for cars and light-duty trucks to a corporate average of 54.5 miles per gallon in the United States (see **Figure 2**) alone will result in fines that nearly quadruple the current penalties paid by some automobile

manufacturers to a total of over $800 million annually [4]. The increase in the price of every new vehicle required to implement technology capable of achieving these standards is estimated to be roughly $7000 per vehicle [5]. Thus, new types of polymers, such as star polymers formulated into specialty fluids for these key applications, present a major opportunity for significant global economic and environmental impact through a variety of mechanisms that are application specific. However, the key to unlocking and understanding the benefits of these polymers as versatile additives to increase fuel efficiency while simultaneously protecting mechanical hardware requires a deep understanding of how polymer architecture impacts solution viscosity over wide ranges of temperature and pressure.

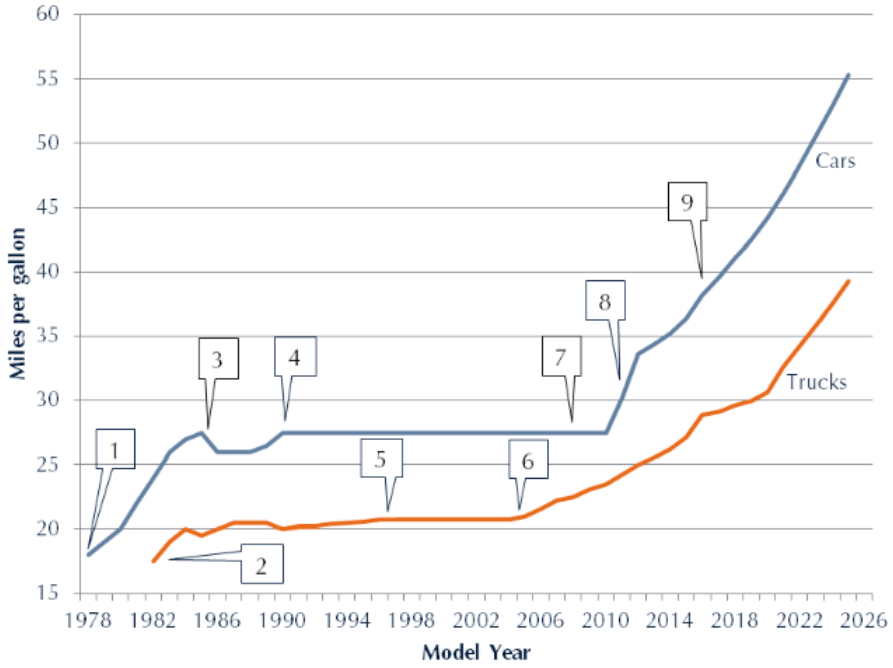

Source: NHTSA Summary of Fuel Economy Performance, NHTSA MY2017-2025 Factsheet

1. 1978-1985: Congress sets car standard (1978-1985)
2. DOT sets truck standard to max feasible (1979-1996)
3. DOT decreased car standard (1986-1989)
4. DOT sets car standard to 27.5 mpg (1990-2010)
5. Congress freezes truck standards at 20.7 mpg (1997-2001)
6. Bush Admin issues new truck targets (2005-2007)
7. EISA changes CAFE to footprint standard (2008-present)
8. Obama Admin issues new car & truck standards (2012-2016)
9. Obama Admin issues new car & truck standards (2017-2025)

Figure 2. Chronology of car and light truck fuel economy standards in the United States [4].

Typically, polymers are added to refinery "base oils" to impart specific lubrication properties to the composite fluid mixture [6, 7, 8]. Base oils are most often refinery blends of paraffinic, naphthenic, and aromatic compounds. For the studies considered for this thesis, octane and toluene are used as the single-component models for base oil. In addition, the understanding of polymer additive and architecture relative to the base oil is less complex if experiments are performed with such a well-characterized single component, such as octane or toluene, given that the role of these "additives" is often varied and quite complex. For example, polymer additives in lubricant base oils can act as friction modifiers through interaction with solid surfaces and bulk fluid to form a tribological film, as is the case in automatic transmissions. In addition, and most pertinent to this research, polymers can be used to significantly modify bulk fluid viscosity not only at ambient conditions, but most importantly at the HTHP operating conditions encountered in automotive applications during normal operating conditions.

A substantial amount of physical property data already exist in the literature on the performance characteristics of conventional, petroleum-derived additives and base oils at atmospheric pressure and temperatures to 100°C [9]. However, very little data exist at typical automotive operating conditions which often far exceed 130°C and 10,000 psia [10]. Data from limited application testing using automotive components suggests that star polymers affect bulk fluid properties in a very different manner than their linear counterparts. Empirical performance data from simulated real world automotive-like conditions further suggest that star polymer additives may have superior and highly beneficial properties that can be exploited commercially given a more thorough understanding of viscosity and density behavior at HTHP conditions [11].

1.2 Toluene as a Candidate Solvent to Commission the HTHP Viscometer

As previously mentioned, toluene is chosen as a convenient low molecular fluid to use to calibrate and evaluate the HTHP rolling ball viscometer/densimeter (RBVD) designed in this thesis study. In addition, substantial toluene viscosity/density database exists for reference and correlation. Toluene is relatively easy to use since it remains a liquid to approximately 110°C at atmospheric pressure [12]. **Figure 3** shows the pressure-temperature map of available published toluene viscosity data taken from a review by Avgeri and coworkers [13]. Even for a compound with a relatively simple structure like toluene, there is still a significant lack of data at temperatures greater than 100°C and pressures greater than 7,500 psia.

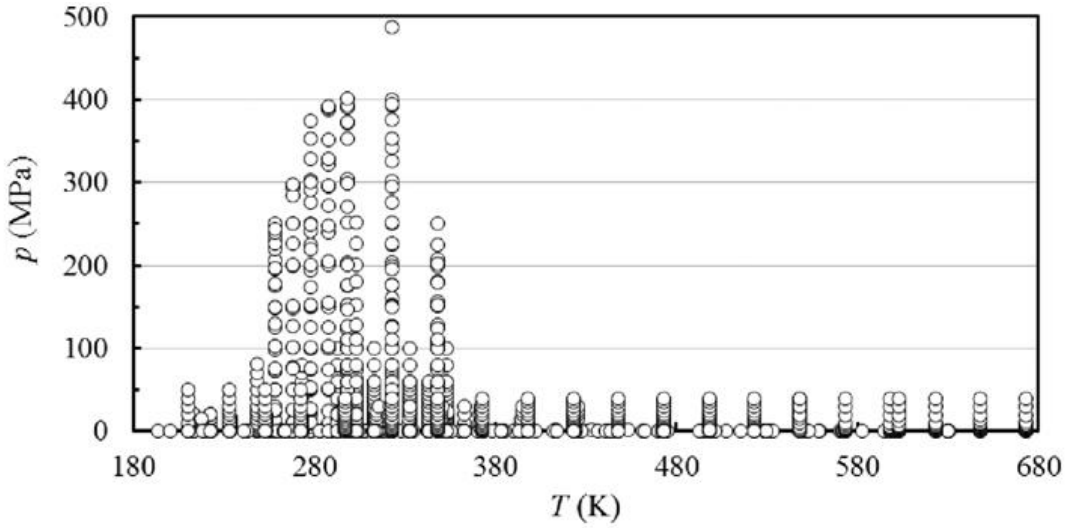

Figure 3. Pressure-temperature plot showing the range of conditions for which toluene viscosity data are available. Each circle represents the available data. [11]

Recent original experimental literature data obtained by Rowane, et al. [14] and the McHugh Group at Virginia Commonwealth University using a "first-generation" RBVD designed

for this thesis further extends the pressure-temperature range of available data for toluene. **Figures 4** shows these original toluene viscosity and density data which both serve to benchmark with existing published data and substantially extend the pressure and temperature range in which data are available.

At low temperatures viscosity increases at a very high rate versus pressure. As temperatures increase, the rate of increase in viscosity versus pressure (i.e., the slope of the viscosity versus pressure curve) decreases substantially, and ultimately becomes less at temperatures above approximately 227°C. As described in a later chapter of this thesis, the addition of a polymer additive appreciably increases toluene viscosity. The data shown in **Figure 3** provide a benchmark for comparison of the toluene impact on the data presented later in this thesis.

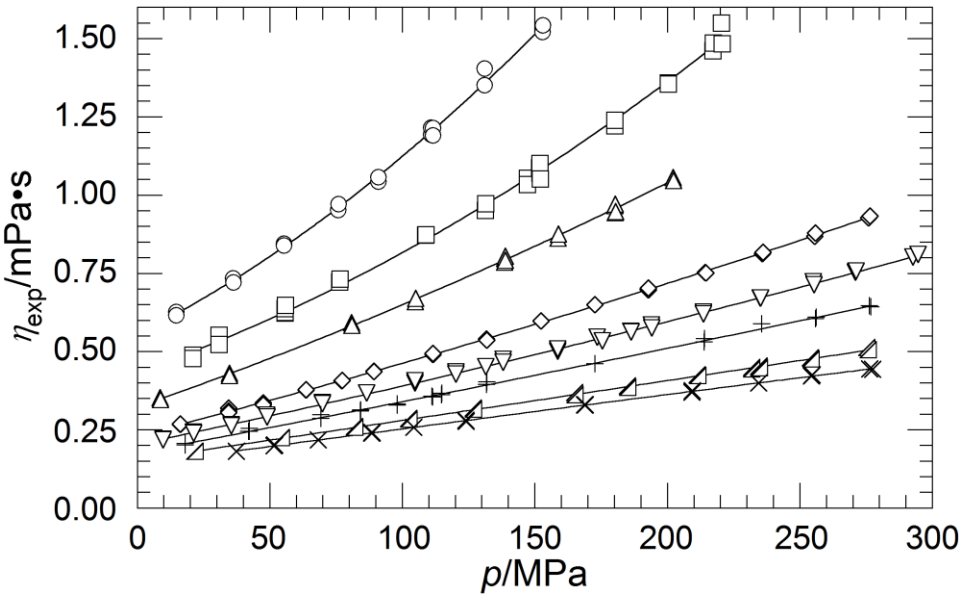

Figure 4. Effect of pressure and temperature on the viscosity of toluene, η_{exp}. ○ - 23°C, □ - 50°C, △ - 74°C, ◇ - 119°C, ▽ - 148°C, + - 179°C, ◿ - 227°C, and × - 262°C . Lines are drawn to guide the eye. [12]

Chapter 2 presents a description of the multi-year design, refinement, and optimization effort associated with the development of the RBVD and the methodology used in this thesis. Chapter 3 details the performance characteristics of the 2nd-generation RBVD initiated to extend the operational range of the RBVD. Chapter 4 follows with a presentation of the calibration, commissioning, and benchmarking of the RBVD. The HTHP toluene study by Rowane and co-workers [14] is highlighted in this chapter since this study serves as the benchmark for comparison to polymer-toluene studies reported in a later chapter in this thesis. Chapter 5 reports viscosity and density data for a star polymer with poly(lauryl methacrylate (LMA) -co- methyl metharcylate (MMA)) arms in octane, a solvent considered a surrogate base oil in the automotive industry. These data provide, for the first time, a measurement of the impact of a commercially-viable LMA-MMA, star polymer additive on a surrogate base oil at extreme operating conditions. Chapter 6 then provides a presentation of original data for HTHP viscosities/densities for linear PS (l-PS) and star PS (s-PS) in toluene. Chapter 7 provides an outlook for potential future experimental studies.

Chapter 2. Rolling Ball Viscometer/Densimeter Design and Development for High-Temperature High-Pressure Measurements

The experimental challenges associated with measurement of viscosity and density at high-temperature and high-pressure require significant technical barriers be overcome to ensure safe operation and robust sealing of all joining surfaces including fittings and transparent windows. At the same time, ease of operation, build-up of the device to operate at extreme conditions, and simplicity of data analysis are also important in order to be practical. In this chapter, an overview of the four types of high-pressure viscometers will be provided. Additionally, the majority of the chapter will contain sections on the development, testing, commissioning, and optimization of the RBVD developed for this thesis.

2.1 Survey of Relevant Viscosity Measurement Techniques

There are generally four types of high-pressure viscometers described in the literature: (1) vibrating wire viscometer [15, 16, 17, 18, 19, 20, 21, 22, 23]; (2) quartz-crystal viscometer [24, 25]; (3) falling body viscometer [26, 27, 28, 29, 30]; and (4) rolling ball viscometer [31, 32].

It is possible to obtain very accurate data using a vibrating wire viscometer, but complexity of operations, potential for mechanical failure, and data analysis often limit the practicality of the

instrument for significant or rapidly moving research programs. The vibrating wire viscometer operates principally by passing a current through a vertically suspended wire between the poles of a magnet. For operation, an alternating current is passed through the wire to initiate oscillation. The electromotive force (emf) developed across the wire is measured using an amplifier. This electromotive force is made up of two components: (1) a voltage developed across the electrical impedance presented by the stationary wire; and (2) a voltage arising from the motion of the wire through the fluid in the presence of the magnetic field. The frequency response of the oscillating wire is related to the density of the surrounding fluid. The width of the resonance curve is related to the viscosity of the fluid. Hence, care is required to accurately operate, calibrate, and interpret the complex vibrating system to ensure valid data.[20] Vibrating wire instruments can be used to determine density and viscosity data for compressed liquid systems at temperatures to 200°C and pressures to 30,000 psia. Caudwell *et al.* [23] determined density and viscosity data for several hydrocarbons including *n*-octane, *n*-decane, *n*-dodecane, *n*-octadecane, 1,3-dimethylbenzene, 1,2,3,4-tetrahydronaphthalene, and 1-methylnaphthalene between 25°C to 200°C and ambient to 30,000 psia. A major advantage vibrating wire instrument is the ability to simultaneously determine density and viscosity. Since most viscosity measurement techniques require either a known density or a fluid density that has to be determined separately, the vibrating wire method eliminates error associated with two separate measurements.

Similarly, the torsional oscillating quartz-crystal viscometer, as used by Kashiwagi and Makita [24], is a complex measurement system of an "oscillator" that is carried out in a vacuum. For this type of viscometer, the electronics are generally housed as close to the fluid of interest that is being heated as possible. The weakness of both the vibrating wire and quartz crystal viscometers is that the reliability of electronics diminishes at high temperature conditions due to

techanical failure and interferences. In addition, the interpretation of the signal obtained with both approaches is mathematically involved. Nevertheless, these techniques have been used by groups to successfully to develop and operate viscometers. However, for the reasons mentioned above their studies have been limited to lower temperatures and do not include mixtures. For example, Oliveira and Wakeham employ a vibrating-wire viscometer to measure the viscosity of five different liquid hydrocarbons, including toluene, to 75°C and ~37,000 psia [19] to a very high degree of accuracy. Vieira dos Santos and Nieto de Castro use a vibrating quartz-crystal viscometer to maximum conditions of 75°C and 30,000 psia [25] to measure toluene and benzene viscosities.

The falling body and rolling ball techniques were develop prior to those mentioned above and are operationally simpler methods for measuring viscosity [33]. The falling body technique uses a bullet-shaped body moving vertically through a fluid. The rolling ball viscometer operates in a similar manner although in this case the rolling speed of the ball is dependent on the angle of inclination, which typically is less than 15 degrees. Experimental viscosity data are interpreted using

$$h = \frac{k\left(r_b - r_{fl}\right)\sin q}{v} \qquad (1)$$

where, η is viscosity in g•cm^{-1}•s^{-1} or cP; k is the viscometer constant in cm^3•s^2; (ρ_b - ρ_{fl}) is the difference in the density of the ball and the fluid in g•cm^{-3}; θ is the angle of the viscometer; and v is the terminal velocity of the rolling ball, cm•s^{-1}. Generally no attempt is made to compute the streamlines in the space between the rolling ball and the inner diameter of the tube. Empirical data

demonstrate that when Reynolds numbers (Re) are less than approximately 50 and data are within the laminar flow regime and provide results that correlate well within three percent to know existing data [33]. As also noted by Hubbard and Brown [33], the friction factor (*f*) should be linear with Re over the range the data are obtained. Hubbard and Brown[38] derived relationships for the Reynolds number, Re (Equation 2), and the friction factor, *f*, (Equation 3). Šesták and Ambros [34] derived the expression shown as Equation (4) for the average shear rate, $\dot{\gamma}$, of a rolling ball viscometer,

$$\mathrm{Re} = \frac{vd^2}{(D+d)}\frac{\rho_{fl}}{\eta} \tag{2}$$

$$f = \frac{5\pi}{42} g \frac{(D+d)^2}{v^2 d}\frac{\left(\rho_b - \rho_{fl}\right)}{\rho_{fl}}\sin\theta \tag{3}$$

$$\bar{\dot{\gamma}} = 2.4v\frac{D}{(D-d)^2} \tag{4}$$

where *D* is the internal diameter of the RBVD (cm), *d* is the diameter of the ball (cm), *v* is the velocity of the ball, and *g* is the gravitational acceleration (cm•s^{-2}).

In order to obtain useful information, the shear rate must be varied at a fixed temperature and pressure. This can be done most easily by varying the angle of inclination; however, this method is indirect and not as easily controlled as in other rheometers. The range of the shear rate provides insight on the internal consistency between the calibration and data acquisition. The range of shear rates for the calibration in this study was 1891 – 23360 s^{-1}.

Careful inspection of Rowane [14] demonstrate that there is no major break in the friction factor vs Re curve and, hence, it is possible to unknowingly generate unreliable data. Therefore, in the present thesis, the Re will be kept well below 50 and generally below 10 to ensure laminar flow streamlines with the RBVD.

2.2 Rolling Ball Viscometer/Densitometer Initial Design

This section describes the initial design phase of a RBVD capable of operating to temperatures of greater than 250°C and pressures to 40,000 psia. Rolling ball viscometers offer a robust design for operating reliably at the extreme temperature and pressure conditions. Measurement of density at these HTHP conditions is also important given the desired application to relevant polymer mixtures in the automotive and lubricant industries. In fact, rolling ball viscometers have a long history of use in and application to the hydrocarbon-based industries. Flowers is credited with the design of the rolling ball viscometer in 1914 as a reliable method to measure viscosity [35]. In 1916, Hersey provided a useful correlation for the variables involved with this apparatus [36]. Later, in 1933, Sage used the rolling ball technique to measure the viscosity of hydrocarbons [37]. Also in 1933, Hoeppler developed a commercial rolling ball viscometer for sale to the oil and gas industries [38]. In 1943, Hubbard and Brown applied dimensional analysis methods to derive relationships between the variables involved in the operation of the rolling ball viscometer [33]. Their analysis led directly to Equation (1). **Table 1** provides additional references and historical context tracking the genesis of the rolling ball viscometer. This table also provides for a comparison of important design and operational parameters used for viscosity measurements. It is worth noting that these operating values were taken from published references that cited *maximum* operating conditions, however, many times

the authors never conducted actual measurements at the reported equipment maximum operating conditions. For example, Harrison [39] lists 350°C and 72,000 psia as the maximum operating condition for the rolling ball viscometer used in their research. However, publications by Harrison only present viscosity data to temperatures of 75°C and pressures to 55,000 psia.

Table 1. References with design and operating parameters for HTHP viscometers. AAD is the Average Absolute Deviation. SD is the Standard Deviation of the AAD.

Year	Authors	$T_{maximum}$ (°C)	$p_{maximum}$ (psia)	Method	Uncertainty (%)	AAD	SD
2016	Zambrano *et al.*[40]	100	20300	Vibrating Wire	1.5	1.2	0.7
2013	Meng *et al.*[15]	90	4350	Vibrating Wire	2.0	1.4	0.3
2011	Meng *et al.*[11]	75	5800	Vibrating Wire	2.8	1.7	0.3
2011	Daridon *et al.*[41]	59	11600	Vibrating Quartz	5.0	1.3	0.9
2009	Baylaucq *et al.*[42]	50	14500	Falling Body	2.0	1.1	0.9
2005	Pensado *et al.*[43]	80	8700	Rolling Ball	2.0	1.9	0.5
2005	Kandil *et al.*[44]	75	5800	Vibrating Wire	3.0	1.8	0.4
2004	Caudwell *et al.*[23]	100	11600	Vibrating Wire	2.0-5.0	1.1	0.5
2003	Avelino *et al.*[18]	50	11600	Vibrating Wire	2.0-3.0	1.3	0.6
2000	Harris[27]	50	58020	Falling Body	1.0	1.4	0.7
1999	Assael *et al.*[20]	97	4350	Vibrating Wire	0.5	1.2	0.4
1997	Vieira dos Santos *et al.*[25]	75	30020	Vibrating Quartz	0.5	1.9	0.9
1996	Abdulagatov and Rasulov[45]	163	4350	Capillary	1.2	9.8	9.5
1995	Dymond *et al.*[29]	75	71360	Falling Body	4.0	1.5	1.1
1992	Olivera *et al.*[19]	75	36550	Vibrating Wire	0.5	2.3	1.6

Table 1 (Cont'd). References with design and operating parameters for HTHP viscometers. AAD is the Average Absolute Deviation. SD is the Standard Deviation of the AAD.

1992	Krall and Sengers[46]	153	4350	Oscillating Disk	0.5	1.6	0.6
1991	Assael *et al*.[21]	50	10300	Vibrating Wire	0.5	1.0	0.5
1991	Dymond *et al.*[28]	100	75280	Falling Body	4.0	4.5	5.8
1982	Kashiwagi *et al*.[47]	75	15950	Vibrating Quartz	2.0	1.0	0.8
1970	Akhundov *et al*.[48]	275	5800	Capillary	2.0-4.0	2.1	1.5
1965	Harrison *et al.* [39]	350	72,000	Rolling Ball	3.0	1.9	0.8

The RBVD design used in this thesis has several important features that distinguish the apparatus from those previously described in the literature. However, in order to provide a starting reference point for this thesis study, **Figure 5** shows an illustration of the 1st-generation RBVD designed in this work. This design utilizes many features found with other high-pressure, variable-volume view cells used by McHugh and co-workers [49]. The body of the viscometer is Inconel 718, a high strength, corrosion-resistant, and non-magnetic nickel chromium steel. Inconel 718 maintains a high tensile strength at temperatures in excess of 300°C, and it is the preferred metal for use in the aerospace and petrochemical industries [50]. Special Metals Corporation reports that Inconel 718 maintains a tensile strength of 156,000 psi for temperatures to 315°C [51], which allows the wall thickness of the viscometer body to be modest. The inside diameter (ID) of our RBVD is 1.5875 cm. The outside diameter (OD) is 6.985 cm, and the maximum working volume is approximately 50 cm^3. 3D Design and Manufacturing LLC manufactured the viscometer to our specifications. The details, drawings and specifications are provided in **Appendix A**. An important feature of this viscometer design is the large sapphire window, secured with o-ring seals,

located at the front of the apparatus to allow for sample and phase behavior observation. Note that none of the falling body or rolling ball viscometers found in the literature contain such a window. A borescope is positioned against that window to determine if the test fluid remains a single phase or whether it solidifies as the temperature and pressure change. This permits important visual observations to be made that are critical to lubricant applications. Equally as important, the window also allows the operator to ensure the ball rolls continuously without sliding during a measurement.

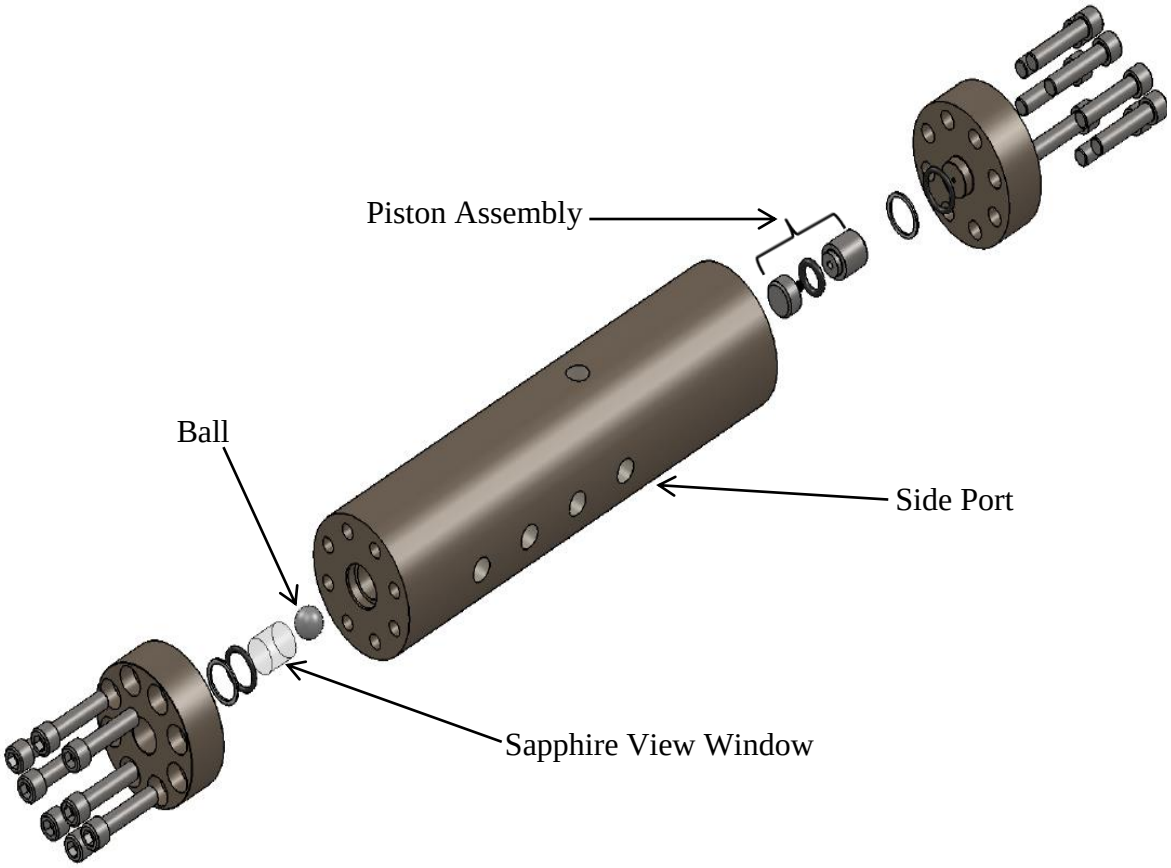

Figure 5. Expanded view of the 1st-generation, rolling ball apparatus used in this study.

It is important to note that the clearance between the viscometer ID and the ball OD is less than 0.25% of the viscometer ID, so any variation in the viscometer or ball dimensions with changes in operating conditions could impact the quality of the viscosity data. The impact of elevated pressures or temperatures on the dimensions of this viscometer are not a concern since Inconel 718 has a low thermal expansion coefficient, 13 $\mu m_{stretch}/m_{length}$•°C, and a compressibility coefficient (inverse of modulus of elasticity) of $3.37 \cdot 10^{-8}$ $psia^{-1}$ (or 4.88 mm^2/N) [29]. In addition, the ball used for this thesis is also made of Inconel 718 to minimize potential thermal expansion effects or possible pressure effects on it as well.

2.3 Pyrex® Tube Insert

This thesis study also investigated an alternative rolling ball design that uses a Pryex® tube, with a precise ID, as an insert into the Inconel viscometer and a close-fitting Pyrex® ball. Preliminary experimental results, not shown here, demonstrate that reliable viscosity measurements with octane can be obtained. However, the roll times for the Pryex® ball are excessively long because of the small difference in density between the ball and n-octane. In general roll times are of the order of 10-to-20 minutes per data point compared to tens of seconds when an Inconel ball is used without an insert for the same solvent. The excessively long roll times are expected to be exacerbated with the Pyrex ball-tube design when measuring more viscous polymer-solvent mixtures considered in this thesis study. Thus, the Pryex® ball and tube design is not chosen for continued evaluations.

2.4 Data Acquisition and Roll Time Measurement

A data acquisition system programmed in LabWindows® is used to acquire, record, log, and write files of data for each experiment at 1000 hertz. Each data file contains temperature, pressure, and roll time measurements when the ball blocks and allows light to pass from the sensors. The software also allows for user inputs to the files such as experiment descriptors. Although the ball roll times can be as short five seconds, the system employed allows accurate measurement of roll time to within ± 0.001 s.

2.5 Small Window Holder Design Modification

Figure 6 shows how the small sapphire window is secured with an elastomeric o-ring. The set screw secures the fiber optic cable that delivers or receives light to the detectors. A series of experiments failed since the window holders leaked which made it difficult to achieve consistent operational pressures in the targeted operational range exceeding 30,000 psi. After careful experimentation the Nitronic 50 steel spacer was identified as the source of the leak. Nitronic 50 is much stronger than 316 SS, however it does exhibit elastic deformation amounting to a decrease in thickness by as much as 0.005 cm at pressures in excess of 20,000 to 40,000 psia. The change in spacer thickness with pressure remained hidden for some time since the deformation of Nitronic 50 recovers when the pressure is released. Therefore, Inconel 718, a harder steel than Nitronic 50, is used for the spacers and, in fact, for the window holder body to eliminate this potential leak source.

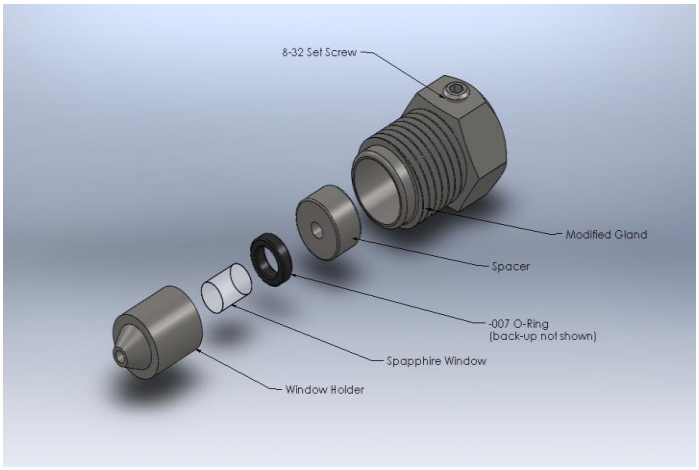

Figure 6. Expanded view of first generation window holder that is inserted into the side port of the viscometer to detect the rolling ball.

2.6 Large Window Holder and End Cap Design

Figure 7 shows a schematic diagram of the large window holder end cap incorporated into the 1st-generation RBVD used in this study. The window holder makes a metal-to-metal seal with the cell body that eliminates the elastomeric o-ring seals previously used by the McHugh group with their variable-volume, view cells [52]. This type of window holder has also been used by other research groups to seal against elevated pressures to temperatures in excess of 300°C. It is important to note that it was also necessary to design the front end of viscometer body to incorporate a "seat" to mate properly with the angled portion of the window holder. The front end cap, with eight bolts, each rated to 185,000 psi ultimate tensile strength, is secured to the viscometer body and directly pushes the window holder against the viscometer seat. Since a leak can occur between the window and the holder body, two other window holder modifications were developed to enhance the reliability and reproducibility of the seal. The first modification was the machining of a small "flat" onto the outside of the cap that pushes the window against the holder

body. The flat allows a small torque wrench to engage the cap without slipping to ensure the cap can be tightened to 17.5 ft-lb torque each time the window holder is assembled. A second modification focused on the design of a cutting device to create reproducible, smooth, and flat disks to seal the window against the window holder body. Both of these design developments enhance the performance of the RBVD by minimizing the occurrence of leaks from the front window holder.

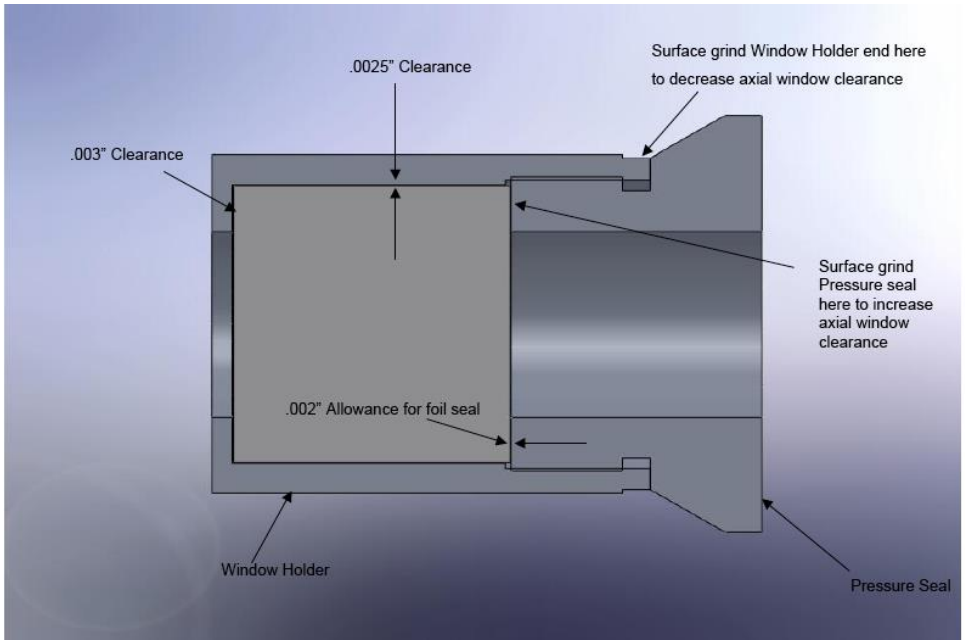

Figure 7. Window holder showing tolerances and machining requirements. A Kapton® film (T_{melt} > 300°C) seals between the window (light gray) and holder body, which makes a metal-to-metal seal with a seat in the viscometer body.

2.7 Pressure Generation and Piston Design

The pressure of the solution of interest is adjusted by moving a floating piston sealed with an elastomeric o-ring as shown in **Figure 5**. Water is the overburden fluid pressurized with a high-pressure generator (HIP Inc., Model 37-5.75-60) to move the piston. It is also important to mention that Inconel 718 has a permeability of 1.001, which means this austenitic metal does not respond to electromagnetic fields. Hence, if a multi-component mixture is studied, it is possible to mix the solution directly in the viscometer by placing a stir bar near the piston and using an external magnet to drive the stir bar. As an alternative, the solution of interest can be mixed by the action of the rolling ball.

Another distinguishing feature with the RBVD developed here and the viscometers reported in the literature, is the incorporation of a linear variable differential transducer (LVDT, Schaevitz Corporation, Model 2000 HR) used to measure the solution density. The LVDT is not shown in **Figure 5**, but a schematic diagram of how the LVDT communicates with the viscometer is shown in **Figure 8**. A magnetic "plug", also known as a core, travels through the high pressure tubing sheathed on the outside with the LVDT. The plug is connected to the piston of the RBVD via a transfer rod so the location of the piston is tracked as it moves and, hence, the volume of the viscometer is obtained from a calibration. Note that LVDT is housed a distance from the viscometer body to keep it from heating beyond approximately 100°C, the working limit for the device. The LVDT output is correlated to the internal volume of the viscometer by calibrating with a known amount of a high purity hydrocarbon fluid, such as octane, for which reliable and accurate density data as a function of temperature and pressure are available (NIST webbook). The viscometer is loaded with a known amount of fluid, the temperature and pressure are fixed,

the reading from the LVDT is recorded, and the fluid density is the determined from an independent source. Since the mass of fluid is known, the fluid volume, that is the viscometer volume, is calculated and correlated to readout of the LVDT. Density information is vital when interpreting, correlating, and calculating solution viscosities, especially in situations where the solution density is unknown. The advantage with this RBVD is that viscosity and density are simultaneously measured once the viscometer/densimeter is calibrated. Details are given in a later section on the volume calibration of the RBVD.

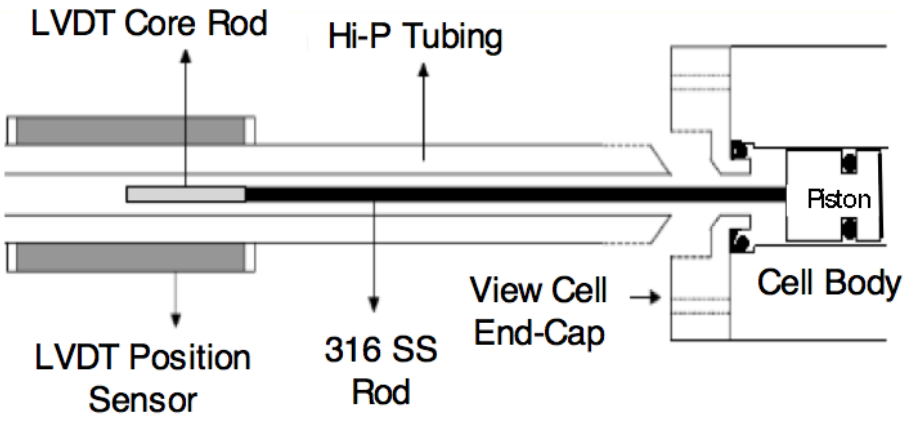

Figure 8. Schematic diagram showing how the location of the piston is determined using an LVDT. Here the cell body represents the 1st-generation RBVD body.

The elastomeric o-rings in this design create a materials compatibility problem with certain chemicals and limits operating temperatures to less than 200°C. The following chapter discusses the design modifications incorporated into the 2nd-generation RBVD to address these operating limitations. Error analysis results are also utilized in the next chapter to guide further refinement of the experimental technique.

Chapter 3. 2nd-Generation RBVD

Although the 1st-generation RBVD apparatus functioned quite well in initial studies at temperatures below approximately 175°C, unforeseen failures occurred with the elastomeric o-rings used to seal the piston and the large window when operating at temperatures in excess of 175°C. At elevated temperatures, it is also possible to contaminate the solution being studied if any impurities are leached from the o-rings or if they degrade.

3.1 2nd-Generation RBVD Modifications

In a modified design, the floating piston is replaced with a metal bellows (1.72 cm OD, BellowsTech, LLC). **Figure 9** shows a mechanical drawing of the 1st-generation RBVD floating piston with an o-ring seal. To accommodate the bellows, the end cap of the RBVD is machined with a 60° cone and the entrance of the viscometer cell body is re-machined with a 59 degree seat to mate with the end cap. It is important to note that the bellows will break if the differential pressure exceeds 15 psig between from the overburden fluid, water, and the fluid of interest. **Figure 10** shows a schematic diagram of the 2nd-generation RBVD with the LVDT rod threaded into the inside bellows face to retrofit seamlessly with the LVDT apparatus.

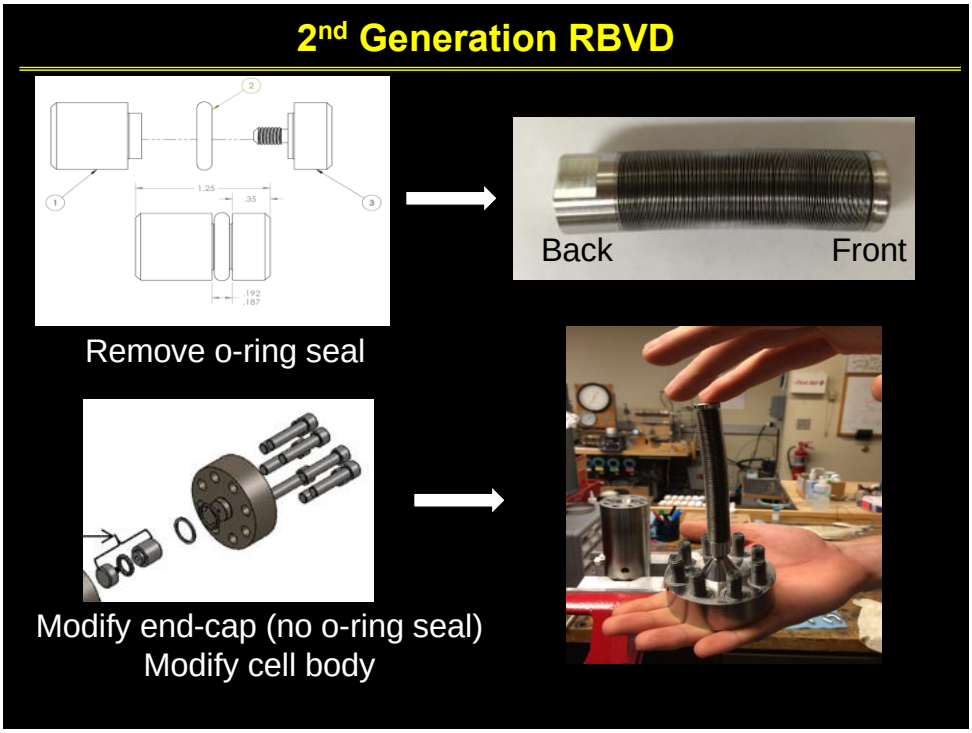

Figure 9. Mechanical drawing of first generation piston assembly sealed with o-ring.

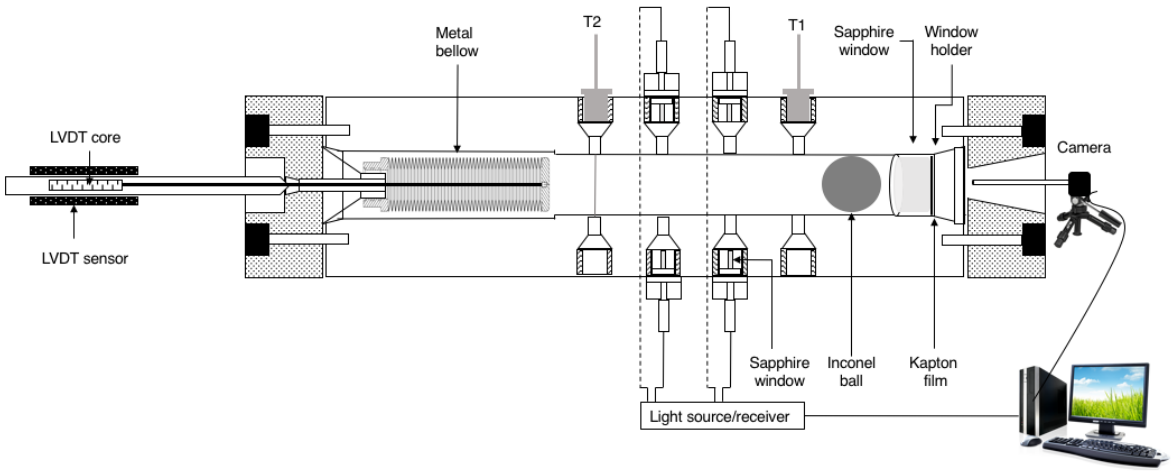

Figure 10. Schematic of the 2nd-generation RBVD developed in this study. T1 and T2 are thermocouples.

Like the prior version, the 2nd-generation RBVD is mounted on the tilt table used to achieve and fix both positive and negative angles for measurement. The internal RBVD temperature is measured at two axial locations with type-K thermocouples (Omega Corp.) calibrated against an immersion thermometer (Fisher Scientific Inc., precision and accuracy to within ± 0.1°C, recalibrated using methods traceable to NIST standards). For temperatures below approximately 150°C, each location is readily maintained constant to within ± 0.1°C and the temperature difference between each location is within ± 0.2°C. At temperatures from 150 to 250°C, each location is maintained constant to within ± 0.3°C and the temperature difference between each location is also generally less than 0.3°C, but never more than ± 0.4°C.

3.2 Impact of Experimental Uncertainties on Further Design Modifications of RBVD

An uncertainty analysis of the experimental technique for viscosity measurement highlights the contribution of each process variable to the accumulated experimental error. The full analysis is shown in the **Appendix B**. Results from this exercise indicate that measurement of the tilt angle of the RBVD (or the inclination angle) is critical to minimizing the accumulated experimental uncertainty of the data. **Figure 11** shows the highest accuracy, readily available, inclinometer on the market (TESA Technology, Model ClinoBEVEL 1 USB, accurate to within 0.01°) that is used to measure the inclination angle to within 0.01°. However, initial experiments revealed that the tilt table to which the inclinometer is mounted flexes slightly when shifted to different angles. An initial solution to resolve this issue involved the design and fabrication of a mounting bracket that allowed the inclinometer to be fixed directly to the RBVD to ensure that error is not introduced as a result of placement or positioning of the inclinometer. With the new

inclinometer and mounting technique, the accumulated overall error for the viscosity obtained with the RBVD is now dominated by the accuracy of available literature data used to calibrate the viscometer. The overall accumulated error following replacement of the inclinometer and redesign of the mounting is now nominally 2.2 percent compared to 4.9 percent before the redesign and replacement of the inclinometer.

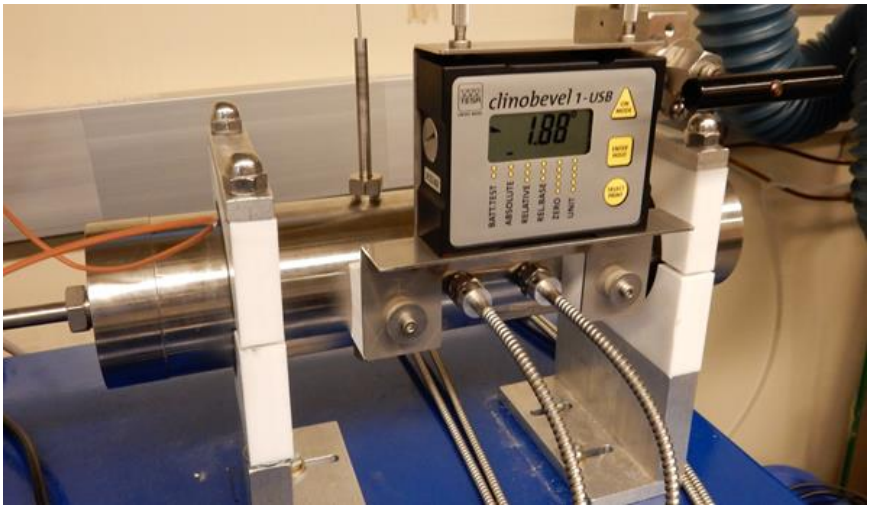

Figure 11. High accuracy inclinometer mounted directly to the RBVD for angle measurement.

Although mounting the inclinometer onto the RBVD ensured proper measurement of the tilt angle, the design created difficulty for stable high temperature operation. Specifically, the mounting bracket precluded proper installation of the heating tape and insulation around the RBVD. This issue was finally resolved by mounting a rigid base onto the tilt table surface to eliminate any flexion or angle change associated with the angle change as seen above. **Figure 12**, shows a photograph of the entire RBVD system including the tilt table, data acquisition system, pressure generator, and other associated hardware.

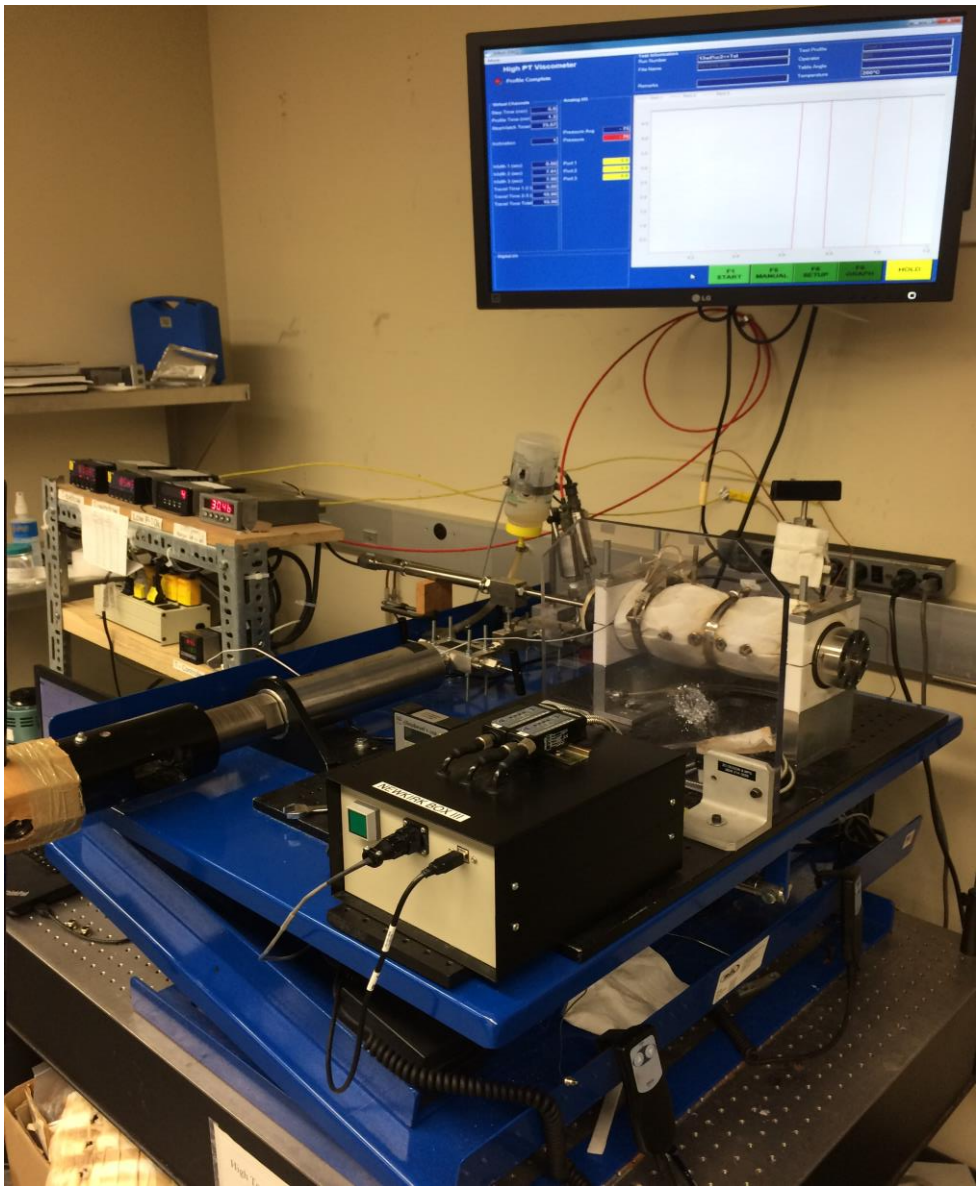

Figure 12. Photograph of complete RBVD system.

Chapter 4. RBVD Calibration, Commissioning, and Benchmarking

As previously described, internal cell volume of the RBVD is measured with a LVDT attached to the end of the RBVD [14]. The LVDT core moves through the sensor region of the LVDT while the opposite end is connected to the inner surface of a metal bellow. Water is delivered to or removed from the internal volume of the bellows that expands/contracts to increase/decrease system pressure.

4.1 RBVD Volume Calibration

The RBVD volume is calibrated using highly accurate n-octane density data reported by Caudwell, *et al.*[23] to 200°C and 30,000 psia and by NIST at temperatures greater than 200°C and pressures less than 15,000 psia. **Figure 13** shows a plot of the internal cell volume versus the transducer reading. The calibration is done at 74, 179, and 262°C and 67 pressures from 2030 to 28,280 psia, which allows for the full linear extension of the bellows. As discussed earlier, the expanded uncertainty analysis is reported in **Appendix B**. As reported, calibration uncertainty, $U_c(\mu)$, is 0.8% of the value of the density, at a confidence level of 95% with a coverage factor, k = 2.

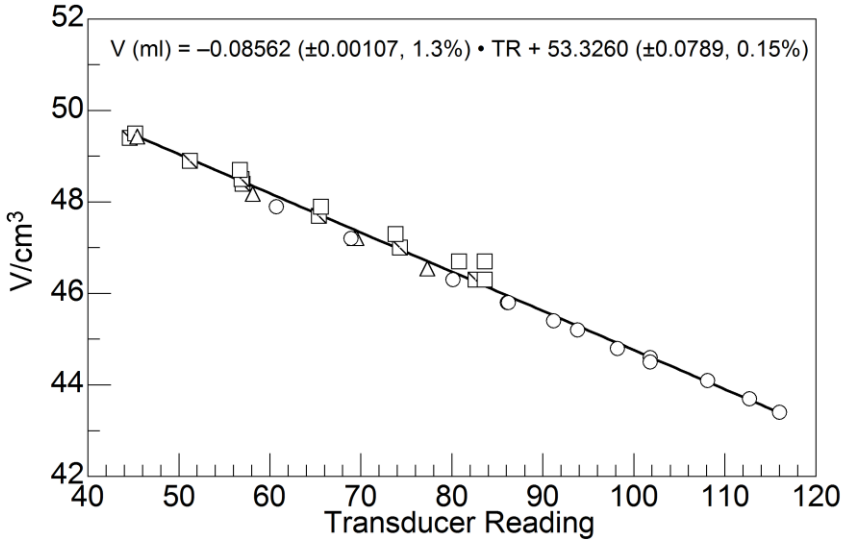

Figure 13. Calibration of RVBD internal cell volume, V, versus the LVDT value.

4.2 Determination of RBVD Calibration Constant

As previously described the governing relationship for the viscosity obtained with the RBVD is shown in **Equation 1** is,

$$h = \frac{k\left(r_b - r_{fl}\right)\sin q}{v} \qquad (1)$$

This equation contains a calibration constant, *k*, that needs to be determined at experimental conditions used in this study. Note that the viscosity calculated in **Equation 1** is inversely related to the time it takes the ball to travel the fixed distance between two sets of windows, L, inside the RBVD. Because the distance between the sets of side windows is fixed, **Equation 1** can be re-written to incorporate this constant length term into a new constant, *K*, in **Equation 5** as,

$$K = \frac{h}{t \times \left(r_b - r_{fl} \right) \sin\theta} \tag{5}$$

where K is equal to k/l. For this thesis study, the balls used in the RBVD are made of Inconel 718, the same metal as the RBVD body, to minimize the effect of temperature on the clearance between the ball and ID of the viscometer and on K. Nevertheless, the viscometer is calibrated to determine K over the full range of temperatures and pressures investigated in this study to account for their influence on K. As described in our earlier work, n-decane viscosity data are used from Caudwell *et al*.[23] at temperatures ranging from 23 to 100°C and Naake *et al*. [53] from 100 to 250°C. **Figure 14** shows one sample set of viscosity data used to determine the effect of temperature and pressure on K. Note that by using these data, a single calibration curve is obtained for temperatures ranging from 100 to 250°C is obtained. The standard uncertainties are $u(t)$ = 0.001 s and $u(\theta)$ = 0.02°. The expanded uncertainty, $U_c(\eta)$, of the viscosity, calculated by applying the law of error propagation to **Equation 5**, is equal to 2.0% at temperatures up to and including 150°C and 3.0% at temperatures greater than 150 up to 250°C, both at a confidence level of 95% with a coverage factor, k = 2.

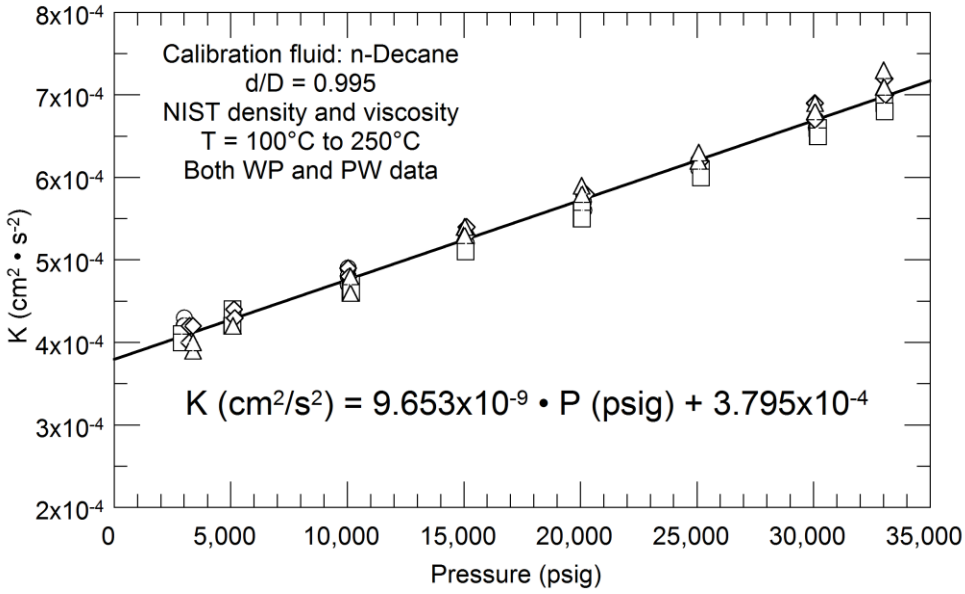

Figure 14. Viscosity calibration with decane at ○ - 100.0°C, □ - 149.6°C, ◇ - 197.4°C, and △ - 249.6°C and for the ball rolling from window to bellows, WP, and from the bellows to the window, PW.

Table 2 provides more information on an example set of calibration data generated at a single temperature to highlight the flow characteristics of the apparatus. Listed in this table are the pressure, Re, *f*, and average shear rate, $\overline{\gamma}$, at 100°C. Reynolds numbers range from 0.5 to 100 and increase with increasing temperature. Conversely, the resistance factors range from 22,000 to 231,200, and decrease with an increase in temperature. **Figure 15** shows a log-log plot of *f* versus *Re* for the complete set of n-decane calibration data obtained in this study. The linear relationship of these data demonstrates laminar flow throughout the calibration range.

Table 2. Example calibration constant, K, Reynolds number, Re, friction factor, *f*, and average shear rate, $\overline{\dot{\gamma}}$, for n-decane viscosity data used to calibrate the RBVD at 100°C. Each pressure entry represents three-to-five measurements at the same pressure.

p (psia)	$K \cdot 10^4$ ($cm^2 \cdot s^{-2}$)	**Re**	$f \cdot 10^{-5}$	$\overline{\dot{\gamma}} \cdot 10^{-4}$ (s^{-1})
3000	4.27	19	1.1	0.97
5090	5.14	15	2.4	0.61
10020	6.18	10	3.6	0.49
15080	6.07	7	3.7	0.49
15100	4.20	7	1.0	0.99
20130	4.18	5	1.0	0.98
25080	5.19	4	2.3	0.63
30110	5.66	3	2.9	0.55

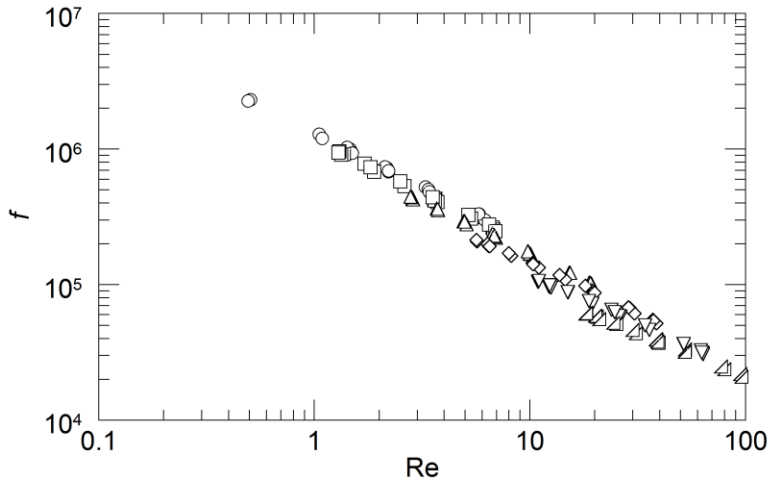

Figure 15. Relationship between the friction factor, *f*, and the Reynolds number, Re. ○ - 46.8°C, □ - 67.6°C, △ - 100.0°C, ◇ - 149.6°C, ▽ - 197.4°C, and ◿ - 249.6°C.

4.3 RBVD Benchmarking Study Using Toluene

After calibration, apparatus commissioning, and technique validation, the RBVD is used to measure simultaneously toluene viscosity and density, to demonstrate the ability to measure data reproducibly, to verify agreement with available literature, and to add new data to the literature. **Table 3** lists a representative toluene density data set for a single temperature at 261.7°C. Complete data and additional data sets are found in our submitted manuscript [14]. Although the density data are listed in increasing order of pressure, the experimental density data are obtained in a non-monotonic manner to minimize any potential experimental artifacts. **Figure 16** shows the Average Absolute Deviation (AAD, **Equation 6**) of toluene density data relative to available NIST data. Multiple points obtained in our study at most pressures superpose and demonstrate data reproducibility. Note also that all data are well within acceptable experimental uncertainty of ± 0.8% and are distributed equally and uniformly about the zero deviation line.

$$AAD/\% = 100 \cdot \frac{1}{N} \sum_{i=1}^{N} \left| \frac{x_{i,\exp} - x_{i,cal}}{x_{i,\exp}} \right| \qquad (6)$$

where N is the number of data points, $x_{i,exp}$ is the value of an experimental data point, and $x_{i,cal}$ is a calculated or literature value from NIST [54]. The calculated AAD is within ± 0.25% indicating excellent agreement with toluene density data reported by NIST.

Table 3. Representative RBVD toluene density data obtained at 261.7°C.

p (psia)	ρ ($kg \cdot m^{-3}$)
5420	697.2
5420	696.5
7480	721.5
7510	720.7
9910	743.2
9910	742.4
12840	764.8
12840	764.8
12850	764.0
12850	764.0
15130	778.9
15140	778.1
17990	794.7
18000	793.8
24490	818.8
24500	818.8
24530	820.6
30340	843.1
30370	844.9
34000	859.2
36890	865.3
36930	867.2
40070	877.0
40250	878.3

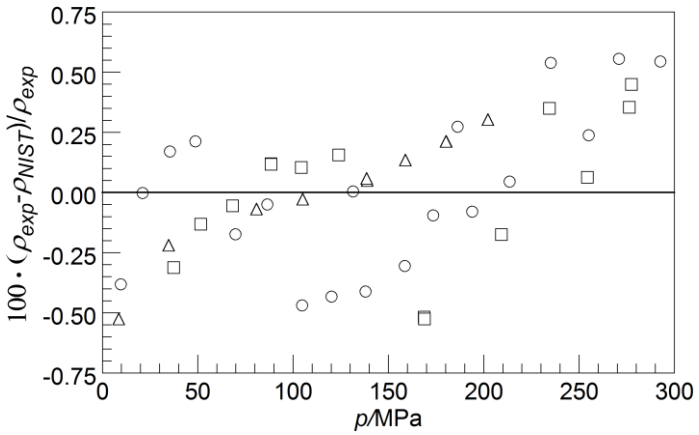

Figure 16. Deviation plot of experimental toluene density (ρ_{exp}) obtained in this study to that obtained from NIST (ρ_{NIST}). △ - 74.2°C, ○ - 178.7°C , and □ - 261.7°C.

Figure 17 shows the effect of pressure and temperature on the viscosity of toluene, η_{exp}, obtained in this benchmarking study at all eight temperatures from approximately 22 to 260°C. **Table 4** provides average absolute deviation AAD, standard deviation of the AAD (SD), maximum deviation (D_{max}, **Equation 7**), and *bias* (**Equation 8**), for each smoothed curve fit to experimental viscosity isotherms. **Table 5** provides a sample set of toluene viscosity data obtained for a single temperature, 178.7°C, of the eight isotherms measured at pressures from 1,000 to 43,000 psia. Listed also are the associated Re, *f*, and γ values for each measurment. Complete data sets are included in Rowane et al. [14].

$$D_{\max} / \% = 100 \bullet Max\left(\left| \frac{x_{i,\,\exp} - x_{i,\,\mathrm{cal}}}{x_{i,\,\exp}} \right| \right) \tag{7}$$

$$bias / \% = 100 \bullet \frac{1}{N} \sum_{i=1}^{N} \left(\frac{x_{i,\,\exp} - x_{i,\,\mathrm{cal}}}{x_{i,\,\exp}} \right) \tag{8}$$

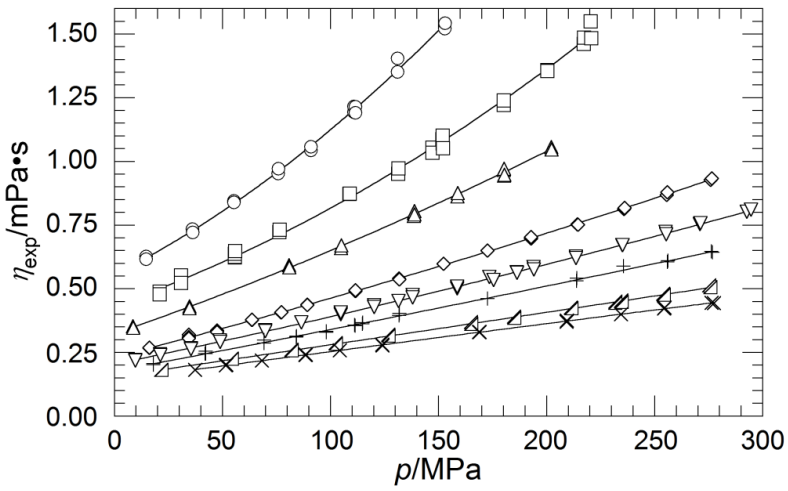

Figure 17. Effect of pressure and temperature on the viscosity of toluene, ηexp, obtained in this study. ○ - 22.7°C, □ - 50.2°C, △ - 74.1°C, ◇ - 119.3°C, ▽ - 148.3°C, + - 178.9°C, ◿ - 227.0°C, and × - 261.7°C. Lines are drawn to guide the eye.

Table 4. Average absolute deviation (AAD), standard deviation (SD), maximum deviation (D_{max}), and bias for each smoothed curve fit to experimental viscosity isotherms.

T (°C)	**AAD** (%)	**SD** (%)	***D_{max}*** (%)	***Bias*** (%)
22.7	1.0	0.7	3.3	0.0
50.2	1.6	1.2	4.6	0.0
74.1	0.9	0.5	1.7	0.1
119.3	0.7	0.7	3.2	0.0
148.3	0.7	0.6	1.8	-0.1
178.9	1.0	1.0	4.1	0.1
227.0	0.6	0.5	1.4	-0.1
261.7	0.4	0.3	1.3	0.3

Table 5. Example RBVD toluene viscosity, Reynolds number, resistance factor, and shear rate data for a single temperature at 178.1°C and pressures from 1,000 to 43,000 psia.

p (psia)	η (mPa·s^{-1})	**Re**	$f \cdot 10^{-5}$	$\overline{\dot{\gamma}} \cdot 10^{-4}$ (s^{-1})
1390	0.221	83.6	0.25	1.87
1410	0.219	86.2	0.24	1.91
3060	0.243	72.4	0.28	1.75
3080	0.240	73.6	0.27	1.76
5130	0.266	63.6	0.30	1.65
5130	0.263	65.8	0.29	1.69
7080	0.296	54.4	0.34	1.55
7090	0.291	57.2	0.32	1.60
10120	0.337	48.1	0.36	1.52
10120	0.334	47.1	0.37	1.48
12150	0.368	41.8	0.39	1.42
12150	0.368	41.2	0.40	1.40
15190	0.400	38.9	0.40	1.41
15190	0.407	37.0	0.42	1.37
17430	0.435	34.9	0.43	1.36
17430	0.428	35.7	0.42	1.37
19060	0.452	33.9	0.43	1.37
19060	0.452	32.3	0.45	1.30
20020	0.475	30.8	0.47	1.30
20020	0.466	31.8	0.45	1.31
23000	0.501	28.4	0.48	1.25
23000	0.509	27.9	0.49	1.25
25160	0.546	24.9	0.53	1.18
25440	0.535	26.0	0.51	1.21
27010	0.566	23.9	0.54	1.17
27020	0.563	24.3	0.53	1.18
28140	0.585	24.1	0.52	1.22
28150	0.576	24.4	0.52	1.21
30980	0.627	20.9	0.58	1.12
30980	0.621	21.1	0.58	1.12
34080	0.672	19.7	0.59	1.12
34100	0.672	19.5	0.59	1.11
36990	0.723	17.5	0.64	1.06
37040	0.714	18.0	0.62	1.08
39290	0.754	16.4	0.66	1.03
39330	0.757	16.2	0.67	1.02
42440	0.802	15.7	0.66	1.04
42710	0.811	15.4	0.68	1.03

The Tait Equation (**Equation 9**) is used to correlate the viscosity data obtained in this study following the method reported by Caudwell et al. [23]. This equation contains three parameters, *D*, *E*, and η_0, which is a reference viscosity at p_0 = 14.7 psia [21,24, 25]. Initially, **Equation 9** is fit to each set of isothermal data by minimizing the *AAD* between calculated and smoothed experimental viscosities. **Table 6** shows that η_0, *D*, and *E* decrease with increasing temperature. The *AAD* and *SD* values are all less than 0.3% indicating that the Tait expression provides a reasonable representation of the high-pressure toluene viscosities measured at each temperature.

$$\eta = \eta_0(T)\left(\frac{p+E}{p_0+E}\right)^D \tag{9}$$

Table 6. Optimized parameters for each set of isothermal viscosity data fit to Tait Equation**.**

T (°C)	**p** (psia)	η_0 (psia•s)	***D***	***E*** (psia)	**AAD** (%)	**SD** (%)
22.7	1160 – 24950	80.35	2.897	52210	0.05	0.17
50.2	3050 - 32050	62.66	2.559	51110	0.06	0.03
74.1	1310 - 29300	47.00	1.458	23680	0.04	0.03
119.3	2320 - 40180	34.23	1.300	21310	0.15	0.16
148.3	1450 - 42790	29.44	1.192	19730	0.26	0.23
178.9	2610 - 40180	25.96	1.129	18880	0.04	0.04
227.0	3340 – 40180	22.48	1.030	18620	0.01	0.01
261.7	5370 - 40320	20.31	0.919	15880	0.02	0.02

The parameters *D* and *E* are fit to quadratic functions of temperature, **Equations 10** and **11**, respectively, to allow for calculating the viscosity at any temperature from 22 to 262°C. Note that parameter *D* is correlated to inverse temperature. The initial fit of these two parameters over the entire experimental temperature range exhibit minima at a temperature near 125°C that translated to very poor fits. Hence, a modified approach is used where *D* and *E* are fit in two different temperature ranges of 20 to 120°C and 120 to 260°C. The 120°C isotherm serves as a convenient break point as it is roughly 10°C greater than the normal boiling point of toluene.

$$D = \sum_{i=0}^{2} d_i (K/T)^i \tag{10}$$

$$E/MPa = \sum_{i=0}^{2} e_i (T/K)^i \tag{11}$$

Equation 12 uses three parameters, A_η, B_η, and C_η, for correlating the temperature variation of the reference viscosities, η_0. Here, again, data in the same two temperature ranges are used for the fit. With an initial estimate for C_η, a linear, least squares fit of **Equation 12** provides a value for B_η from the slope and for A_η from the intercept. Optimized values for A_η, B_η, and C_η are obtained by minimizing the *AAD* in each temperature range.

$$\ln \eta_0 = \ln A_\eta + \left(\frac{B_\eta}{T - C_\eta} \right) \tag{12}$$

Finally, for each temperature range, re-optimized values for A_η, B_η, C_η, d_0, d_1, d_2, e_0, e_1, and e_2 are obtained simultaneously using a non-linear optimization routine that minimizes the *AAD* between calculated and smoothed experimental viscosities. **Appendix C** summarizes the method to correlate toluene viscosity data to the Tait Equation. **Table 7** lists parameter values from this re-optimization along with values for the *AAD*, *SD*, D_{max}, and *bias*. The temperature variation of *D* and *E* is similar to that reported in the literature [21, 24, 25, 55]. The *AAD* in each temperature range is less than 0.4%, which is much lower than the estimated experimental uncertainty of ± 2%. **Figure 18** shows the deviation plot for the data obtained in this study compared to calculations using the Tait Equation. The very low values for the *bias* shown in **Table 7** establishes that the deviations are evenly distributed about zero.

Table 7. Best fit parameters for the Tait Equation used to represent experimental viscosities in two temperature ranges. (Note that calculations necessitate absolute temperature units of K and pressure unites of mPa).

T *range* *(°C)* =	22.7 - 100	**T *range*** *(°C)* =	100 – 262
$10^3 A_\eta$ (mPa·s)	3.0468	$10^2 A_\eta$ (mPa·s)	4.7176
$10^{-3} B_\eta$ (K)	2.5661	$10^{-2} B_\eta$ (K)	4.7407
$10^{-2} C_\eta$(K)	-1.9691	$10^{-1} C_\eta$(K)	9.8448
d_0	4.1582	$10 d_0$	-8.9288
$10^{-3} d_1$ (K)	-3.5207	$10^{-3} d_1$ (K)	1.2282
$10^{-5} d_2$ (K)^2	9.4327	$10^{-5} d_2$ (K)^2	-1.3770
$10^{-3} e_0$ (MPa)	2.1503	$10^{-2} e_0$ (MPa)	2.5916
e_1 (MPa/K)	-8.6609	e_1 (MPa/K)	-2.2697
$10^3 e_2$ (MPa/K^2)	9.0820	$10^5 e_2$ (MPa/K^2)	-9.5633
AAD (%)	0.33	*AAD (%)*	0.30
SD (%)	0.65	*SD (%)*	0.26
D_{max} *(%)*	3.94	D_{max} *(%)*	0.84
Bias (%)	-0.09	*Bias (%)*	0.06

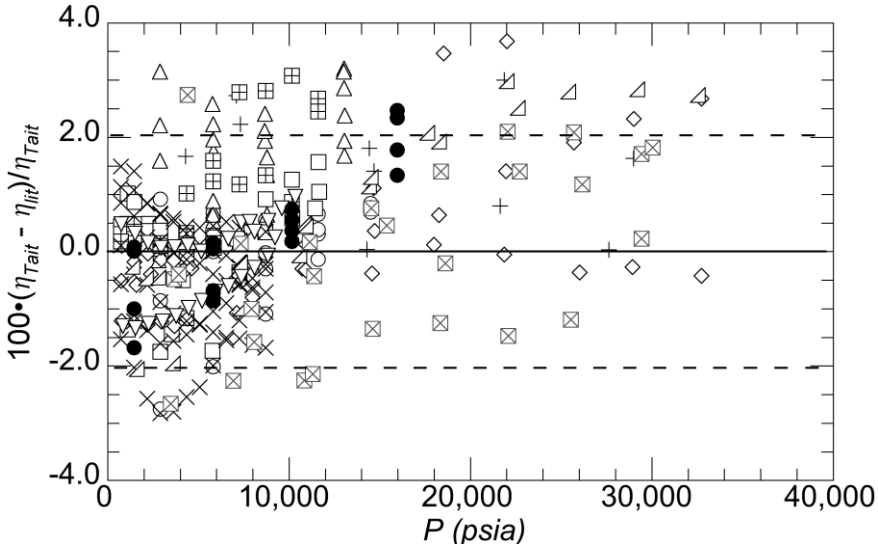

Figure 18. Comparison of literature data, η_{lit}, to viscosities from this study, η_{Tait}. ○ - Baylaucq et al.[42], □ - Avelino *et al.*[18], △ - Caudwell *et al.*[55], ◇ - Olivera and Wakeham [19], ＋ - Dymond *et al.*[29], ⊞ - Daridon *et al.*[41], × - Pensado *et al.*[43], ⊿ - Harris [26], ▽ - Assael *et al.*[20], ● - Kashwagi and Makita [24], ⊠ - Vieria dos Santos and Nieto de Castro [25].

Table 8 compares literature sources for toluene viscosities with experimental viscosities from the present study calculated with the Tait Equation. The *AAD* values are consistently lower than the ± 2.0% estimated experimental uncertainty for the data reported in the present study, with the expection of the data of Dymond et al. [29] and Wilbur and Jonas [56]. The larger *AAD* for the comparison to data from Dymond et al.[29] may be a result of the modestly large experimental uncertainty of ± 4% reported by these authors. In contrast, Wilbur and Jonas [56] do not report an experimental uncertainty for the viscosity and, more imporantly, they report data for deuterated toluene, which is not expected to have precisely the same viscosity as toluene. Comparisons of available viscosity data in the literature with data from the present study calculated with the Tait expression using **Equation 12**, up to 58,000 psia.

Table 8. Comparison of toluene literature viscosities and viscosities from this study calculated with the Tait Equation using the best fit parameters.

Year	Authors	T (°C)	P (psia)	Method	Accuracy (±%)	AAD (%)	D_{max} (%)
2015	This Study [14]	23-262	1300-43500	Rolling Ball	2	0.3	3.9
2011	Daridon et al.[41]	20-59	14-11600	Vibrating Quartz	5	1.3	3.1
2009	Baylaucq et al.[42]	20-50	14-14500	Falling Body	2	0.7	2.8
2005	Pensado et al.[43]	30-80	14-8700	Rolling Ball	2	0.9	2.8
2004	Caudwell et al.[55]	50-100	14-13000	Vibrating Wire	2-5	1.6	3.2
2003	Avelino et al.[18]	-25-50	14-11600	Vibrating Wire	2-3	0.7	1.8
2000	Harris[26]	-18-50	14-58000	Falling Body	1	1.7	5.4
1997	Vieira dos Santos, N.C. [25]	25-75	14-30000	Vibrating Quartz	0.5	1.3	2.7
1995	Dymond et al.[29]	25-75	14-71000	Falling Body	4	1.5	4.5
1992	Olivera, Wakeham [19]	30-75	14-36500	Vibrating Wire	0.5	1.6	10.4
1991	Assael et al.[20]	30-50	14-10000	Vibrating Wire	0.5	0.6	1.3
1991	Dymond et al.[29]	25-100	14-75000	Falling Body	4	3.6	13.4
1982	Kashiwagi, Makita [24]	25-75	14-16000	Vibrating Quartz	2	0.8	2.5
1974	Wilbur, Jonas [56]	-35-200	14-51000	Rolling Ball	N/A	3.5	10.7

It is important to note that data in the present study are limited to 43,000 psia; and, therefore part of the comparison considers extrapolated viscosity values**.** **Figure 19** shows 11 out of 13 sources have *AAD* values less than 1.7%. Five of the 11 sources have *AAD* values less than 1.0% and these five sources use four unique viscometric techniques.

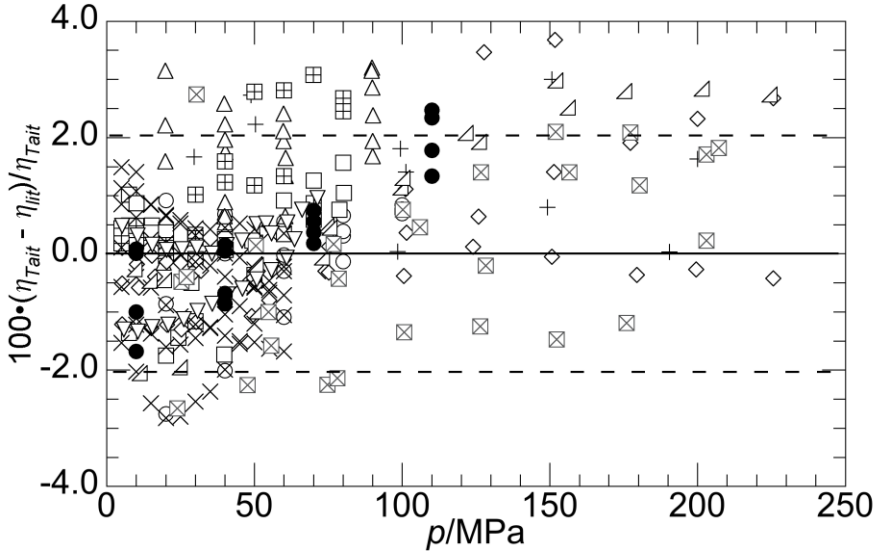

Figure 19. Comparison of available literature data, η_{lit}, and viscosities from this study calculated with the Tait Equation using the best fit parameters, η_{Tait}. Three of the points reported by Olivera and Wakeham exhibit a deviation greater than ± 6%, and do not show up on this graph. ○ - Baylaucq et al., □ - Avelino *et al.*, △ - Caudwell *et al.*, ◇ - Olivera and Wakeham, ＋ - Dymond *et al.*, ⊞ - Daridon *et al.*, × - Pensado *et al.*, ⊿ - Harris, ▽ - Assael *et al.*, ● - Kashwagi and Makita, ⊠ - Vieria dos Santos and Nieto de Castro.

Only 21 out of 378 data points used in this comparison in **Figure 19** show a deviation greater than ± 3%. Of those 21, seven are reported by Olivera and Wakeham [19]; and six of those are at a single temperature of at 30°C. Nine of the 21 points are reported by Harris [26] with six of these points at 25°C, and three points at 50°C and pressures from 54,000 to 58,000 psia. Three of the 21 points are reported by Caudwell *et al*.[55], one by Daridon *et al*.[41], and one by Dymond *et al*.[29].

Collectively, the data of Kashiwagi and Makita [24] and Baylaucq et al.[42] show no obvious trends in the deviation although this collective data set does contain four points that deviate from ± 2.0 to 3.0 percent. The data reported by Pensado *et al*.[43] and Vieria dos Santos and Nieto de Castro cluster consistently around zero deviation and are within the ± 2.0 percent experimental uncertainty of the data from the present study. The results shown in **Figure 19** and **Table 8** validate the reliability and accuracy of the RBVD technique used here given that the reported high pressure viscosities are in close agreement with viscosities obtained using other viscometric techniques. In addition, the high-temperature, high-pressure viscosities reported in the present study extend the available toluene data base to temperatures as high as 262°C and pressures to 43,500 psia.

Chapter 5. Impact of Star Polymers on Solution Viscosity

After thoroughly benchmarking of the RVBD with toluene to temperatures of 260°C and pressures exceeding 40,000 psia, results are presented from studies on the impact of star polymer-solvent mixtures on solution viscosity. Two types of star polymer systems are studied: (1) a industrially-relevant polymer with an ethylene glycol dimethacrylate (EGDMA) core attaching copolymer "arms" of methyl methacrylate (MMA) and lauryl methacrylate (LMA); and (2) a set of three low polydispersity commercially purchased polystyrene star polymers. The same validated techniques are used to as those refined during the commissioning phase described in Chapter 4.

5.1 Highly-Branched and Star Polymer Background

Over the past few decades, advances in polymer chemistry have led to the creation of a variety of polymers with unique, well-defined, and highly branched architectures. **Figure 20** provides illustrations of several of these highly-branched polymer architectures from Gao *et al* [57]. Star polymers used for this study have a fixed number of branches (or "arms"). These polymers are globular and not typically exhibit chain entanglements. Star polymers can also be synthesized to incorporate a variety or a large number of functional groups within a single molecule. Thus, they can be tailored to specific uses such as viscosity modifiers and friction

modifiers for lubricants. In addition, they hold widespread potential for use in catalysis, coatings, and drug delivery [58, 59, 60, 61]. Despite this potential, fundamental research on the physical chemistry properties of star polymers is still in its infancy, especially at HTHP. Nevertheless, recall from the introductory and background information presented in this thesis that some star polymers have been shown in limited empirical studies to provide superior performance in maintaining lubricant film thickness and improved frictional properties at high temperatures and pressures in automotive applications. Therefore, if the RBVD can be used to understand and correlate physical and structural features of star polymers to desirable performance attributes, such as improved fuel economy, substantial industrial R&D time and money can be saved compared to running large, costly, and statistically designed empirical matrix tests.

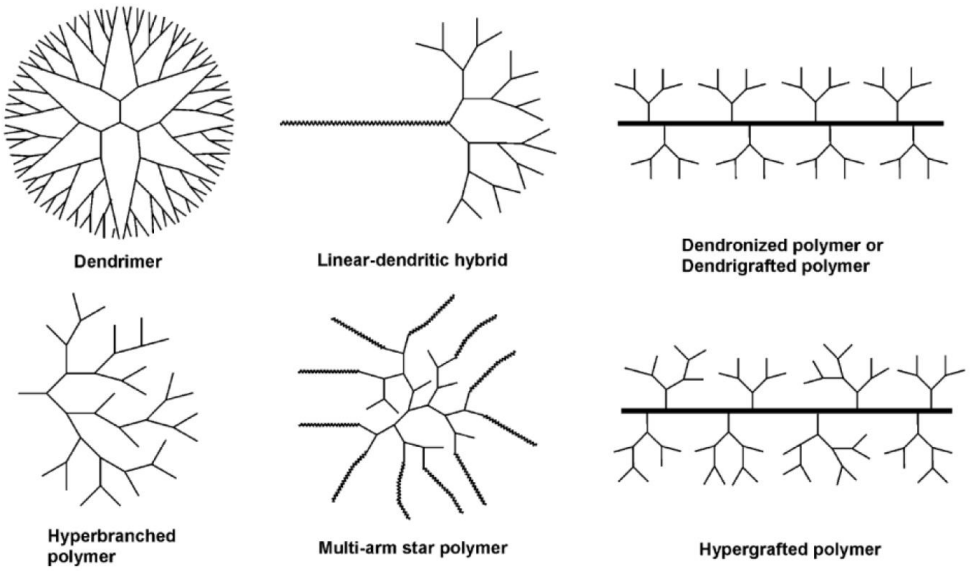

Figure 20. Highly branched polymer structures [57].

5.2 Impact of MMA-LMA Industrially-Relevant Star Polymer on Solution Viscosity

An industrially relevant star polymer is initially used (supplied by Afton Chemical Corporation) to investigate the impact of polymer architecture on HTHP viscosity. The randomly distributed repeat groups in the copolymer "arms" are methyl methacrylate (MMA) and lauryl methacrylate (LMA). The "core" of the star polymer is made of ethylene glycol dimethacrylate (EGDMA). The star polymer is synthesized in a paraffinic-naphthenic "base oil" solvent. A generalized synthesis of this type of polymer is shown schematically in **Figure 21**.

The star polymer, designated as 60ML45RS, is chosen for the first set of star polymer experiments. The Mw (in kilo-Daltons, kDa) of each arm and the total polymer as measured by gel permeation chromatography analysis using a polystyrene standard were specified as ~44 kDa and ~595 kDa, respectively. The polydispersity index (PDI) of the arms and star polymer as a whole are 1.25 and 1.36, respectively. The 60ML45RS polymer has a high MMA to LMA ratio of 0.6 that, based on empirical data from linear polymer counterparts, is of interest for study because this higher MMA content is generally less soluble in base oil yet it improves lubricant friction modifier performance significantly. Thus, from a lubricant applications standpoint, this polymer is representative of a material that would be of high commercial interest.

A mixture of 2.4 weight percent (wt%) 60ML45RS in n-octane is used for these studies since this amount of polymer is representative of that used industrially. N-octane is selected because a significant amount of HTHP viscosity literature data exists, and it is an acceptable surrogate for the base oil in which the star polymer would typically be blended in industrial applications. Results are shown for experiments with two different diameter balls with ball outer diameter (OD)-to-viscometer inner diameter (ID) ratios: 0.998 and 0.995. **Figure 22** shows that

although the two sets of data differ slightly in a systematic way, the aforementioned ratio has little effect on the measured viscosity within expected experimental error. Note also that the Re for these experiments is generally maintained at less than 100, which ensures laminar flow between the ball OD and RBVD ID. Importantly, recognize that each set of data was obtained independently, six months apart, and they still represent acceptable variation. These results not only validate the technique developed, but also demonstrate how robust and repeatable the RBVD is by being able to repeat within nominal error over such an extended period. Detailed data associated with **Figure 22** are provided in **Appendix D** for reference. A step-by-step procedure for assembly of the RBVD is provided in **Appendix E**.

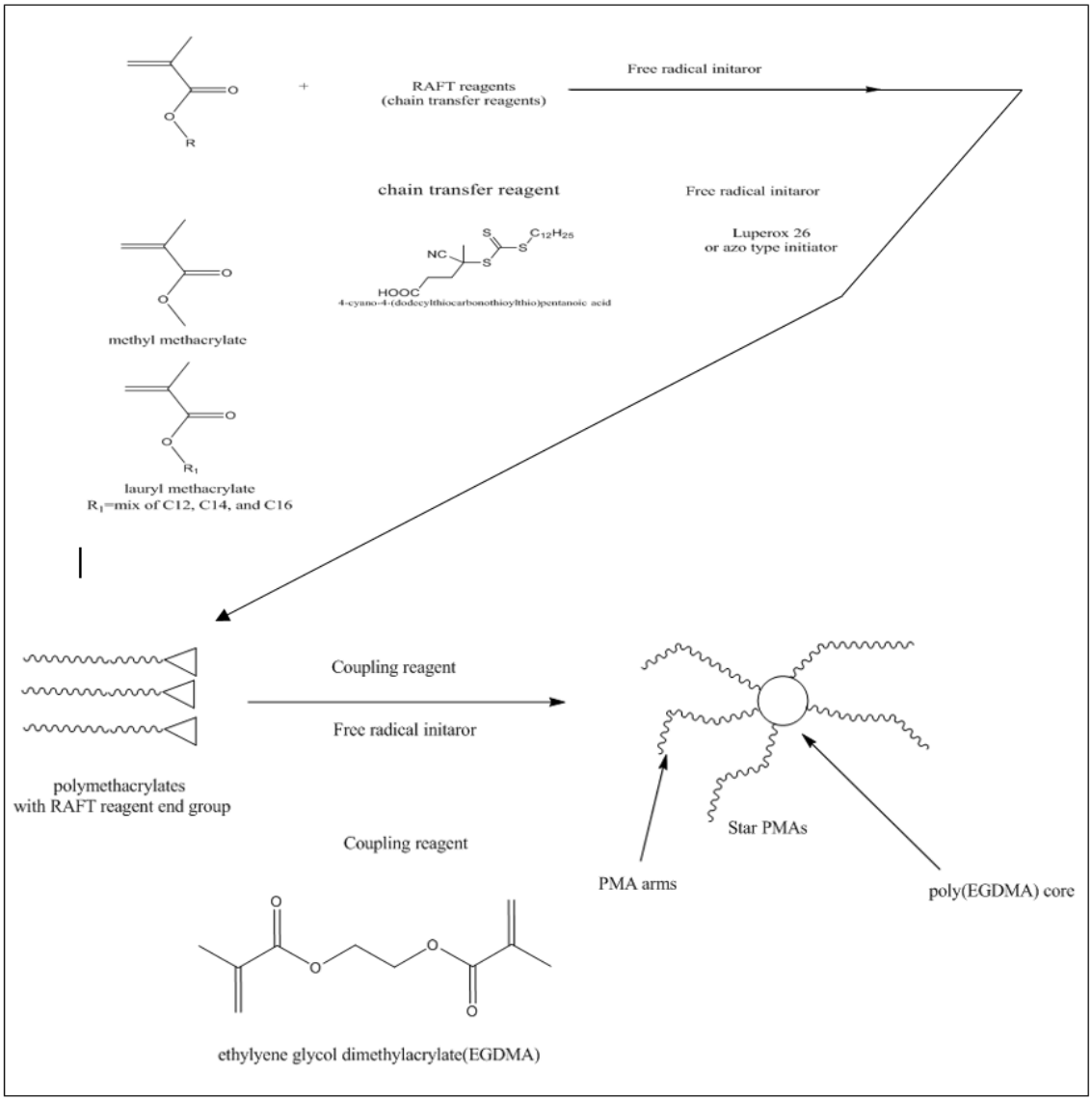

Figure 21. Schematic representation of EGDMA star polymers synthesis.

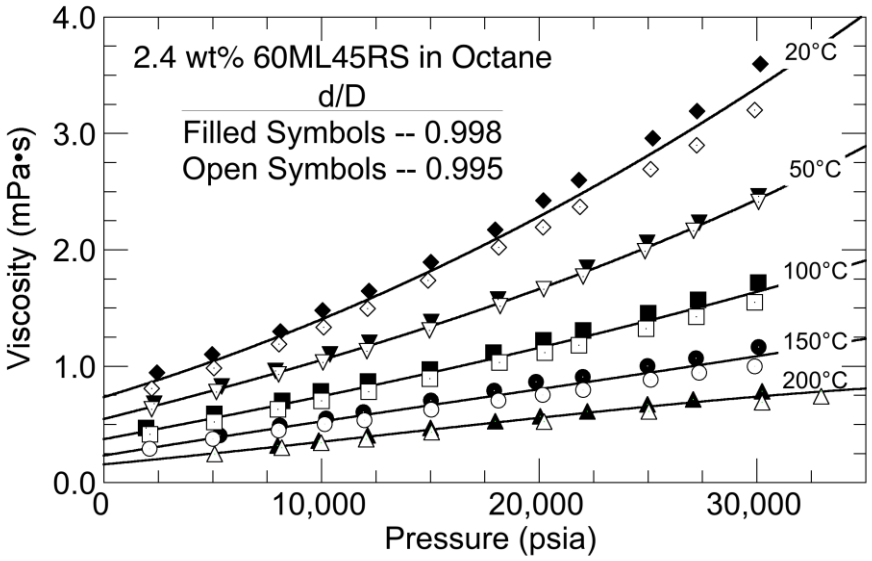

Figure 22. Effect of temperature, pressure, and ball OD (d) on viscosity of a 2.4 wt% 60ML45RS-n-octane solution obtained in this study. Here D represents the inside diameter of the RBVD. Note that the size of the symbol hides the error bars.

Figures 23, **24**, **25**, **26, and 27** show comparisons of 2.4 wt% 60ML45RS in n-octane solution viscosity to pure n-octane viscosity at nominal temperatures from 20, 50, 100, 150, and 200°C, respectively. Both viscosity curves show an expected decrease as the temperature increases. However, even at 200°C the 2.4 wt% 60ML45RS in n-octane solution maintains higher viscosity to pressures near 30,000 psia. As previously mentioned, this is an important finding as these temperatures and pressures are relevant to a variety of automotive applications. Additionally, these results are developed using much less costly testing than is commonly used in industry.

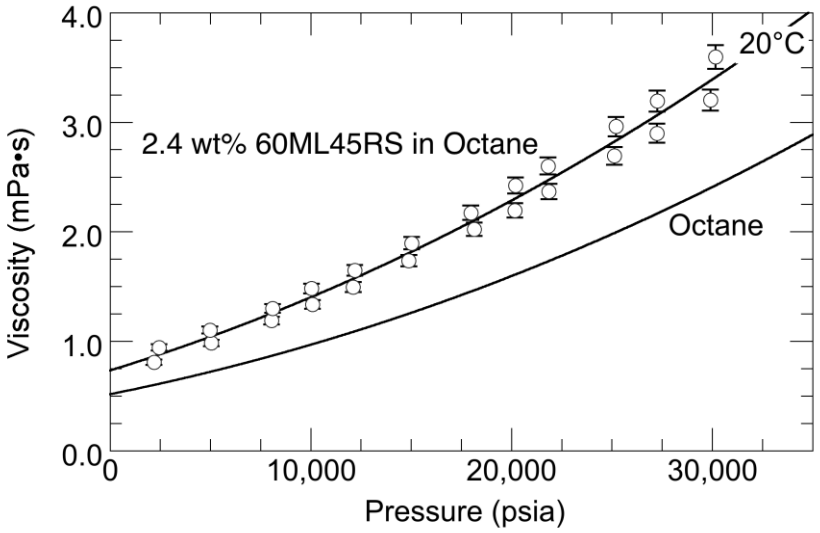

Figure 23. Comparison of 2.4 wt% 60ML45RS in n-octane solution and pure n-octane viscosities at 20°C.

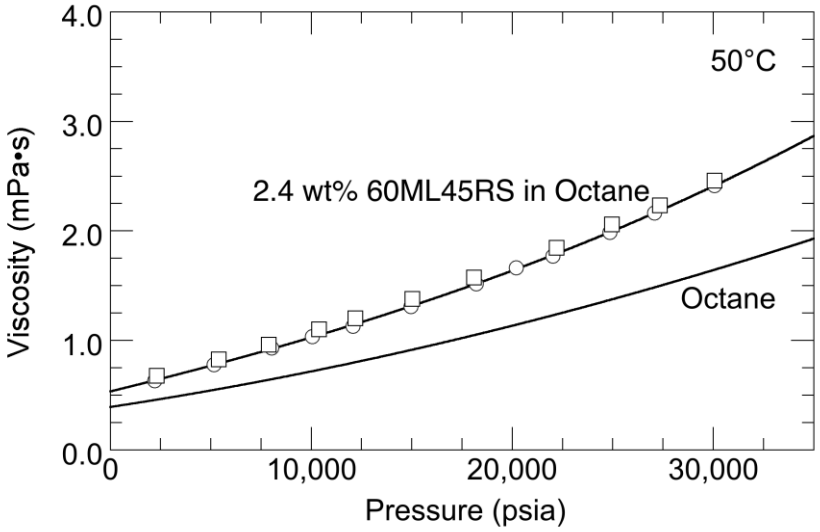

Figure 24. Comparison of 2.4 wt% 60ML45RS in n-octane solution and pure n-octane viscosities at 50°C.

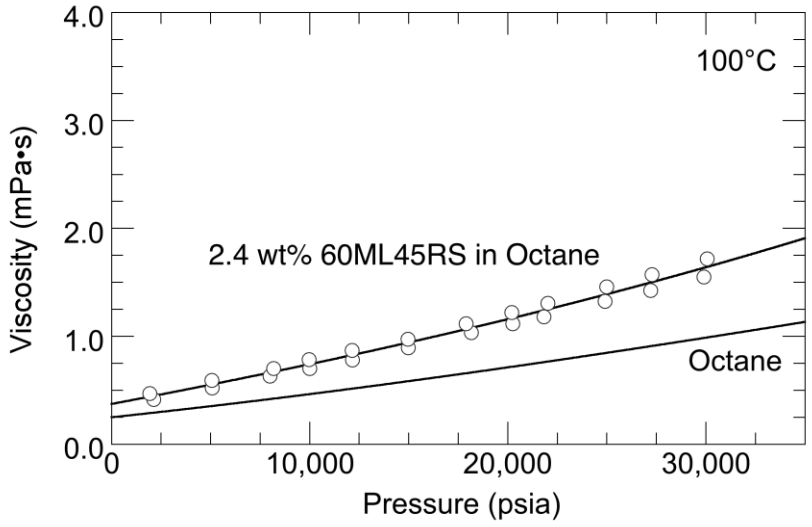

Figure 25. Comparison of 2.4 wt% 60ML45RS in n-octane solution and pure n-octane viscosities at 100°C.

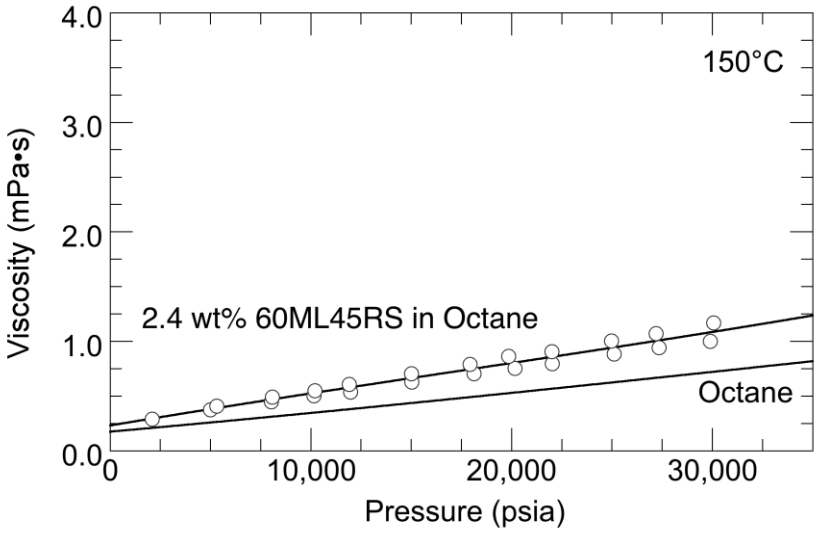

Figure 26. Comparison of 2.4 wt% 60ML45RS in n-octane solution and pure n-octane viscosities at 150°C.

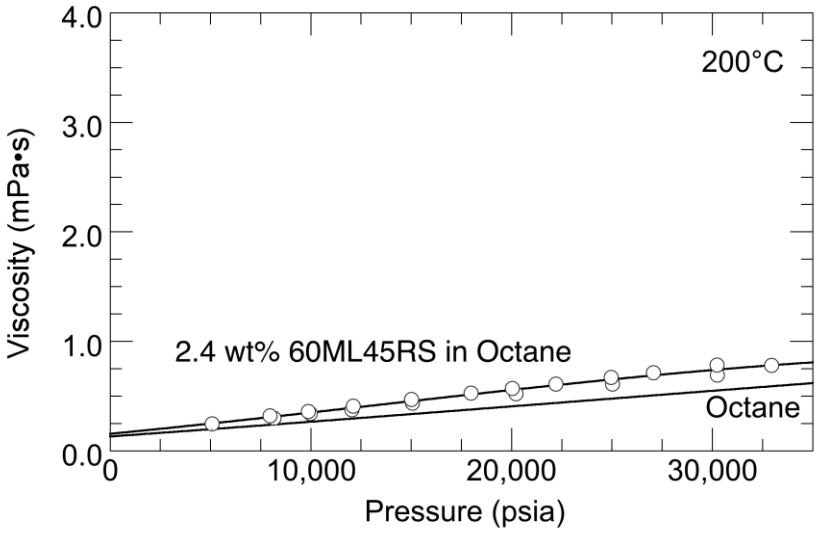

Figure 27. Comparison of 2.4 wt% 60ML45RS in n-octane solution and pure n-octane viscosities at 200°C.

Figure 28 shows a cross plot of the viscosity data as isobars. As mentioned, the pressure levels shown here are representative of those found in automotive. Based on the capability of the RVBD to be used with high molecular weight polymer solutions under reasonable industrially relevant experimental conditions that allow for significant research and development without the use of lengthy or expensive alternative tests, a next phase of comparative research is undertaken. Thus, these data motivate the approach in the next Chapter where a one-to-one comparison is made with well-characterized star polymer solutions.

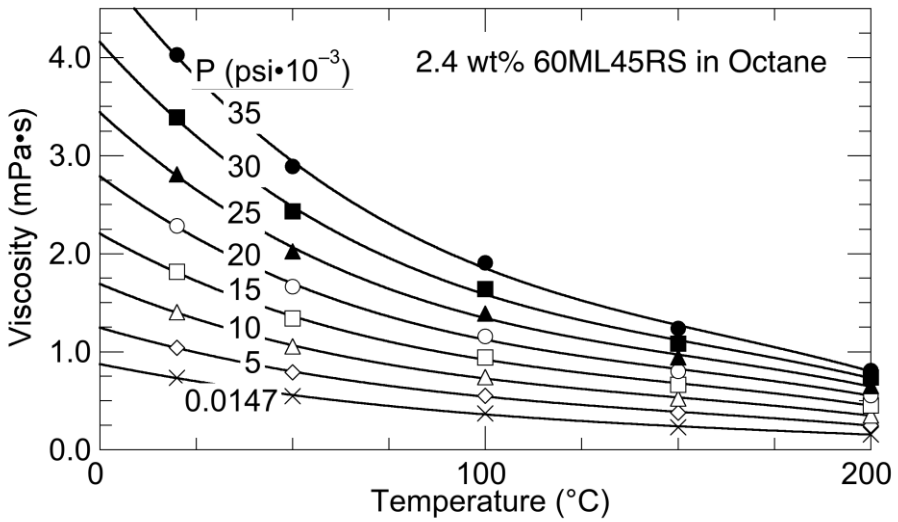

Figure 28. Impact of temperature on isobaric viscosity behavior for a solution of 2.4 wt% 60ML45RS in n-octane.

5.3 Impact of Well-Characterized, Star Polystyrene on Solution Viscosity

This section provides results and discussion on the use of the RBVD to simultaneously measure density and viscosity of three different three-arm star polystyrene (s-PS) polymer solutions at 2 wt% in toluene. In addition, pure toluene data are also presented to allow for evaluation of the impact of each s-PS. Toluene is an ideal solvent for s-PS, and is also a reasonable surrogate for base oil in this situation. The s-PS used here were obtained commercially as neat purified solid powders and are well characterized to facilitate data interpretation. All have narrow polydispersity indices (PDI) and are atactic as determined by nuclear magnetic resonance spectroscopy analysis. A summary of the properties of these polymers is provides as **Table 9**. Detailed analytical reports for these polymers are provided as **Appendix F**. All data measured and reported in this section demonstrate, for the first time, the actual impact of the star architecture

on critical fluid properties of viscosity and density at extreme operating conditions representative of automotive applications.

Table 9. Summary of star-polystyrene properties

s-PS	# of arms	Arm Mw (kDa)	Polymer Mw (kDa)	PDI
45k	3	15.4	41.2	1.08
100k	3	36.0	97.6	1.07
300k	3	108	305	1.06

The first set of plots compares each 2 wt% s-PS polymer solution (in toluene) with pure toluene to evaluate the impact on density of HTHP on each. **Figure 29** provides the aforementioned comparison for s-PS(45k) at 38, 107, 171, and 255°C. **Figure 30** shows the same comparison for s-PS(100k) at 45, 106, 194 °C. The same plot is provided for s-PS(300k) as **Figure 31** at 43, 110, and 173°C.

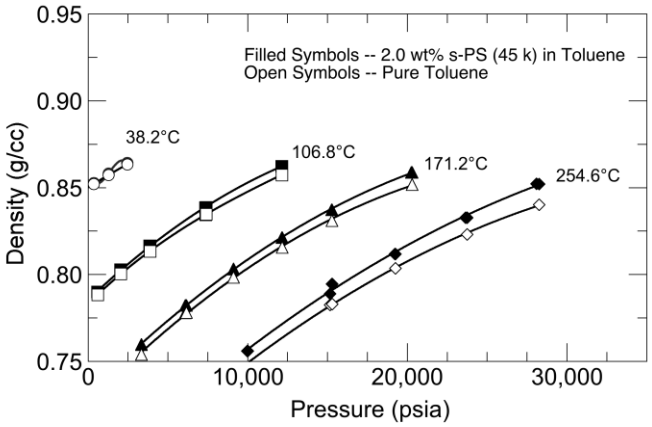

Figure 29. Comparison of density for 2.0 wt% s-PS(45)-toluene solution to pure toluene at 38, 107, 171, and 255°C.

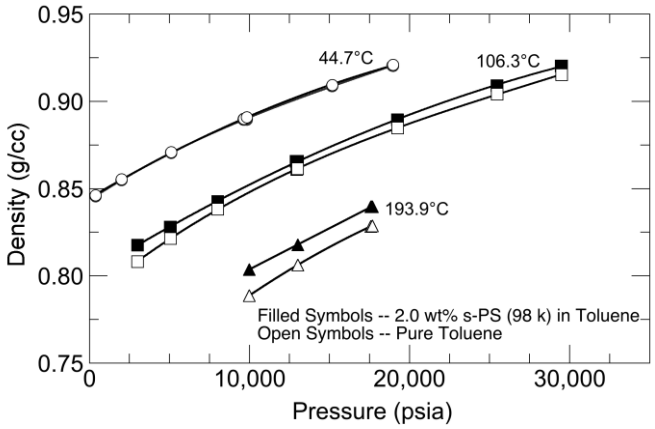

Figure 30. Comparison of density for 2.0 wt% s-PS(100)-toluene solution to pure toluene at 45, 106, 194 °C.

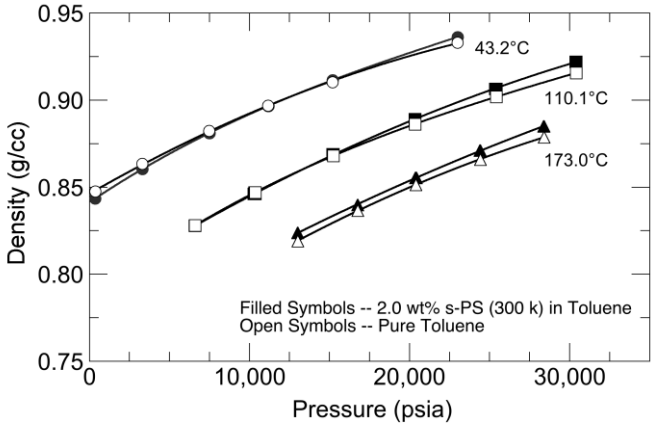

Figure 31. Comparison of density for 2.0 wt% s-PS(300)-toluene solution to pure toluene at 43, 110, and 173°C.

Two percent by weight additive or polymer treat rate (in base oil or solvent) is generally considered by the lubricant industry as the lower end of what is required to elicit a HTHP response significant enough to differentiate performance from pure solvent alone. The next set of plots compares each 2 wt% s-PS polymer solution (in toluene) with pure toluene to evaluate the impact

of HTHP on viscosity of each respective temperature. **Figures 32, 33, 34,** and **35** provide the aforementioned comparison for s-PS(45k) at 38, 107, 171, and 255°C, respectively. **Figures 36, 37,** and **38** shows a comparison for 2 wt% s-PS polymer solution (in toluene) with pure toluene at for a higher total molecular weight s-PS(100k) at 45, 106, and 194°C. Similar plots are provided for s-PS(300k) at 38, 107, 171, and 255°C, respectively, in **Figures 39, 40, 41,** and **42**.

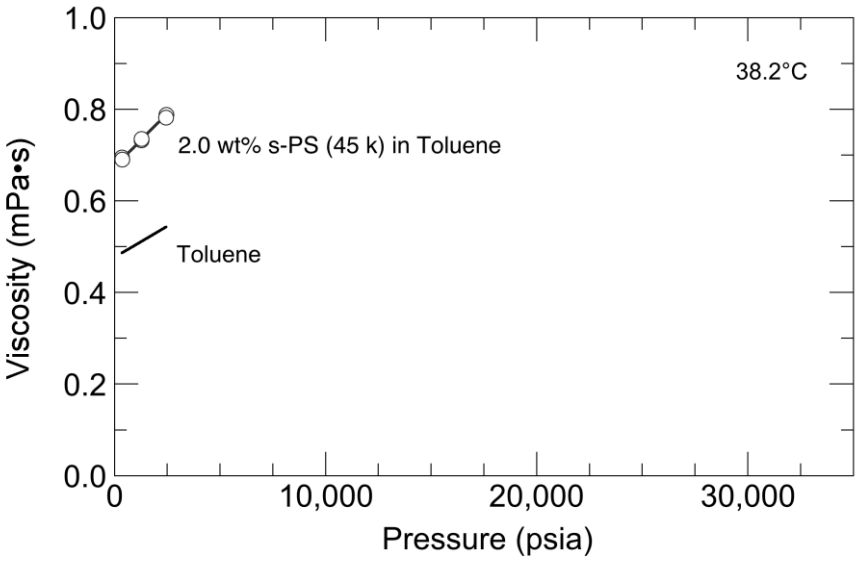

Figure 32. Comparison of 2.0 wt% s-PS(45k)-toluene solution viscosity to pure toluene viscosity at 38°C.

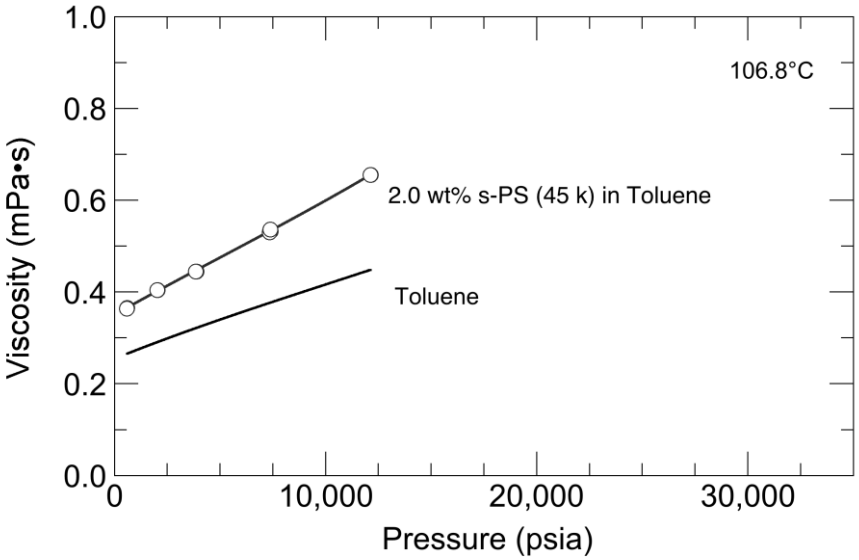

Figure 33. Comparison of 2.0 wt% s-PS(45k)-toluene solution viscosity to pure toluene viscosity at 107°C.

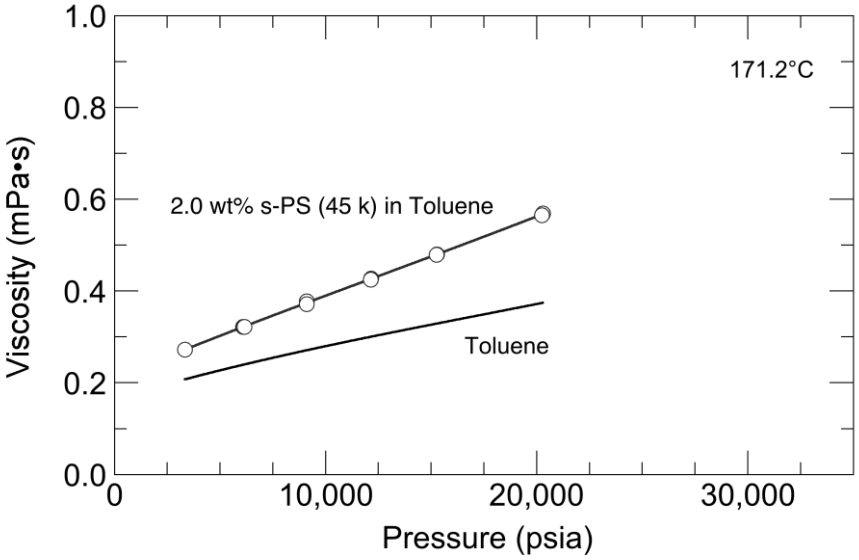

Figure 34. Comparison of 2.0 wt% s-PS(45k)-toluene solution viscosity to pure toluene viscosity at 171°C.

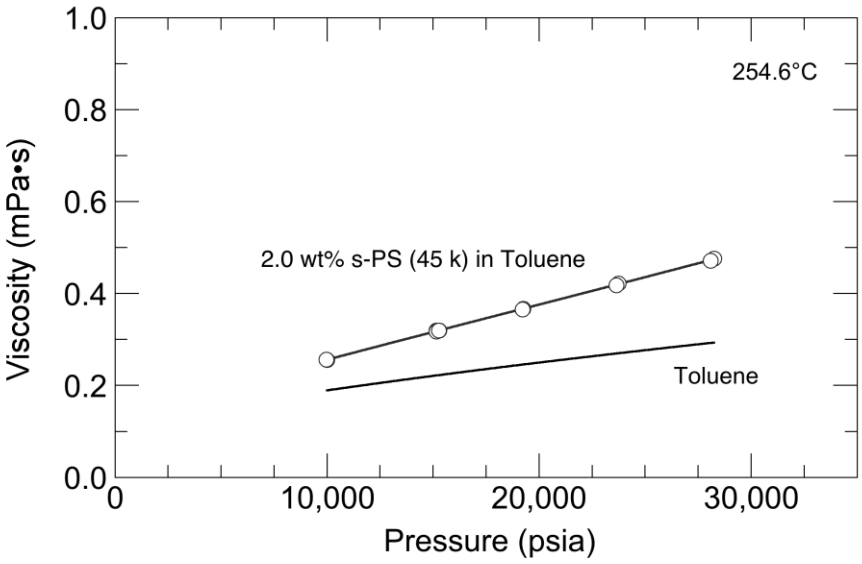

Figure 35. Comparison of 2.0 wt% s-PS(45k)-toluene solution viscosity to pure toluene viscosity at 255°C.

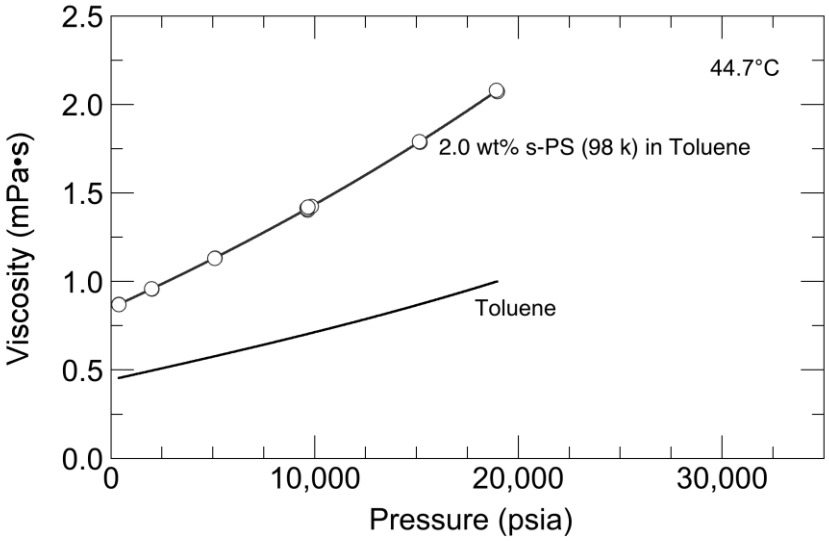

Figure 36. Comparison of 2.0 wt% s-PS(100k)-toluene solution viscosity to pure toluene viscosity at 45°C.

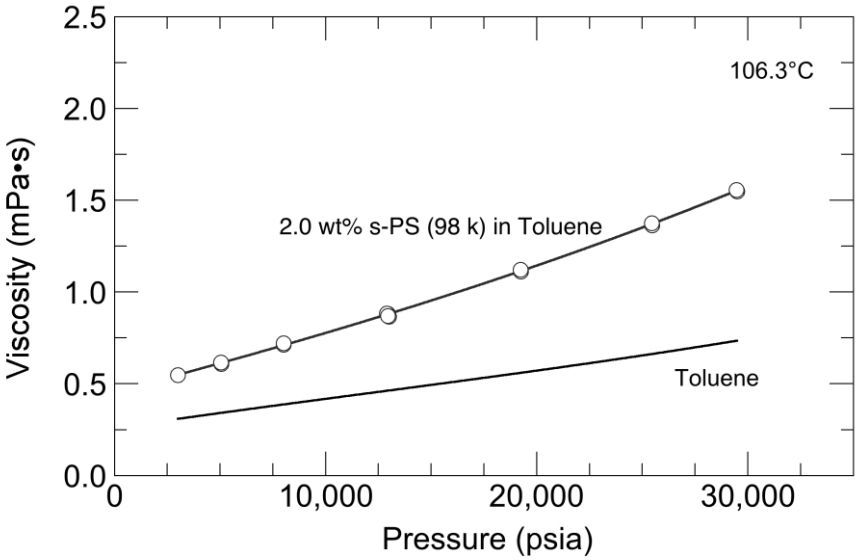

Figure 37. Comparison of 2.0 wt% s-PS(100k)-toluene solution viscosity to pure toluene viscosity at 106°C.

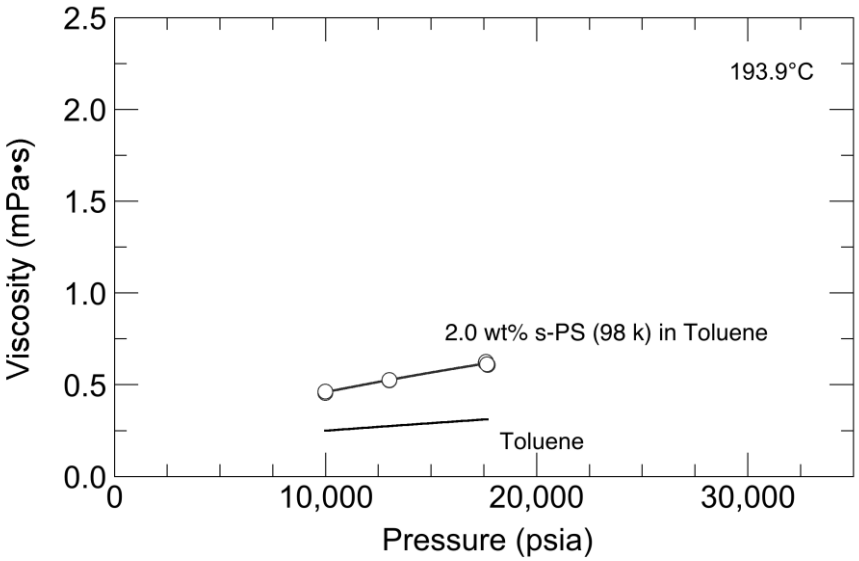

Figure 38. Comparison of 2.0 wt% s-PS(100k)-toluene solution viscosity to pure toluene viscosity at 194°C.

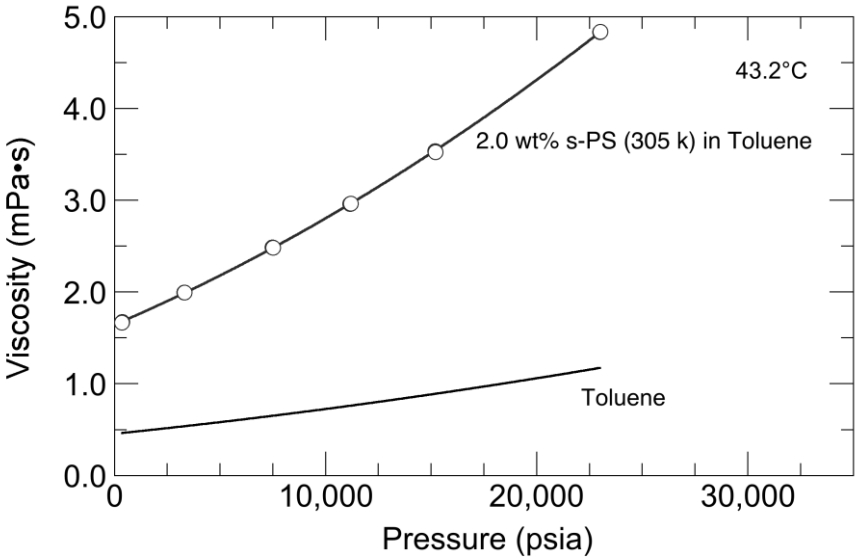

Figure 39. Comparison of 2.0 wt% s-PS(300k)-toluene solution viscosity to pure toluene viscosity at 43°C.

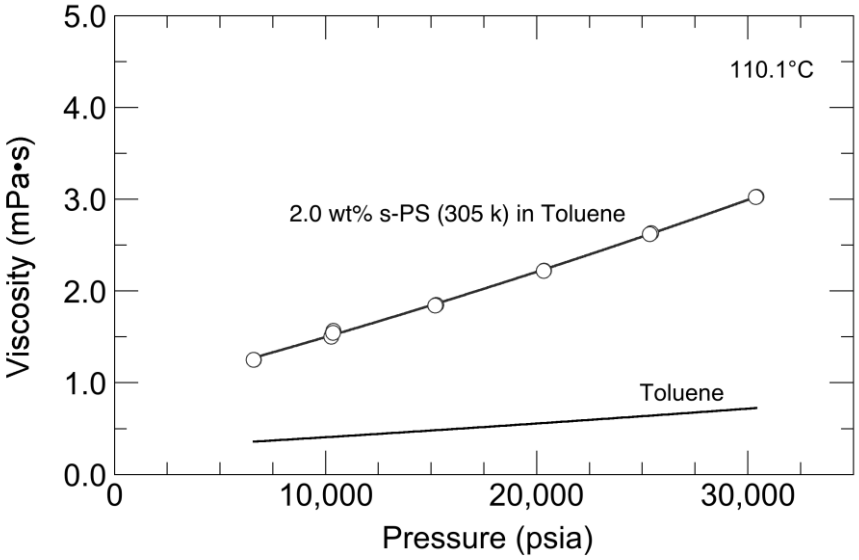

Figure 40. Comparison of 2.0 wt% s-PS(300k)-toluene solution viscosity to pure toluene viscosity at 110°C.

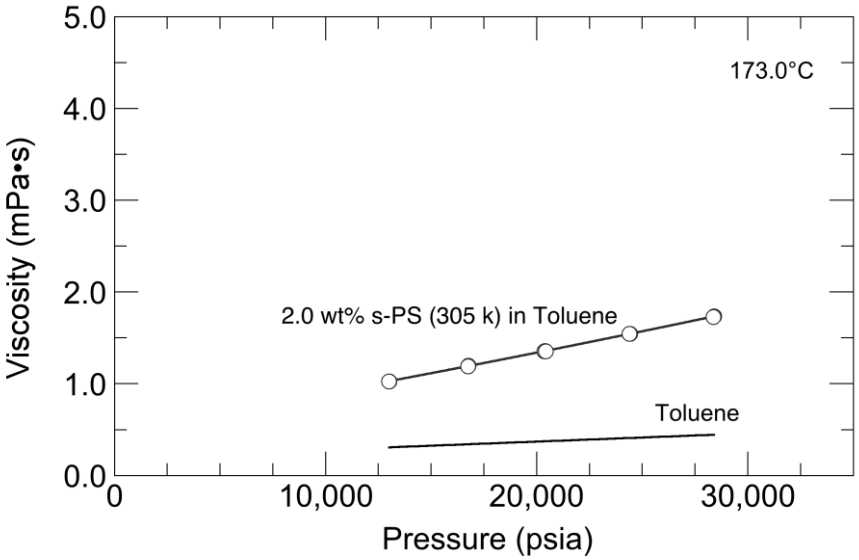

Figure 41. Comparison of 2.0 wt% s-PS(300k)-toluene solution viscosity to pure toluene viscosity at 173°C.

Figures 42, **43**, and **44** highlights the significant impact of s-PS molecular weight on solution viscosity at HTHP conditions for the 2.0 wt% solutions of each of the three s-PS polymers at approximately 40, 110, and 180°C, respectively. Detailed tables associated with all RBVD tests run to generate all s-PS data in this section are found in **Appendix G**.

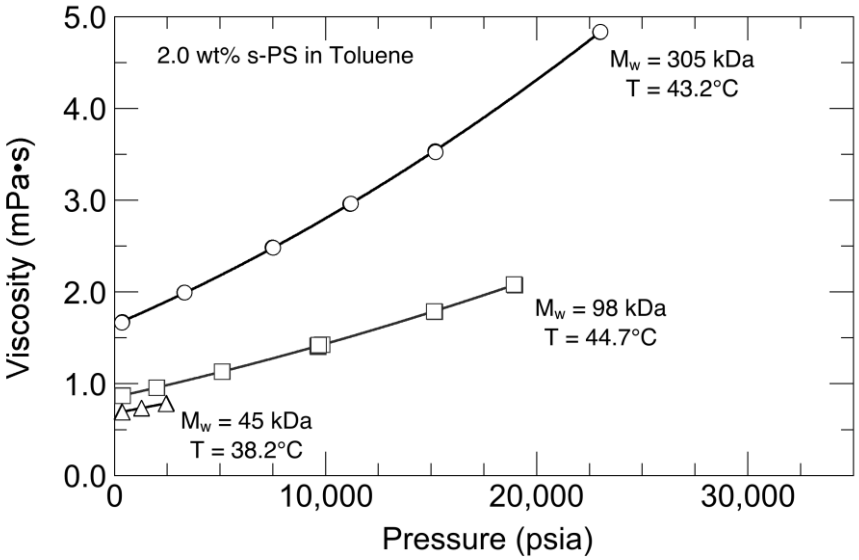

Figure 42. Effect of s-PS molecular weight/arm molecular weight on viscosity at ~40°C.

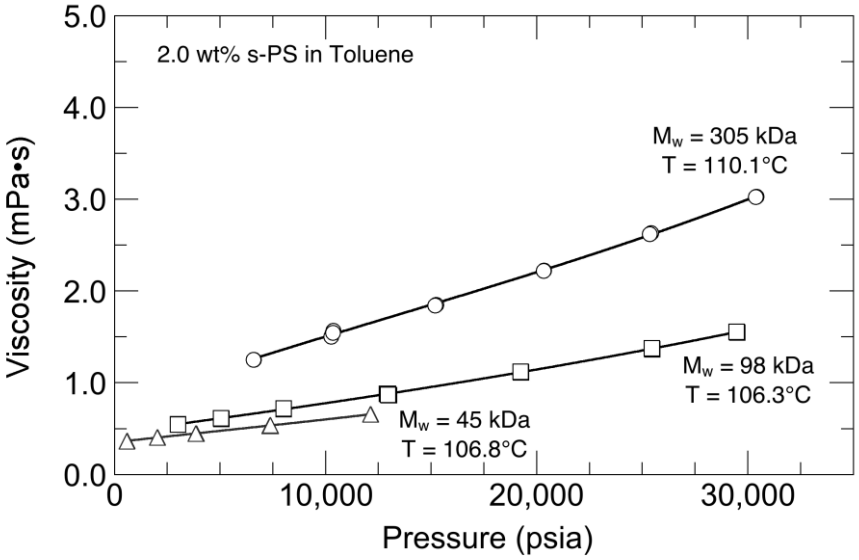

Figure 43. Effect of s-PS molecular weight/arm molecular weight on viscosity at ~110°C.

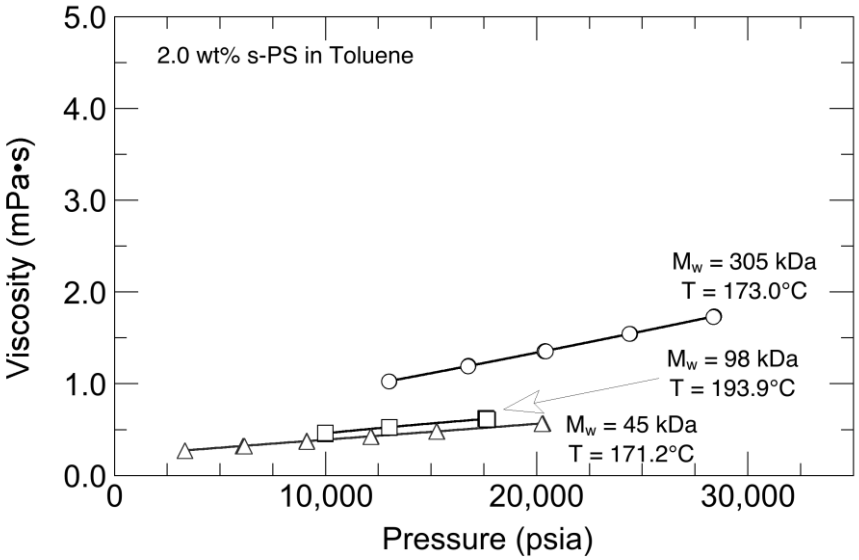

Figure 44. Effect of s-PS molecular weight/arm molecular weight on viscosity at ~180°C.

The ability to observe the impact of arm molecular weights ranging from approximately 15, 36, or 108 kDa for each of these three-arm s-PS polymers at HTHP conditions enables significant efficiency advances in evaluation and screening of polymer technology for industrial lubricant applications to be implemented. For the s-PS polymers evaluated, it is evident that viscosity increases significantly at HTHP with increasing arm Mw. This effect on viscosity is likely due to the expected increase in hydrodynamic radius of the s-PS polymer as arm Mw increases.

Chapter 6. Conclusions and Future Directions for HTHP RBVD Research

6.1 Conclusions

Modern automotive applications such as transmission clutch plates, combustion chambers, diesel fuel injector tips, and axle gears and friction plates operate at temperatures that can exceed 250°C and pressures of 40,000 psig. Industrial practice is to add homopolymers and copolymers to base oils to modify bulk fluid viscosity and frictional properties for these demanding applications. However, designing polymeric additives for lubricants and predicting their performance is limited by the lack of available high-temperature, high-pressure (HTHP) viscosity and density data needed to test contemporary lubricity models. In this thesis, a major objective covered in detail is the design, development, and commissioning of a rolling ball viscometer/densitometer (RBVD) capable of simultaneously determining fluid densities and viscosities at temperatures in excess of 250°C and pressures of 40,000 psig. Three significant and novel features of this RBVD apparatus that distinguish and differentiate it from other apparatus of this type are: (1) specially designed metal-to-metal and sapphire-to-metal seated surfaces capable of eliminating temperature- and chemically-sensitive elastomeric seals; (2) use of a bellows piston to eliminate significant temperature and operational constraints; and (3) incorporation of a linear variable differential transducer (LVDT) to simultaneously permit determination of solution density and viscosity.

Data are presented show that the RBVD is capable of measuring viscosities with an accuracy of ± 2 to 3 percent and densities to ± 0.7 percent, including at the extreme operating conditions targeted. The information generated with both the PS and LMA-MMA star polymers can be used to test contemporary viscosity models. This research also provides direction toward future development of novel polymer additives capable of optimally extending the performance of lubricants to extreme temperature and pressure regimes. In addition, the RBVD designed, developed, and commissioned as a key component of this thesis work has put into place a robust tool capable of simultaneously producing density and viscosity data in an efficient manner. Commissioning data generated as part of this work clearly served to benchmark this RBVD against available literature data, and showed that all of the data produced was well within the range of acceptability compared to others in the field. In addition, indirect empirical results from lubricant research using automotive hardware with star polymers additives was greatly clarified with direct RVBD testing using star polymers in this thesis work.

Also of significant importance is that in addition to operation at HTHP conditions, the RVBD can, for the first time, evaluate polymer-solvent mixtures at these extreme conditions representative of industrial applications. Recall that historically, in the lubricant and other industries, polymer mixture and lubricant evaluations were conducted using a large number of expensive hardware tests in a statistically designed matrix study whereby the results can only be evaluated based on indirect performance.

A second objective of this thesis is the measurement of HTHP viscosities of star polymer-solvent mixtures to determine the impact of star polymer architecture on solution viscosity at extreme conditions similar to those that might be experienced in automotive applications. Data

are presented for an industrially-relevant star polymer in n-octane to assess the impact of the star configuration on solvent viscosity at extreme conditions. The star polymer used in this instance consists of an ethylene glycol dimethacrylate core with poly(lauryl methacrylate-*co*-methyl methacrylate) (LMA-MMA) arms. The star polymer has a total weight averaged molecular weight (Mw) and Mw of each arm of 575,000, and 45,000, respectively. The copolymer arms of the star polymer have an LMA-to-MMA mole ratio of 0.6.

The results of further viscosity studies are presented for a model system of well-characterized commercially available narrow polydispersity index (PDI) star polystyrenes (PS) in toluene. Each PS is evaluated at a 2 percent by weight concentration in toluene to evaluate the effect of arm molecular weigh on viscosity. Each three-arm star polymer has arm and total molecular weights ([arm Mw] total star Mw) of ([15,400] 41,200), ([36,000] 97,600), and ([108,000] 305,000). In this instance, the viscosity of star polymer-toluene mixture increased by more than a factor of three for the star with the highest Mw arms.

6.2 Future Directions for HTHP Research

Given the ability of the RBVD to measure polymer mixture viscosity and density simultaneously as well as save tremendous resource on traditional research techniques, there is significant opportunity to use the system. Initially, a study of a star polymer matrix consisting of EGDMA core with varied MMA to LMA ratios and arm molecular weights is of significant interest given the promising findings from the single polymer evaluated in this thesis.

A second significant undertaking for the RBVD that is currently in process in the re-design of the small side window holders. These small window holders contain the only remaining elastomeric o-rings that can deteriorate over time. Although these o-rings have proven to be much

less problematic than the others on the system that were eliminated during the 2nd-generation design modifications, eliminating them would completely remove all elastomers and associated potential leaks from the entire system. As a result, long-term or extended high temperature operation would not be limited by any o-rings in the system. A schematic of the mechanical drawing for the new small window holder design is presented in **Figure 45**. A photograph of the complete new small window holder is provided as **Figure 46**.

Given the work presented in this thesis, the associated novel capabilities of the RBVD, and the tremendous amount of high value work to be undertaken, the future work associated with simultaneous HTHP viscosity and density measurements is bright. The oil, lubricant, and polymer industries will find significant benefit and time-savings versus traditional empirical methods of testing.

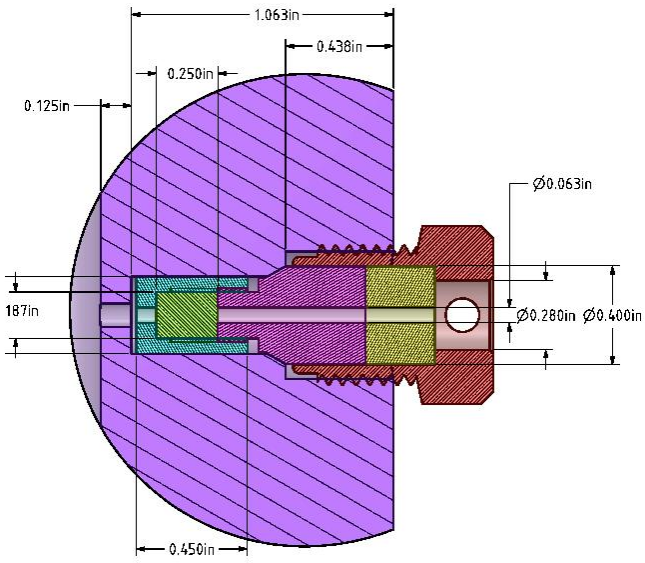

Figure 45. Schematic diagram of new RBVD small window holders currently being implemented.

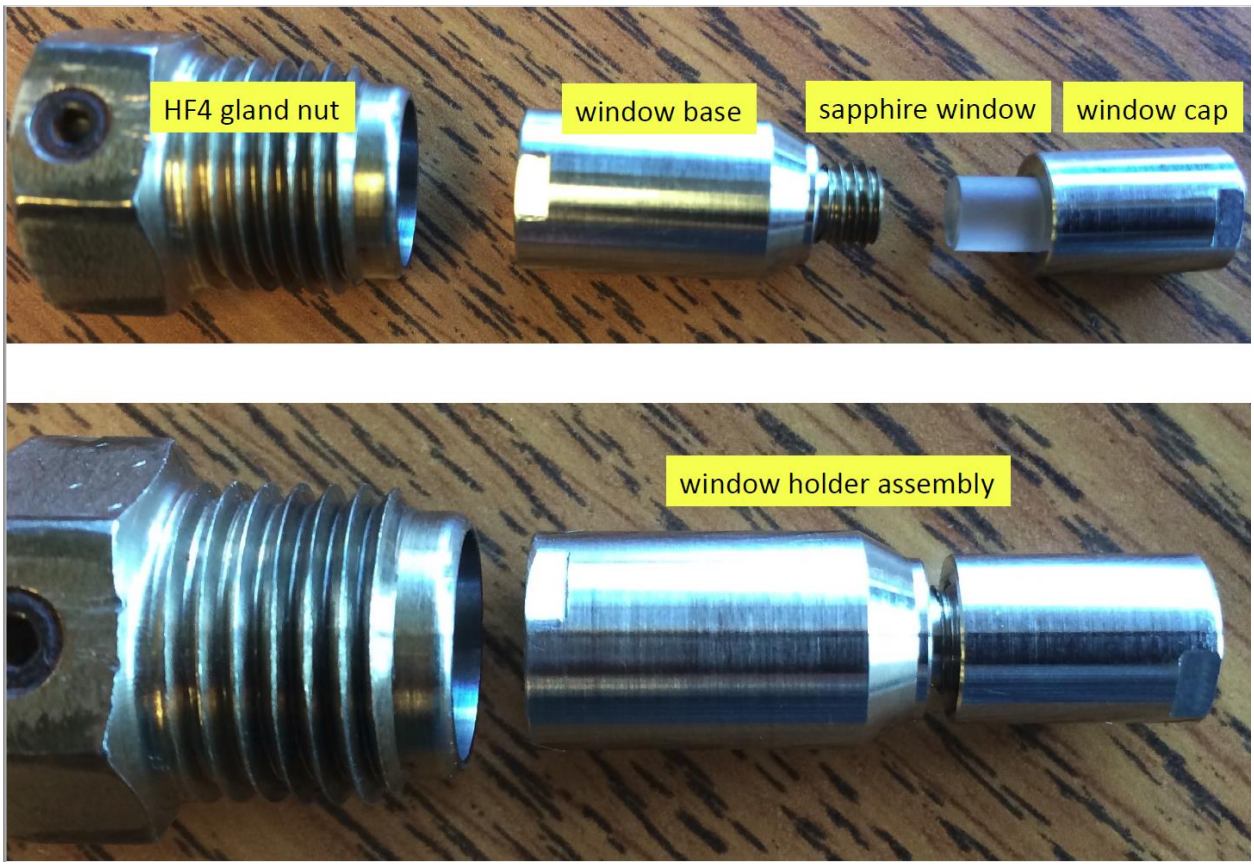

Figure 46. Newly designed and fabricated small window holder that eliminates all elastomeric o-rings.

List of References

List of References

[1] Newkirk, M., Executive Panel Chairman/Moderator, "Balancing Regulations and Customer Expectations in Future Powertrain, Fuel, and Lubricant Vehicle Systems," Society of Automotive Engineers Powertrain, Fuels, and Lubricants Meeting, Baltimore, Maryland, October 25, 2016.

[2] Beene, R. (2016) Industry blindsided as CAFE fines jump. Automotive News.

[3] Guinther, G. (2016). Efficiency Losses Due to Friction. M. Newkirk. Richmond.

[4] Cunningham, L. (2016). CAFÉ Cost Looking Forward. M. Newkirk. Richmond.

[5] Warnecke, W., Keynote Address, Society of Automotive Engineers Powertrain, Fuels, and Lubricants Meeting, Baltimore, Maryland, October 24, 2016.

[6] Mary, C., Philippon, D., Lafarge, L., Laurent, D., Rondelez, F., Bair, S., & Vergne, P. (2013). New insight into the relationship between molecular effects and the rheological behavior of polymer-thickened lubricants under high pressure. *Tribology Letters*, *52*(3), 357-369.

[7] Klaus, E., Tewksbury, E., Jolie, R., Lloyd, W., & Manning, R. (1965). Effect of Some High-Energy Sources on Polymer-Thickened Lubricants. In *The Effects of Polymer Degradation on Flow Properties of Fluids and Lubricants Containing Polymers*. ASTM International.

[8] Tang, Z., & Li, S. (2014). A review of recent developments of friction modifiers for liquid lubricants (2007–present). *Current Opinion in Solid State and Materials Science*, *18*(3), 119-139.

[9] Fox, M. F. (2010). *Chemistry and Technology of Lubricants* (Vol. 107115). R. M. Mortier, & S. T. Orszulik (Eds.). London: Springer.

[10] Robinson, J. W., Zhou, Y., Qu, J., Erck, R., & Cosimbescu, L. (2016). Effects of star-shaped poly (alkyl methacrylate) arm uniformity on lubricant properties. *Journal of Applied Polymer Science*, *133*(26).

[11] Covitch, M. J. (1998). *How polymer architecture affects permanent viscosity loss of multigrade lubricants* (No. 982638). SAE Technical Paper.

[12] Goodwin, R.D. (1989). *J Phys Chem Ref Data* 18, 1565-1636.

[13] Avgeri, S., Assael, M.J., Huber, M.L., Perkins, R.A. (2015). *J Phys Chem Ref Data* 44, 033101.

[14] Rowane, A. J., Mallepally, R., Bamgbade,B.A., Newkirk, M.S., (2016). High-Temperature, High-Pressure Viscosities and Densities of Toluene. *Journal of Chemical Thermodynamics*, pending publication.

[15] Meng, X., Qiu, G., Wu, J., & Abdulagatov, I. M. (2013). Viscosity measurements for 2, 3, 3, 3-tetrafluoroprop-1-ene (R1234yf) and trans-1, 3, 3, 3-tetrafluoropropene (R1234ze (E)). *The Journal of Chemical Thermodynamics*, *63*, 24-30.

[16] Meng, X., Zhang, J., & Wu, J. (2011). Compressed Liquid Viscosity of 1, 1, 1, 3, 3-Pentafluoropropane (R245fa) and 1, 1, 1, 3, 3, 3-Hexafluoropropane (R236fa). *Journal of Chemical & Engineering Data*, *56*(12), 4956-4964.
[17] Caetano, F. J. P., da Mata, J. C., Fareleira, J. M. N. A., Oliveira, C. M. B. P., & Wakeham, W. A. (2004). Viscosity measurements of liquid toluene at low temperatures using a dual vibrating-wire technique. *International Journal of Thermophysics*, *25*(1), 1-11.
[18] Avelino, H. M. T., Fareleira, J. M. N. A., & Wakeham, W. A. (2003). Simultaneous measurement of the density and viscosity of compressed liquid toluene. *International Journal of Thermophysics*, *24*(2), 323-336.
[19] Oliveira, C. M. B. P., & Wakeham, W. A. (1992). The viscosity of five liquid hydrocarbons at pressures up to 250 MPa. *International Journal of Thermophysics*, *13*(5), 773-790.
[20] Assael, M. J., Dalaouti, N. K., & Polimatidou, S. (1999). The Viscosity of Toluene in the Temperature Range from 210 to 370 K at Pressures up to 30 MPa. *International Journal of Thermophysics*, *20*(5), 1367-1377.
[21] Assael, M. J., Papadaki, M., & Wakeham, W. A. (1991). Measurements of the viscosity of benzene, toluene, and m-xylene at pressure up to 80 MPa. *International Journal of Thermophysics*, *12*(3), 449-457.
[22] Kandil, M. E., Marsh, K. N., & Goodwin, A. R. (2005). Vibrating Wire Viscometer with Wire Diameters of (0.05 and 0.15) mm: Results for Methylbenzene and Two Fluids with Nominal Viscosities at T= 298 K and p= 0.01 MPa of (14 and 232) mPa·s at Temperatures between (298 and 373) K and Pressures below 40 MPa. *Journal of Chemical & Engineering Data*, *50*(2), 647-655.
[23] Caudwell, D., Goodwin, A. R., & Trusler, J. M. (2004). A robust vibrating wire viscometer for reservoir fluids: results for toluene and n-decane. *Journal of Petroleum Science and Engineering*, *44*(3), 333-340.
[24] Kashiwagi, H., & Makita, T. (1982). Viscosity of twelve hydrocarbon liquids in the temperature range 298–348 K at pressures up to 110 MPa. *International Journal of Thermophysics*, *3*(4), 289-305.
[25] dos Santos, F. V., & de Castro, C. N. (1997). Viscosity of toluene and benzene under high pressur. *International Journal of Thermophysics*, *18*(2), 367-378.
[26] Harris, K. R., Malhotra, R., & Woolf, L. A. (1997). Temperature and density dependence of the viscosity of octane and toluene. *Journal of Chemical & Engineering Data*, *42*(6), 1254-1260.
[27] Harris, K. R. (2000). Temperature and density dependence of the viscosity of toluene. *Journal of Chemical & Engineering Data*, *45*(5), 893-897.
[28] Dymond, J. H., Awan, M. A., Glen, N. F., & Isdale, J. D. (1991). Transport properties of nonelectrolyte liquid mixtures. VIII. Viscosity coefficients for toluene and for three mixtures of toluene+ hexane from 25 to 100 C at pressures up to 500 MPa. *International journal of thermophysics*, *12*(2), 275-287.
[29] Dymond, J. H., Glen, N. F., Isdale, J. D., & Pyda, M. (1995). The viscosity of liquid toluene at elevated pressures. *International Journal of Thermophysics*, *16*(4), 877-882.
[30] Et-Tahir, A., Boned, C., Lagourette, B., & Xans, P. (1995). Determination of the viscosity of various hydrocarbons and mixtures of hydrocarbons versus temperature and pressure. *International Journal of Thermophysics*, *16*(6), 1309-1334.

[31] Pensado, A. S., Comunas, M. J. P., Lugo, L., & Fernández, J. (2006). High-pressure characterization of dynamic viscosity and derived properties for squalane and two pentaerythritol ester lubricants: pentaerythritol tetra-2-ethylhexanoate and pentaerythritol tetranonanoate. *Industrial & Engineering Chemistry Research*, *45*(7), 2394-2404.
[32] Wilbur, D. J., & Jonas, J. (1973). Fourier transform NMR in liquids at high pressure. II. 19F chemical shift in benzotrifluorides. *Journal of Magnetic Resonance (1969)*, *10*(3), 279-289.
[33] Hubbard, R. M., Brown, G. G. (1943). Viscosity of n-Pentane. *Industrial & Engineering Chemistry*, *35*(12), 1276-1280.
[34] Šesták, J., & Ambros, F. (1973). On the use of the rolling-ball viscometer for the measurement of rheological parameters of power law fluids. *Rheologica acta*, *12*(1), 70-76.
[35] Flowers, A.E. (1914). Viscosity measurement and a new viscometer. *Proceedings of the American. Society of Testing Materials*, 14II (1914) 565-616.
[36] Hersey, M.D. (1916). The theory of the torsion and rolling-ball viscometers, and their use in measuring the effect of pressure on viscosity. *Journal of Washington Academy of Science*, 6, 525-530.
[37] Sage, B.H. (1933). Measurement of viscosities of liquids saturated with gases at high pressures. *Industrial and Engineering Chemistry and Analysis Education*, 5, 261-263.
[38] Hoeppler, F. (1933). The eccentric fall of spheres through liquids or gases in cylinders, *Z. Techique Physik*, 14, 165-169.
[39] Harrison, D. E., Gosser, R. B. (1965). Rolling ball viscometer for use at temperatures to 400° C under pressures to 5 kilobar. *Review of Scientific Instruments*, *36*(12), 1840-1843.
[40] Zambrano, J. R., M. Sobrino, et al. (2016). "Contributing to accurate high pressure viscosity measurements: Vibrating wire viscometer and falling body viscometer techniques." *The Journal of Chemical Thermodynamics*, 96: 104-116.
[41] Daridon, J. L., Cassiède, M., Paillol, J. H., & Pauly, J. (2011). Viscosity measurements of liquids under pressure by using the quartz crystal resonators. *Review of Scientific Instruments*, *82*(9), 095114.
[42] Baylaucq, A., Watson, G., Zéberg-Mikkelsen, C., Bazile, J. P., & Boned, C. (2009). Dynamic Viscosity of the Binary System 1-Propanol+ Toluene as a Function of Temperature and Pressure†. *Journal of Chemical & Engineering Data*, *54*(9), 2715-2721.
[43] Pensado, A. S., Comuñas, M. J., Lugo, L., & Fernández, J. (2005). Experimental dynamic viscosities of 2, 3-dimethylpentane up to 60 MPa and from (303.15 to 353.15) K using a rolling-ball viscometer. *Journal of Chemical & Engineering Data*, *50*(3), 849-855.
[44] Kandil, M. E., Marsh, K. N., & Goodwin, A. R. (2005). Vibrating Wire Viscometer with Wire Diameters of (0.05 and 0.15) mm: Results for Methylbenzene and Two Fluids with Nominal Viscosities at T= 298 K and p= 0.01 MPa of (14 and 232) mPa·s at Temperatures between (298 and 373) K and Pressures below 40 MPa. *Journal of Chemical & Engineering Data*, *50*(2), 647-655.
[45] Abdulagatov, I. M., & Rasulov, S. M. (1996). Viscosity of N-Pentane, N-Heptane and Their Mixtures within the Temperature Range from 298 K up to Critical Points at the Saturation Vapor Pressure. *Berichte der Bunsengesellschaft für Physikalische Chemie*, *100*(2), 148-154.
[46] Krall, A. H., Sengers, J. V., Kestin, J. (1992). Viscosity of liquid toluene at temperatures from 25 to 150. degree. C and at pressures up to 30 MPa. *Journal of Chemical and Engineering Data*, *37*(3), 349-355.

[47] Kashiwagi, H., & Makita, T. (1982). Viscosity of twelve hydrocarbon liquids in the temperature range 298–348 K at pressures up to 110 MPa. *International Journal of Thermophysics*, *3*(4), 289-305.
[48] Akhundov, T. S., S. M. Ismail-Zade, et al. (1970). Experimental Investigation of the Viscosity of Toluene at High Pressure and Temperature. *Izv. Vyssh. Uchebn. Zaved., Neft Gaz*, **79,** 80-82.
[49] Meilchen, M. A., Hasch, B. M., McHugh, M. A. (1991). Effect of copolymer composition on the phase behavior of mixtures of poly (ethylene-co-methyl acrylate) with propane and chlorodifluoromethane. *Macromolecules*, *24*(17), 4874-4882.
[50] D. Roylance, Pressure Vessels. 2001. Pages 1-10.
[51] Special Metals Corporation: Inconel Alloy 718, www.specialmetals.com.
[52] Mallepally, R. R., Gadepalli, V. S., Bamgbade, B. A., Cain, N., McHugh, M. A. (2016). Phase Behavior and Densities of Propylene and Hexane Binary Mixtures to 585K and 70 MPa. *Journal of Chemical & Engineering Data*, *61*(8), 2818-2827.
[53] Naake, L.-D. (2002). The Viscosity of n-Decane to High Temperatures of 573K and High Pressures of 300 Mpa. *Zeitschrift für Physikalische Chemie International Journal of Research in Physical Chemistry and Chemical Physics*. 216, 1295-1322.
[54] Lemmon, E.W., McLinden, M.O., Friend, D.G. Retrieved 2015) Thermophysical properties of fluid systems.in: P.J. Lindstrom, W.G. Mallard, (Eds.), NIST Chemistry Webbook, NIST Standard Reference Database Number 69, Gathersburg MD, 20899.
[55] Caudwell, J.P.M. Trusler, V. Vesovic, W.A. Wakeham, *Journal of Chemical Engineering Data*, 55 (2010).
5396-5396.
[56] Wilbur, D. J., & Jonas, J. (1973). Fourier transform NMR in liquids at high pressure. II. 19F chemical shift in benzotrifluorides. *Journal of Magnetic Resonance (1969)*, *10*(3), 279-289.
[57] Gao, C., & Yan, D. (2004). Hyperbranched polymers: from synthesis to applications. *Progress in Polymer Science*, *29*(3), 183-275.
[58] Bosman, A. W., Vestberg, R., Heumann, A., Fréchet, J. M., & Hawker, C. J. (2003). A modular approach toward functionalized three-dimensional macromolecules: From synthetic concepts to practical applications. *Journal of the American Chemical Society*, *125*(3), 715-728.
[59] Ho, A. K., Iin, I., Gurr, P. A., Mills, M. F., & Qiao, G. G. (2005). Synthesis and characterization of star-like microgels by one-pot free radical polymerization. *Polymer*, *46*(18), 6727-6735.
[60] Sk, U. H., & Kojima, C. (2015). Dendrimers for theranostic applications. *Biomolecular Concepts*, *6*(3), 205-217.
[61] Cameron, D. J., & Shaver, M. P. (2011). Aliphatic polyester polymer stars: synthesis, properties and applications in biomedicine and nanotechnology. *Chemical Society Reviews*, *40*(3), 1761-1776.

APPENDICIES

APPENDIX A. Detailed Mechanical Drawings and Specifications for the RBVD

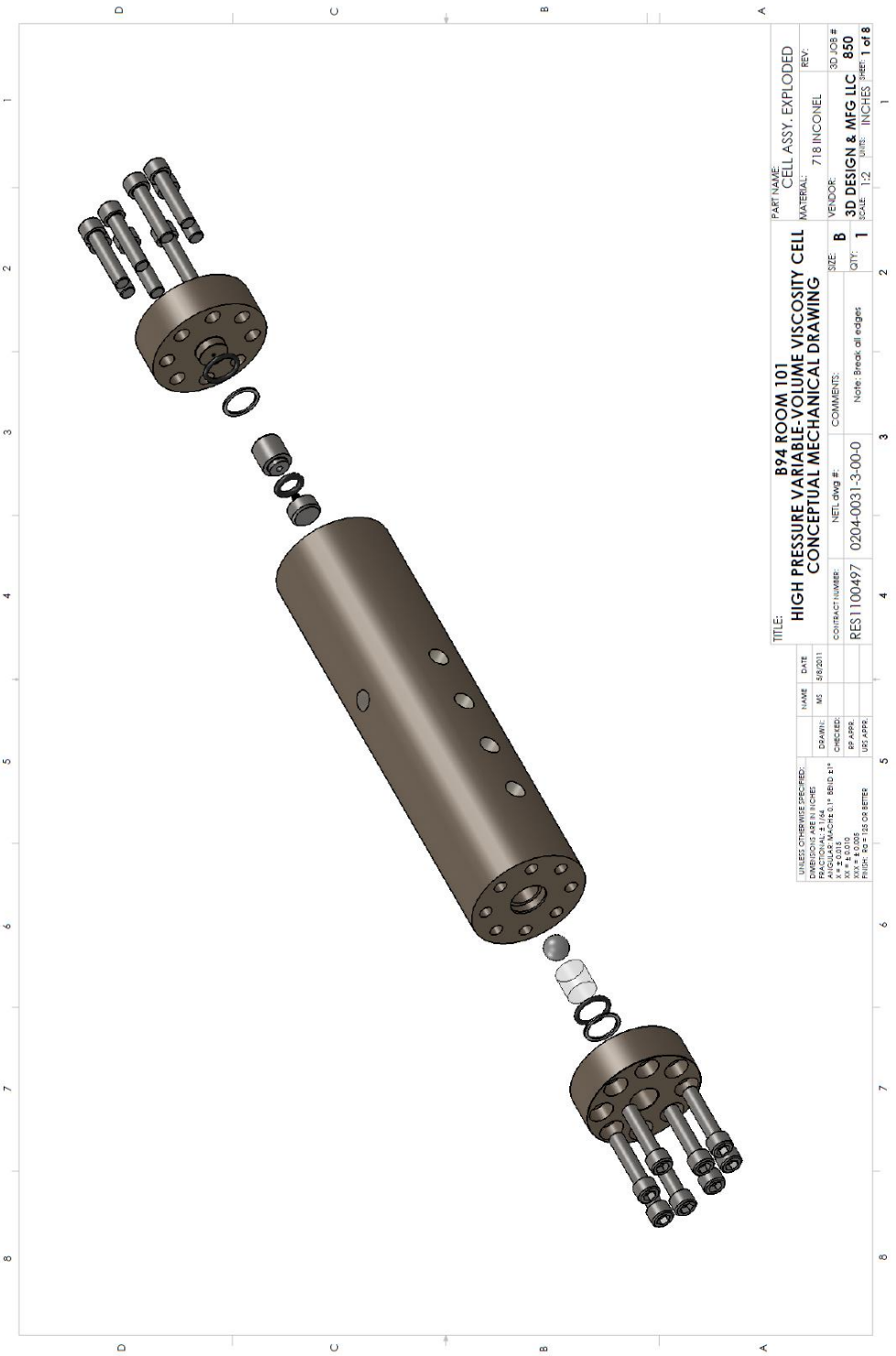

ITEM NO.	SHEET NO.	PART DESCRIPTION	QTY.
1	3	Cell Body	1
2	4	End Cap-Input	1
3		-116 Oring	2
4		-116 Backup Ring	2
5		Sapphire Window	1
6	5	End Cap- ViewPort	1
7		Test Ball	1
8		SHCS 3/8-24x1-5/8	16
9	6	Piston- Part 1	1
10	7	Piston- Part 2	1
11		-206 Oring	1
12		Stir-Bar	1

SECTION A-A
SCALE 1 : 2

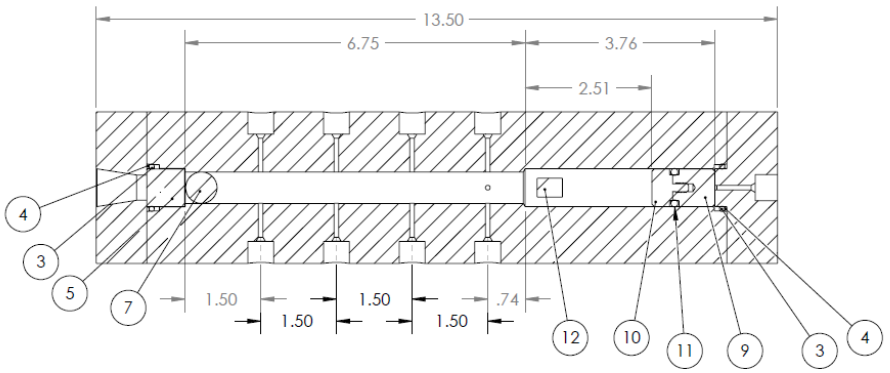

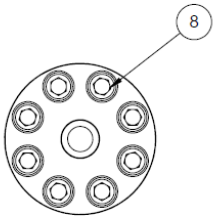

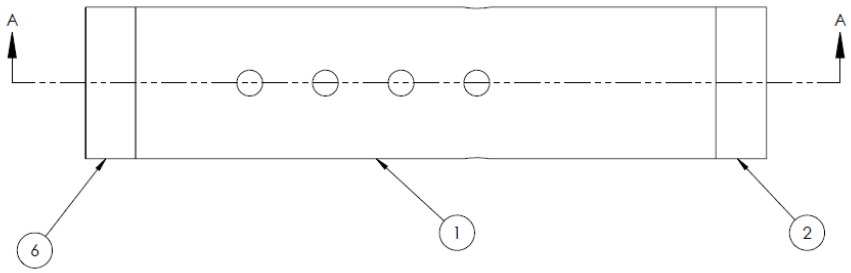

UNLESS OTHERWISE SPECIFIED:		NAME	DATE
DIMENSIONS ARE IN INCHES FRACTIONAL: ± 1/64 ANGULAR: MACH ± 0.1° BEND ±1° X = ± 0.015 XX = ± 0.010 XXX = ± 0.005 FINISH: Ra = 125 OR BETTER	DRAWN:	MS	5/8/2011
	CHECKED:		
	RP APPR.		
	URS APPR.		

TITLE:				PART NAME:	
B94 ROOM 101 HIGH PRESSURE VARIABLE-VOLUME VISCOSITY CELL CONCEPTUAL MECHANICAL DRAWING				CELL ASSEMBLY	
				MATERIAL: 718 INCONEL	REV:
CONTRACT NUMBER:	NETL dwg #:	COMMENTS:	SIZE: B	VENDOR:	3D JOB #
RES1100497	0204-0031-3-00-0	Note: Break all edges	QTY: 1	3D DESIGN & MFG LLC	850
				SCALE: 1:2 UNITS: INCHES	SHEET: 2 of 8

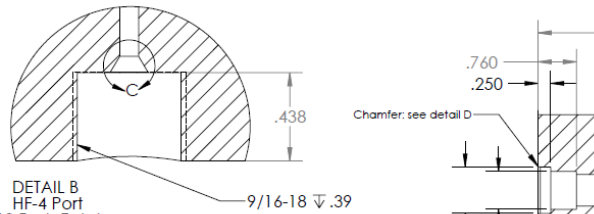

DETAIL B
HF-4 Port
10 Ports Total
SCALE 2 : 1

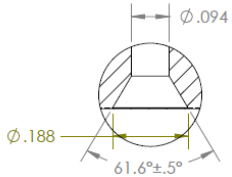

DETAIL C
SCALE 4 : 1

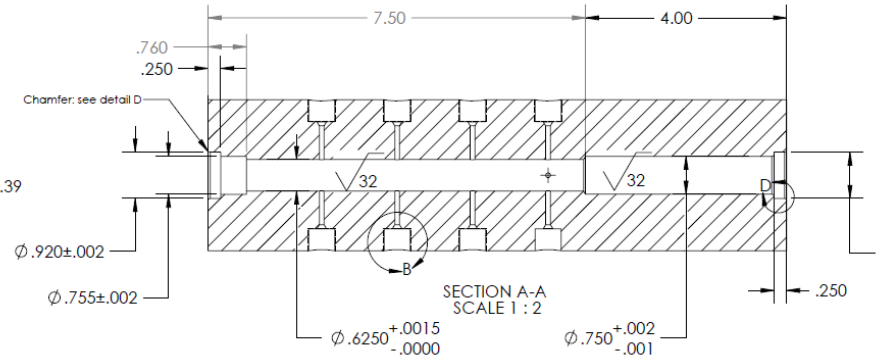

SECTION A-A
SCALE 1 : 2

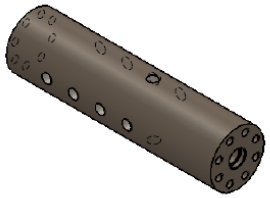

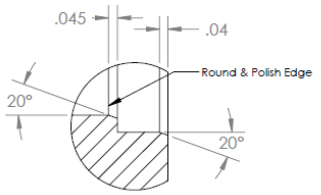

DETAIL D
SCALE 2 : 1

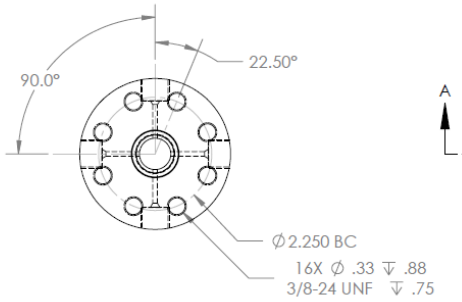

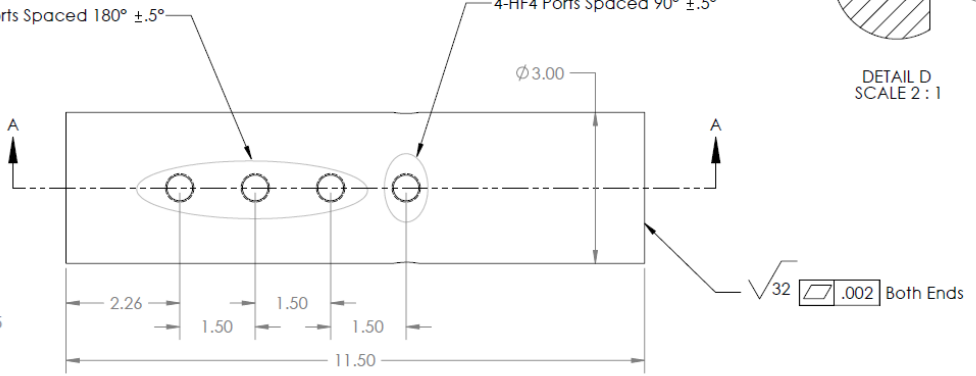

UNLESS OTHERWISE SPECIFIED: DIMENSIONS ARE IN INCHES FRACTIONAL: ± 1/64 ANGULAR: MACH± 0.1° BEND ±1° X = ± 0.015 XX = ± 0.010 XXX = ± 0.005 FINISH: Ra = 125 OR BETTER		NAME	DATE
	DRAWN:	MS	5/8/2011
	CHECKED:		
	RP APPR.		
	URS APPR.		

TITLE: B94 ROOM 101 HIGH PRESSURE VARIABLE-VOLUME VISCOSITY CELL CONCEPTUAL MECHANICAL DRAWING				PART NAME: CELL BODY
				MATERIAL: 718 INCONEL / REV:
CONTRACT NUMBER: RES1100497	NETL dwg #: 0204-0031-3-00-0	COMMENTS: Note: Break all edges	SIZE: B / QTY: 1	VENDOR: 3D DESIGN & MFG LLC / 3D JOB # 850
				SCALE: 1:2 / UNITS: INCHES / SHEET: 3 of 8

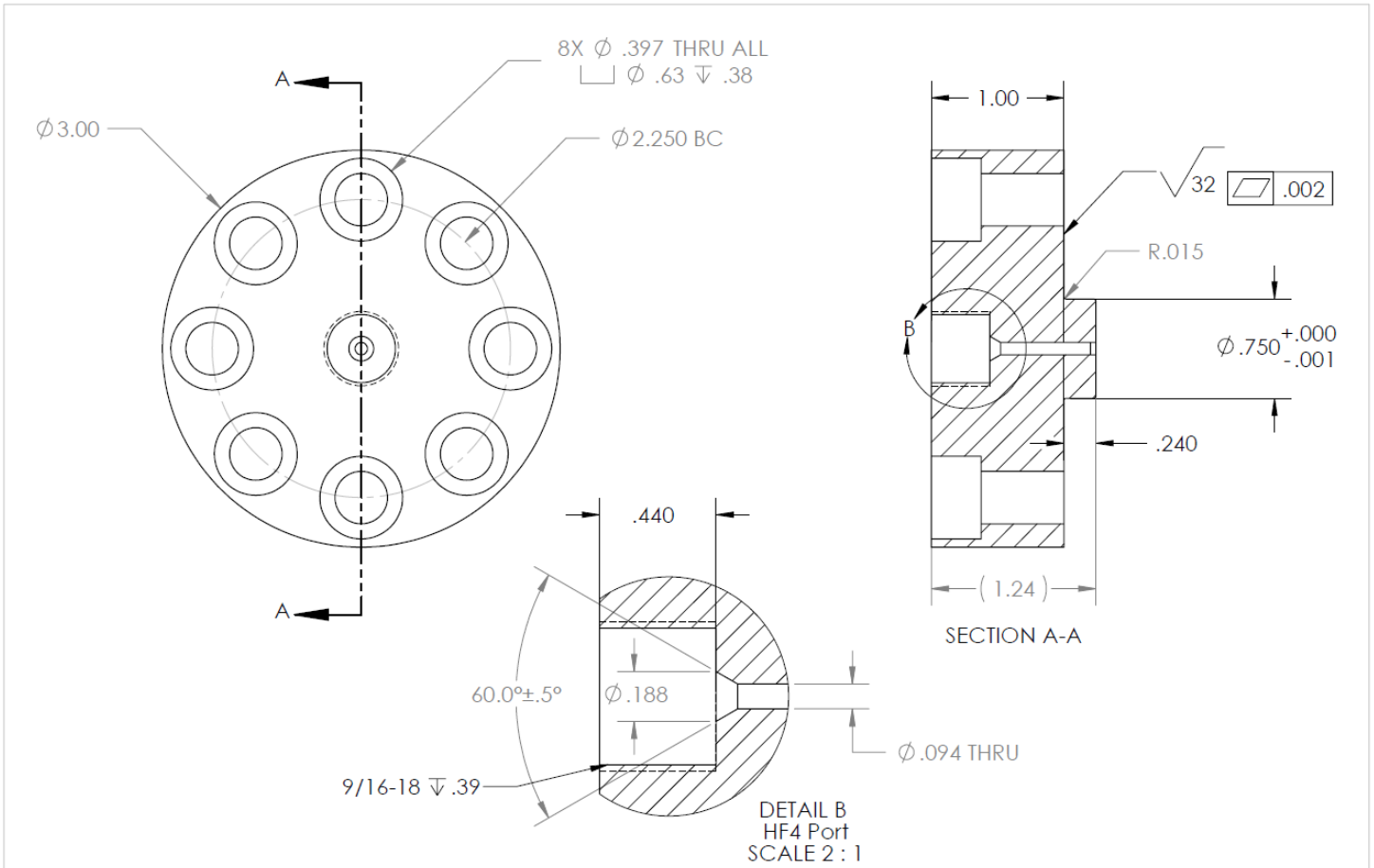
8X ⌀ .397 THRU ALL
⌴ ⌀ .63 ↧ .38
A
⌀3.00
⌀2.250 BC
A
1.00
32
.002
R.015
B
⌀.750 +.000 -.001
.240
(1.24)
SECTION A-A
.440
60.0°±.5°
⌀.188
⌀.094 THRU
9/16-18 ↧.39
DETAIL B
HF4 Port
SCALE 2 : 1
UNLESS OTHERWISE SPECIFIED:
DIMENSIONS ARE IN INCHES
FRACTIONAL: ± 1/64
ANGULAR: MACH± 0.1° BEND ±1°
X = ± 0.015
XX = ± 0.010
XXX = ± 0.005
FINISH: Ra = 125 OR BETTER
NAME
DATE
DRAWN:
MS
5/8/2011
CHECKED:
RP APPR.
URS APPR.
TITLE:
B94 ROOM 101
HIGH PRESSURE VARIABLE-VOLUME VISCOSITY CELL
CONCEPTUAL MECHANICAL DRAWING
CONTRACT NUMBER:
RES1100497
NETL dwg #:
0204-0031-3-00-0
COMMENTS:
Note: Break all edges
SIZE:
A
QTY:
1
PART NAME:
END CAP-INPUT
MATERIAL:
718 INCONEL
REV:
VENDOR:
3D DESIGN & MFG LLC
3D JOB #
850
SCALE:
Full
UNITS:
INCHES
SHEET:
4 of 8
5
4
3
2
1

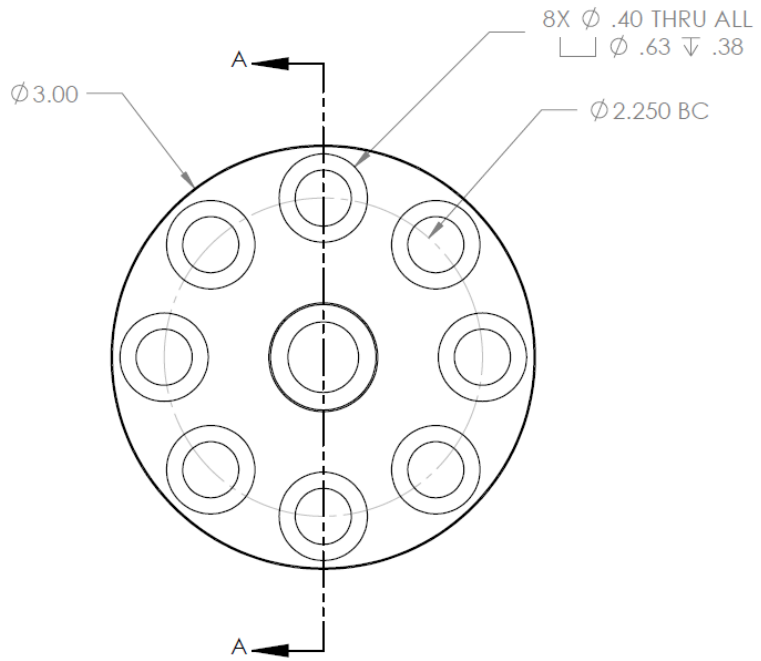

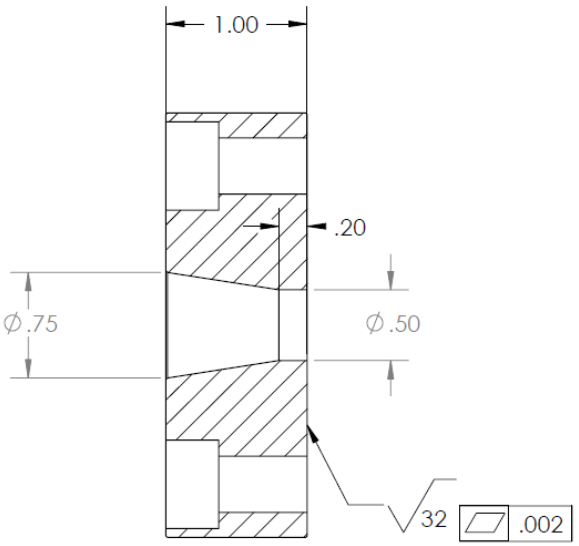

SECTION A-A

UNLESS OTHERWISE SPECIFIED:		NAME	DATE
DIMENSIONS ARE IN INCHES FRACTIONAL: ± 1/64 ANGULAR: MACH± 0.1° BEND ±1° X = ± 0.015 XX = ± 0.010 XXX = ± 0.005 FINISH: Ra = 125 OR BETTER	DRAWN:	MS	5/8/2011
	CHECKED:		
	RP APPR.		
	URS APPR.		

TITLE:
B94 ROOM 101
HIGH PRESSURE VARIABLE-VOLUME VISCOSITY CELL
CONCEPTUAL MECHANICAL DRAWING

CONTRACT NUMBER:	NETL dwg #:	COMMENTS:	SIZE:	QTY:
RES1100497	0204-0031-3-00-0	Note: Break all edges	A	1

PART NAME: END CAP-VIEWPORT
MATERIAL: 718 INCONEL
REV:
VENDOR: **3D DESIGN & MFG LLC**
3D JOB # **850**
SCALE: Full UNITS: INCHES SHEET: **5 of 8**

5 4 3 2 1

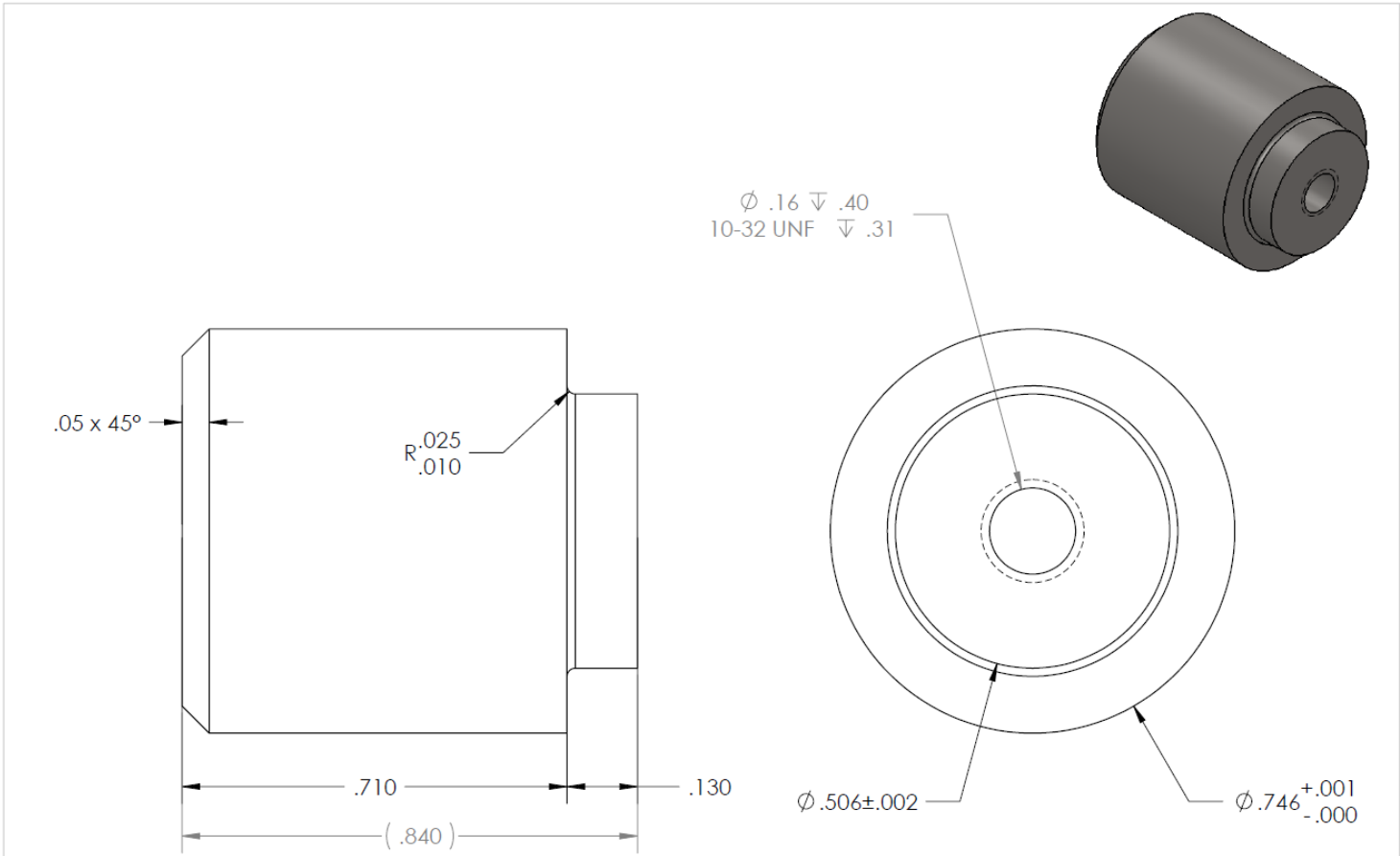

UNLESS OTHERWISE SPECIFIED:		NAME	DATE
DIMENSIONS ARE IN INCHES FRACTIONAL: ± 1/64 ANGULAR: MACH± 0.1° BEND ±1° X = ± 0.015 XX = ± 0.010 XXX = ± 0.005 FINISH: Ra = 125 OR BETTER	DRAWN:	MS	5/8/2011
	CHECKED:		
	RP APPR.		
	URS APPR.		

TITLE:
B94 ROOM 101
HIGH PRESSURE VARIABLE-VOLUME VISCOSITY CELL
CONCEPTUAL MECHANICAL DRAWING

CONTRACT NUMBER:	NETL dwg #:	COMMENTS:	SIZE:	QTY:
RES1100497	0204-0031-3-00-0	Note: Break all edges	A	1

PART NAME: PISTON-PART 1

MATERIAL: 316 STAINLESS STEEL

REV:

VENDOR: **3D DESIGN & MFG LLC**

3D JOB # **850**

SCALE: 4:1 UNITS: INCHES SHEET: **6 of 8**

5 4 3 2 1

Note: Threads shown are for reference only

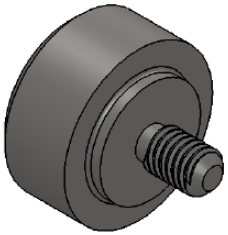

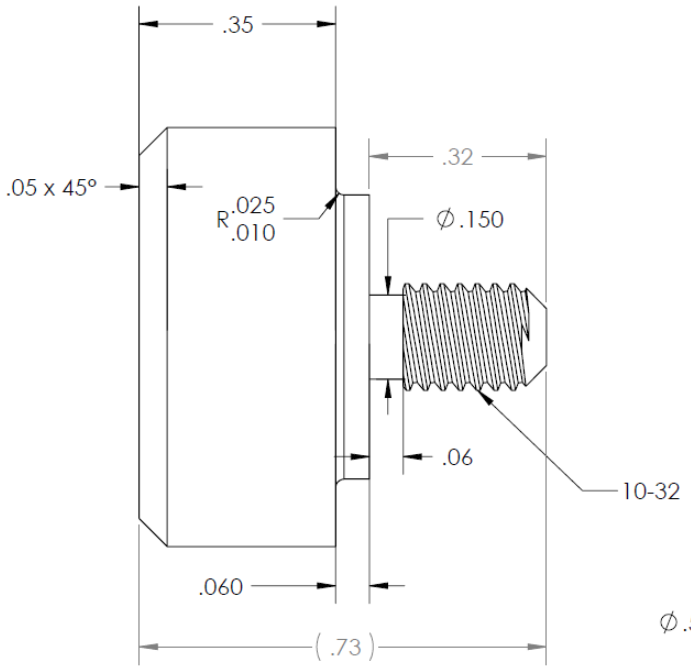

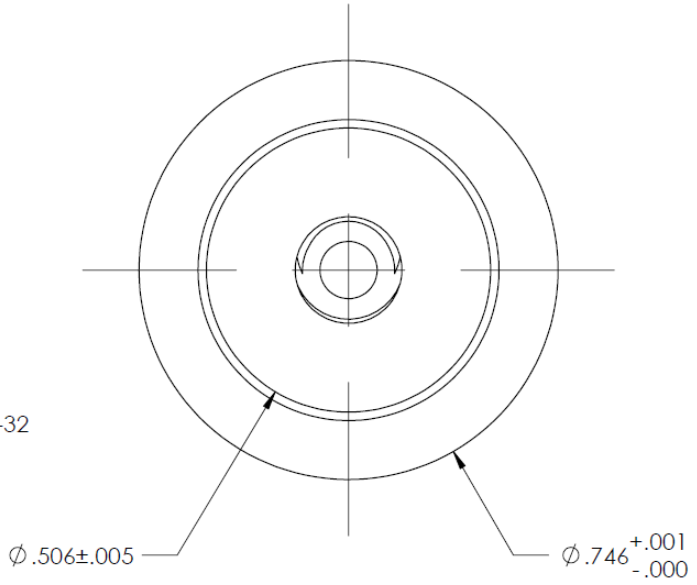

UNLESS OTHERWISE SPECIFIED: DIMENSIONS ARE IN INCHES FRACTIONAL: ± 1/64 ANGULAR: MACH± 0.1° BEND ±1° X = ± 0.015 XX = ± 0.010 XXX = ± 0.005 FINISH: Ra = 125 OR BETTER		NAME	DATE
	DRAWN:	MS	5/8/2011
	CHECKED:		
	RP APPR.		
	URS APPR.		

TITLE:
B94 ROOM 101
HIGH PRESSURE VARIABLE-VOLUME VISCOSITY CELL
CONCEPTUAL MECHANICAL DRAWING

CONTRACT NUMBER:	NETL dwg #:	COMMENTS:	SIZE:	QTY:
RES1100497	0204-0031-3-00-0	Note: Break all edges	A	1

PART NAME: PISTON-PART 2
MATERIAL: 316 STAINLESS STEEL
REV:
VENDOR: **3D DESIGN & MFG LLC**
3D JOB # **850**
SCALE: 4:1 UNITS: INCHES SHEET: **7 of 8**

5 4 3 2 1

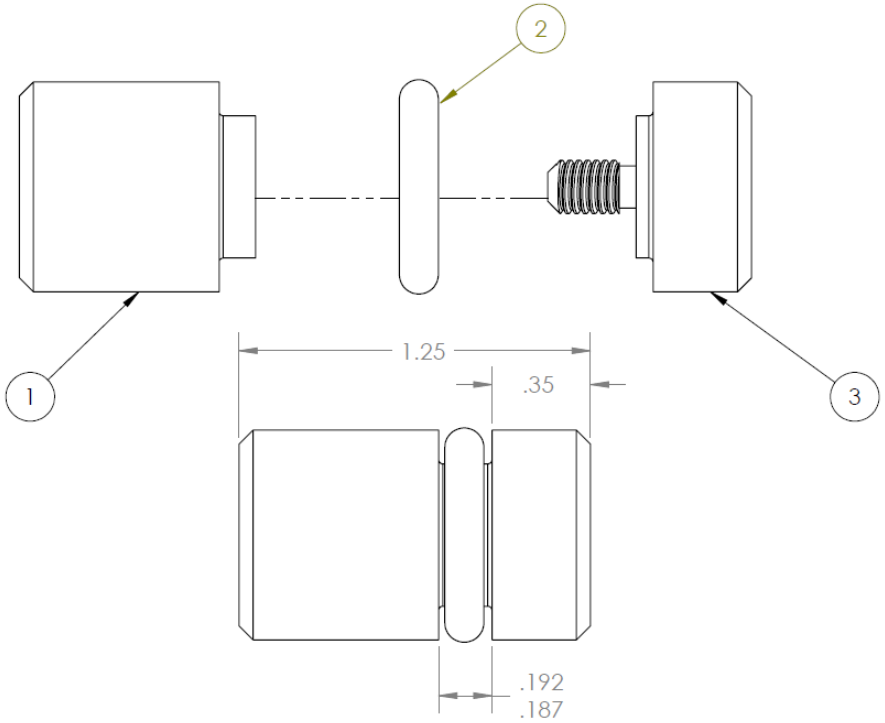

ITEM NO.	SHEET NO.	PART DESCRIPTION	QTY.
1	6	Piston-Part 1	1
2		-206 Oring	1
3	7	Piston-Part 2	1

UNLESS OTHERWISE SPECIFIED:
DIMENSIONS ARE IN INCHES
FRACTIONAL: ± 1/64
ANGULAR: MACH± 0.1° BEND ±1°
X = ± 0.015
XX = ± 0.010
XXX = ± 0.005
FINISH: Ra = 125 OR BETTER

	NAME	DATE
DRAWN:	MS	5/8/2011
CHECKED:		
RP APPR.		
URS APPR.		

TITLE:
B94 ROOM 101
HIGH PRESSURE VARIABLE-VOLUME VISCOSITY CELL
CONCEPTUAL MECHANICAL DRAWING

CONTRACT NUMBER:	NETL dwg #:	COMMENTS:	SIZE:	QTY:
RES1100497	0204-0031-3-00-0	Note: Break all edges	A	1

PART NAME: PISTON ASSEMBLY
MATERIAL: 316 STAINLESS STEEL
REV:
VENDOR: **3D DESIGN & MFG LLC**
3D JOB # **850**
SCALE: 2:1
UNITS: INCHES
SHEET: **8 of 8**

5 4 3 2 1

APPENDIX B. Rolling Ball Viscometer System Error and Sensitivity Analysis

A complete analysis consisting of all terms needed to determine system sensitivity to each controllable factor was undertaken. The first step is to start with the basic equation (A-1) for determination of the constant, *k*, for the system.

$$k = \frac{\mu v}{(\rho_b - \rho_{fl}) \sin\theta} \tag{A-1}$$

In order to transform the equation and express it in a measurable term of *t* (time), both sides of the equation (A-1) are divided by velocity to get a new viscometer machine constant, *K' = k/l*, shown by equation (A-2).

$$K' = \frac{k}{l} = \frac{\mu}{(\rho_b - \rho_{fl}) t \sin\theta} \tag{A-2}$$

From equation (2), the overall error expression for K, σ_K, is written as is shown by equation (A-3).

$$\sigma_{K'} = \sqrt{\left(\frac{\partial K'}{\partial \mu}\right)^2 \partial\sigma_\mu^2 + \left(\frac{\partial K'}{\partial \rho_b}\right)^2 \partial\sigma_{\rho_b}^2 + \left(\frac{\partial K'}{\partial \rho_{fl}}\right)^2 \partial\sigma_{\rho_{fl}}^2 + \left(\frac{\partial K'}{\partial t}\right)^2 \partial\sigma_t^2 + \left(\frac{\partial K'}{\partial \theta}\right)^2 \partial\sigma_\theta^2} \tag{A-3}$$

The magnitude of the individual partial derivatives can each be evaluated to allow a sensitivity analysis to be conducted for each experimental variable are shown below as equations A-4, -5, -6, -7, -8, and -9.

$$\frac{\partial K\prime}{\partial \rho_b} = \frac{1}{(\rho_b - \rho_{fl})(t_2 - t_1)\sin\theta} \tag{A-4}$$

$$\frac{\partial K\prime}{\partial \rho_b} = -\frac{\mu}{(t_2 - t_1)\sin\theta} * \frac{1}{(\rho_b - \rho_{fl})^2} \tag{A-5}$$

$$\frac{\partial K\prime}{\partial \rho_{fl}} = \frac{\mu}{(t_2 - t_1)\sin\theta} * \frac{1}{(\rho_b - \rho_{fl})^2} \tag{A-6}$$

$$\frac{\partial K\prime}{\partial t} = -\frac{1}{(t_2 - t_1)^2} * \frac{\mu}{(\rho_b - \rho_{fl})\sin\theta} \tag{A-7}$$

$$\frac{\partial K\prime}{\partial \theta} = -\frac{\cos\theta}{\sin^2\theta} * \frac{\mu}{(t_2 - t_1)(\rho_b - \rho_{fl})} \tag{A-8}$$

$$\frac{\partial K\prime}{\partial \sin\theta} = -\frac{1}{\sin^2\theta} * \frac{\mu}{(t_2 - t_1)(\rho_b - \rho_{fl})} \tag{A-9}$$

These equations were input to a spreadsheet to allow parametric evaluation of the variables to determine sensitivity. Some of the reference data needed for this evaluation are provided here.

$\frac{\Delta\mu}{\mu} = 0.02$

$\Delta\rho_b = 0.002\ g/cm^3$ [29]

$\frac{\Delta\rho_{fl}}{\rho_{fl}} = 0.002$ for μ<cP

$\frac{\Delta\rho_{fl}}{\rho_{fl}} = 0.008$ for μ>cP]

Δt = 0.001 s (high speed data acquisition rate for time measurement)

$\Delta\theta$ = 0.1° (error associated with inclinometer angle measurement)

$\rho_{ball} = 8.22\ g/cm^3$

Sample data are presented in Table A-1 below. Table A-2 below shows the error analysis with calculated values for the derivative terms. By varying each parameter in the spreadsheet and from an evaluation of the equations above, it can be readily seen that the error associated with the angle measurement has the most significant impact on the accumulated experimental error.

Appendix Table B-1. Sample error analysis data for density and viscosity of n-decane.

T (°C)	P (psig)	Angle (°)	Δt (s)	Density (g/cc)	Viscosity (mPa•s)	K' = k/l (cm^2/s^2)
23.0	2062	34.3	121.9	0.813	42.4	0.0835
22.8	4117	34.2	163.9	0.820	58.2	0.0853
23.0	5295	34.1	187.6	0.824	68.2	0.0877
22.8	6100	34.1	212.3	0.826	77.4	0.0879
22.9	8236	34.2	276.3	0.832	104.0	0.0903
23.0	10210	34.2	349.6	0.837	134.0	0.0926
50.4	2308	29.2	43.0	0.799	14.1	0.0908
50.3	5124	29.1	58.4	0.809	20.0	0.0951
50.4	8292	29.3	81.2	0.819	28.9	0.0983
50.4	10010	29.2	95.6	0.824	35.2	0.1020
50.4	12080	29.3	117.5	0.830	43.9	0.1030
50.4	15050	29.4	152.3	0.837	60.0	0.1080
50.5	18230	29.2	200.9	0.845	82.3	0.1130
50.5	20050	29.1	237.4	0.848	98.2	0.1150
50.5	23180	29.2	304.0	0.855	131.6	0.1200
50.5	25090	29.3	352.7	0.858	156.5	0.1230
101.5	3050	10.8	32.0	0.773	4.0	0.0905
101.4	5305	10.9	38.9	0.784	5.0	0.0917
101.5	8194	10.9	48.1	0.795	6.5	0.0962
101.4	10200	10.9	55.5	0.802	7.7	0.0993
101.4	12100	10.9	63.0	0.809	9.0	0.1030
101.4	15240	10.9	75.8	0.818	11.6	0.1090
101.4	18320	10.8	93.0	0.826	14.7	0.1140
101.4	20003	10.8	101.4	0.830	16.7	0.1190
101.3	22039	10.9	114.7	0.835	19.3	0.1210
101.6	25200	10.8	135.6	0.842	23.9	0.1280
151.1	8295	9.4	25.2	0.774	2.7	0.0884
151.3	10140	9.2	28.5	0.781	3.1	0.0903
151.2	12310	9.4	31.9	0.790	3.6	0.0926
151.4	15230	9.2	37.2	0.799	4.3	0.0973
151.4	18240	9.3	42.3	0.808	5.2	0.1020
151.3	20280	9.3	46.3	0.814	5.9	0.1060
151.3	22340	9.2	51.1	0.819	6.6	0.1100
151.4	24980	9.3	56.9	0.826	7.7	0.1140

Appendix Table B-2. Error analysis calculated values.

$dK/d\mu$	$(dK/d\mu)^2 \bullet \sigma_\mu^2$	$dK/d\theta$	$(dK/d\theta)^2 \bullet \sigma_\theta^2$	$dK/d\rho_b$	$(dK/d\rho_b)^2 \bullet \sigma_{\rho b}^2$	$dK/d\rho_{fl}$	$(dK/d\rho_{fl})^2 \bullet \sigma_{\rho fl}^2$	dK/dt	$(dK/dt)^2 \bullet \sigma_t^2$	$dK/d\sin\theta$	$(dK/d\sin\theta)^2 \bullet \sigma_{\sin\theta}^2$
0.00197	2.8E-06	-0.123	4.6E-08	-0.0113	5.081E-10	0.0113	5.38E-09	-6.85E-04	4.69E-19	-0.148	6.70E-08
0.00147	2.9E-06	-0.126	4.8E-08	-0.0115	5.318E-10	0.0115	5.73E-09	-5.21E-04	2.71E-19	-0.152	7.02E-08
0.00129	3.1E-06	-0.130	5.1E-08	-0.0119	5.627E-10	0.0119	6.11E-09	-4.68E-04	2.19E-19	-0.156	7.46E-08
0.00114	3.1E-06	-0.130	5.1E-08	-0.0119	5.655E-10	0.0119	6.18E-09	-4.14E-04	1.71E-19	-0.157	7.49E-08
0.00087	3.3E-06	-0.133	5.4E-08	-0.0122	5.980E-10	0.0122	6.63E-09	-3.27E-04	1.07E-19	-0.161	7.87E-08
0.00069	3.4E-06	-0.136	5.7E-08	-0.0125	6.296E-10	0.0125	7.07E-09	-2.65E-04	7.02E-20	-0.165	8.27E-08
0.00642	3.3E-06	-0.162	8.0E-08	-0.0122	5.984E-10	0.0122	6.11E-09	-2.11E-03	4.46E-18	-0.186	1.05E-07
0.00475	3.6E-06	-0.171	8.9E-08	-0.0128	6.582E-10	0.0128	6.89E-09	-1.63E-03	2.65E-18	-0.195	1.16E-07
0.00340	3.9E-06	-0.175	9.3E-08	-0.0133	7.053E-10	0.0133	7.57E-09	-1.21E-03	1.47E-18	-0.201	1.23E-07
0.00290	4.2E-06	-0.183	1.0E-07	-0.0138	7.617E-10	0.0138	8.28E-09	-1.07E-03	1.14E-18	-0.209	1.33E-07
0.00235	4.3E-06	-0.184	1.0E-07	-0.0140	7.810E-10	0.0140	8.60E-09	-8.79E-04	7.72E-19	-0.211	1.36E-07
0.00181	4.7E-06	-0.194	1.1E-07	-0.0147	8.701E-10	0.0147	9.76E-09	-7.15E-04	5.11E-19	-0.222	1.50E-07
0.00138	5.2E-06	-0.204	1.3E-07	-0.0154	9.519E-10	0.0154	1.09E-08	-5.66E-04	3.21E-19	-0.233	1.66E-07
0.00118	5.3E-06	-0.207	1.3E-07	-0.0156	9.794E-10	0.0156	1.13E-08	-4.86E-04	2.36E-19	-0.237	1.71E-07
0.00092	5.8E-06	-0.216	1.4E-07	-0.0164	1.070E-09	0.0164	1.25E-08	-3.96E-04	1.57E-19	-0.247	1.86E-07
0.00079	6.1E-06	-0.220	1.5E-07	-0.0167	1.120E-09	0.0167	1.32E-08	-3.49E-04	1.22E-19	-0.252	1.93E-07
0.02240	3.3E-06	-0.475	6.9E-07	-0.0122	5.911E-10	0.0122	5.66E-09	-2.83E-03	8.00E-18	-0.483	7.11E-07
0.01834	3.4E-06	-0.479	7.0E-07	-0.0123	6.086E-10	0.0123	5.98E-09	-2.36E-03	5.55E-18	-0.487	7.23E-07
0.01488	3.7E-06	-0.502	7.7E-07	-0.0130	6.713E-10	0.0130	6.79E-09	-2.00E-03	4.00E-18	-0.511	7.95E-07
0.01290	3.9E-06	-0.518	8.2E-07	-0.0134	7.169E-10	0.0134	7.38E-09	-1.79E-03	3.20E-18	-0.528	8.48E-07
0.01138	4.2E-06	-0.536	8.7E-07	-0.0139	7.682E-10	0.0139	8.03E-09	-1.63E-03	2.66E-18	-0.546	9.07E-07
0.00942	4.8E-06	-0.568	9.8E-07	-0.0148	8.741E-10	0.0148	9.35E-09	-1.44E-03	2.08E-18	-0.579	1.02E-06
0.00776	5.2E-06	-0.598	1.1E-06	-0.0154	9.526E-10	0.0154	1.04E-08	-1.23E-03	1.50E-18	-0.609	1.13E-06
0.00712	5.6E-06	-0.622	1.2E-06	-0.0160	1.030E-09	0.0160	1.14E-08	-1.17E-03	1.37E-18	-0.633	1.22E-06
0.00624	5.8E-06	-0.627	1.2E-06	-0.0163	1.069E-09	0.0163	1.19E-08	-1.05E-03	1.11E-18	-0.638	1.24E-06
0.00534	6.5E-06	-0.668	1.4E-06	-0.0173	1.195E-09	0.0173	1.35E-08	-9.41E-04	8.85E-19	-0.680	1.41E-06
0.03278	3.1E-06	-0.537	8.8E-07	-0.0119	5.649E-10	0.0119	5.41E-09	-3.51E-03	1.23E-17	-0.545	9.04E-07
0.02946	3.3E-06	-0.558	9.5E-07	-0.0121	5.895E-10	0.0121	5.76E-09	-3.16E-03	1.00E-17	-0.565	9.72E-07
0.02600	3.4E-06	-0.562	9.6E-07	-0.0125	6.208E-10	0.0125	6.19E-09	-2.91E-03	8.44E-18	-0.570	9.89E-07
0.02265	3.8E-06	-0.601	1.1E-06	-0.0131	6.881E-10	0.0131	7.03E-09	-2.62E-03	6.84E-18	-0.609	1.13E-06
0.01975	4.2E-06	-0.626	1.2E-06	-0.0138	7.644E-10	0.0138	7.99E-09	-2.42E-03	5.87E-18	-0.634	1.22E-06
0.01804	4.5E-06	-0.647	1.3E-06	-0.0143	8.192E-10	0.0143	8.68E-09	-2.29E-03	5.24E-18	-0.656	1.31E-06
0.01654	4.8E-06	-0.677	1.4E-06	-0.0148	8.771E-10	0.0148	9.42E-09	-2.14E-03	4.60E-18	-0.685	1.43E-06
0.01478	5.2E-06	-0.697	1.5E-06	-0.0154	9.427E-10	0.0154	1.03E-08	-1.99E-03	3.98E-18	-0.706	1.52E-06

APPENDIX C. Schematic Showing How to Calculate Tait Parameters

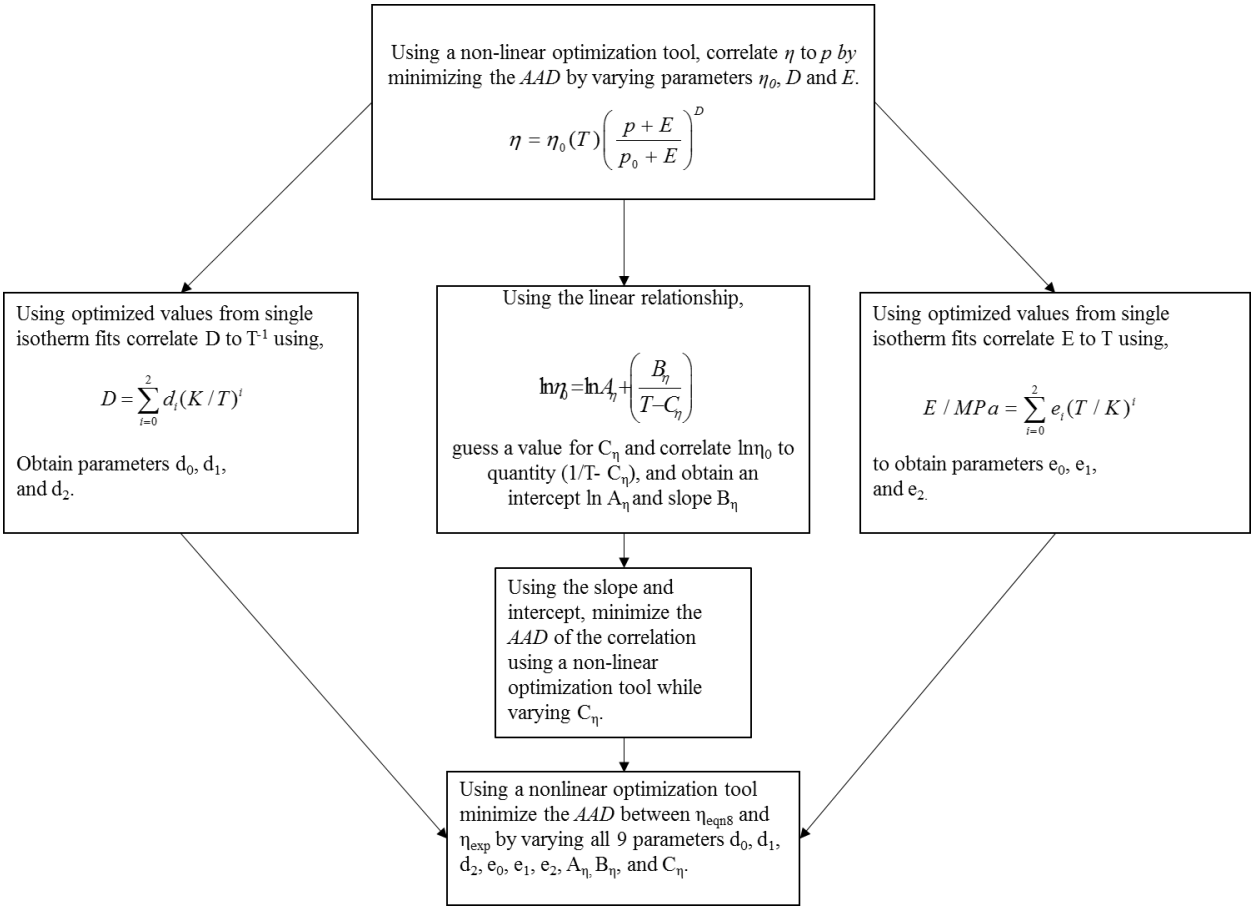

APPENDIX D. Detailed and Summary Data for all s-PMA-LMA Experiments Conducted

From Window to Piston

File Name	T (°C)	P (psig)	Angle (°)	Between Light Ports 2 and 3 Start Time (s)	Stop Time (s)	Dif (s)	Velocity (cm/s)	Internal Cell Volume (mL)	Density (g/cc)	k/l	Viscosity (mPa•s)	Re	Octane Viscosity for Comparison (mPa•s)
140604.001.HS1-1	23.3	2442	12.04	157.9	209.1	51.2	0.043	46.02	0.711	0.012	0.953	2.6	0.608
140604.003.HS1-1	23.2	4975	12.03	169.4	224.0	54.6	0.041	45.24	0.723	0.013	1.103	2.1	0.718
140604.014.HS1-1	23.2	8102	12.01	187.1	245.3	58.2	0.038	44.40	0.737	0.014	1.294	1.7	0.866
140604.005.HS1-1	23.3	10037	11.99	205.9	268.8	62.9	0.035	43.98	0.744	0.015	1.478	1.4	0.965
140604.008.HS1-1	23.4	12190	11.98	211.7	277.3	65.7	0.034	43.52	0.751	0.016	1.637	1.2	1.083
140604.016.HS1-1	23.4	15029	12.02	222.6	292.6	70.1	0.032	43.00	0.761	0.017	1.891	1.0	1.252
140604.010.HS1-1	23.5	17972	12.02	234.7	309.4	74.7	0.030	42.51	0.769	0.019	2.173	0.8	1.440
140604.012.HS1-1	23.4	20197	12.01	248.1	327.6	79.5	0.028	42.15	0.776	0.020	2.440	0.7	1.595
140604.018.HS1-1	23.4	21821	11.98	263.6	345.2	81.6	0.027	41.92	0.780	0.021	2.597	0.6	1.714
140604.020.HS1-1	23.3	25212	12.02	293.6	379.4	85.7	0.026	41.45	0.789	0.022	2.956	0.5	1.979
140604.022.HS1-1	23.3	27259	11.97	287.0	375.8	88.9	0.025	41.18	0.794	0.023	3.190	0.5	2.148
140604.024.HS1-1	23.2	30166	11.97	300.2	394.2	94.0	0.024	40.84	0.801	0.025	3.588	0.4	2.407

From Piston to Window

File Name	T (°C)	P (psig)	Angle (°)	Between Light Ports 3 and 2 Start Time (s)	Stop Time (s)	Dif (s)	Velocity (cm/s)	Internal Cell Volume (mL)	Density (g/cc)	k/l	Viscosity (mPa•s)	Re	Octane Viscosity for Comparison (mPa•s)
140604.002.HS1-1	23.3	2433	12.00	94.8	144.7	50.0	0.045	49.80	0.657	0.012	0.933	2.5	0.608
140604.004.HS1-1	23.2	4969	12.00	103.2	157.5	54.3	0.041	48.36	0.676	0.013	1.101	2.0	0.718
140604.015.HS1-1	23.3	8108	12.01	129.3	187.5	58.3	0.038	47.57	0.687	0.014	1.304	1.6	0.866
140604.006.HS1-1	23.3	10039	12.01	115.8	178.4	62.7	0.036	47.10	0.694	0.015	1.483	1.3	0.966
140604.009.HS1-1	23.4	12192	12.01	96.0	162.0	66.0	0.034	46.05	0.710	0.016	1.658	1.1	1.083
140604.017.HS1-1	23.4	15021	12.02	129.7	199.7	70.0	0.032	45.30	0.722	0.017	1.898	1.0	1.251
140604.011.HS1-1	23.5	17969	12.02	126.9	201.2	74.3	0.030	44.88	0.729	0.019	2.173	0.8	1.439
140604.013.HS1-1	23.3	20195	12.03	148.3	226.1	77.8	0.029	44.42	0.736	0.020	2.404	0.7	1.598
140604.019.HS1-1	23.3	21809	12.03	150.6	231.7	81.1	0.027	43.83	0.746	0.021	2.602	0.6	1.715
140604.021.HS1-1	23.3	25218	12.03	112.8	198.2	85.5	0.026	43.44	0.753	0.022	2.963	0.5	1.979
140604.023.HS1-1	23.2	27245	12.03	159.4	247.6	88.2	0.025	42.98	0.761	0.023	3.195	0.5	2.150
140604.025.HS1-1	23.3	30174	12.03	154.5	248.1	93.5	0.024	42.48	0.770	0.025	3.604	0.4	2.403

From Window to Piston

File Name	T (°C)	P (psig)	Angle (°)	Between Light Ports 2 and 3 Start Time (s)	Stop Time (s)	Dif (s)	Velocity (cm/s)	Internal Cell Volume (mL)	Density (g/cc)	k/l	Viscosity (mPa•s)	Re	Octane Viscosity for Comparison (mPa•s)
140604.026.HS1-1	53.4	2282	12.05	137.1	171.1	34.0	0.065	46.15	0.709	0.012	0.630	6	0.441
140604.036.HS1-1	53.6	5401	12.07	129.1	167.3	38.2	0.058	45.19	0.724	0.013	0.785	4	0.535
140604.028.HS1-1	53.6	7880	12.00	140.6	181.7	41.1	0.054	44.26	0.739	0.014	0.907	3	0.616
140604.030.HS1-1	53.7	10382	12.03	148.9	192.9	44.0	0.051	43.64	0.749	0.015	1.046	3	0.703
140604.032.HS1-1	53.8	12191	11.91	150.9	197.2	46.3	0.048	43.23	0.757	0.016	1.147	3	0.768
140604.034.HS1-1	53.7	15030	12.09	164.9	213.6	48.7	0.046	42.64	0.767	0.017	1.322	2	0.879
140604.042.HS1-1	53.7	18098	11.97	177.6	229.5	51.9	0.043	42.25	0.774	0.019	1.507	2	1.005
140604.038.HS1-1	53.7	20050	11.96	180.5	233.3	52.8	0.042	41.74	0.784	0.020	1.606	2	1.089
140604.040.HS1-1	53.6	22198	11.95	190.3	245.3	55.0	0.040	41.40	0.790	0.021	1.758	1	1.187
140604.044.HS1-1	53.8	24955	12.07	195.6	252.9	57.3	0.039	41.01	0.798	0.022	1.970	1	1.313
140604.046.HS1-1	53.7	27349	11.97	201.2	260.3	59.1	0.038	40.68	0.804	0.023	2.125	1	1.432
140604.048.HS1-1	53.7	30070	12.00	223.2	284.2	61.0	0.036	40.32	0.811	0.025	2.328	1	1.570

From Piston to Window

File Name	T (°C)	P (psig)	Angle (°)	Between Light Ports 3 and 2 Start Time (s)	Stop Time (s)	Dif (s)	Velocity (cm/s)	Internal Cell Volume (mL)	Density (g/cc)	k/l	Viscosity (mPa•s)	Re	Octane Viscosity for Comparison (mPa•s)
140604.027.HS1-1	53.6	2337	11.99	86.8	121.5	34.8	0.064	46.15	0.709	0.012	0.642	6	0.442
140604.037.HS1-1	53.7	5414	12.01	78.8	117.1	38.3	0.058	45.19	0.724	0.013	0.784	4	0.535
140604.029.HS1-1	53.6	7898	11.98	81.3	123.5	42.2	0.053	44.26	0.739	0.014	0.930	3	0.617
140604.031.HS1-1	53.7	10399	12.00	81.9	126.9	45.0	0.049	43.64	0.749	0.015	1.067	3	0.703
140604.033.HS1-1	53.7	12191	12.00	83.2	129.9	46.7	0.048	43.23	0.757	0.016	1.164	2	0.769
140604.035.HS1-1	53.6	15038	11.99	108.3	157.9	49.6	0.045	42.64	0.767	0.017	1.333	2	0.880
140604.043.HS1-1	53.6	18108	11.98	74.7	126.9	52.3	0.043	42.25	0.774	0.019	1.519	2	1.006
140604.039.HS1-1	53.8	20048	11.97	84.2	137.3	53.0	0.042	41.74	0.784	0.020	1.614	2	1.088
140604.041.HS1-1	53.7	22209	11.97	111.0	166.6	55.6	0.040	41.40	0.790	0.021	1.782	1	1.186
140604.045.HS1-1	53.6	24959	11.97	118.2	176.1	57.8	0.038	41.01	0.798	0.022	1.971	1	1.316
140604.047.HS1-1	53.7	27339	11.96	122.9	182.4	59.4	0.037	40.66	0.804	0.023	2.133	1	1.431
140604.049.HS1-1	53.6	30075	11.97	127.7	189.3	61.6	0.036	40.32	0.811	0.025	2.343	1	1.573

From Window to Piston

File Name	T (°C)	P (psig)	Angle (°)	Between Light Ports 2 and 3 Start Time (s)	Stop Time (s)	Dif (s)	Velocity (cm/s)	Internal Cell Volume (mL)	Density (g/cc)	k/l	Viscosity (mPa•s)	Re	Octane Viscosity for Comparison (mPa•s)
140602.001.HS1-1	98.3	1913	12.06	95.2	118.5	23.2	0.096	49.34	0.663	0.012	0.428	12	0.292
140602.003.HS1-1	98.4	5058	11.99	113.2	139.8	26.5	0.084	47.82	0.684	0.013	0.539	8	0.359
140602.027.HS1-1	98.4	8176	12.08	101.7	130.1	28.4	0.078	46.79	0.699	0.014	0.640	7	0.429
140602.005.HS1-1	98.5	9951	12.05	99.6	130.1	30.4	0.073	46.05	0.710	0.015	0.719	6	0.470
140602.007.HS1-1	98.6	12125	11.97	125.0	156.8	31.9	0.070	45.45	0.720	0.016	0.795	5	0.521
140602.025.HS1-1	98.4	14952	12.08	121.2	153.9	32.7	0.068	44.75	0.731	0.017	0.890	4	0.592
140602.009.HS1-1	98.4	17882	11.97	142.4	177.5	35.1	0.063	44.09	0.742	0.019	1.018	4	0.668
140602.011.HS1-1	98.3	20183	11.95	127.1	163.4	36.4	0.061	43.65	0.749	0.020	1.114	3	0.729
140602.015.HS1-1	98.3	22003	12.04	131.2	168.2	37.0	0.060	43.31	0.755	0.021	1.190	3	0.778
140602.013.HS1-1	98.3	24984	12.03	135.6	174.0	38.4	0.058	42.80	0.764	0.022	1.323	3	0.861
140602.017.HS1-1	98.4	27275	11.97	139.8	179.5	39.7	0.056	42.44	0.771	0.023	1.429	2	0.926
140602.019.HS1-1	98.4	30054	11.92	143.0	183.9	40.9	0.054	42.05	0.778	0.025	1.556	2	1.007
140602.022.HS1-1	98.3	32084	11.95	149.5	191.0	41.5	0.054	41.76	0.783	0.026	1.648	2	1.068

From Piston to Window

File Name	T (°C)	P (psig)	Angle (°)	Between Light Ports 3 and 2 Start Time (s)	Stop Time (s)	Dif (s)	Velocity (cm/s)	Internal Cell Volume (mL)	Density (g/cc)	k/l	Viscosity (mPa•s)	Re	Octane Viscosity for Comparison (mPa•s)
140602.002.HS1-1	98.3	1953	12.06	54.1	77.1	23.0	0.097	49.34	0.663	0.012	0.424	12	0.293
140602.004.HS1-1	98.4	5092	12.07	58.9	85.3	26.4	0.084	47.82	0.684	0.013	0.540	8	0.360
140602.028.HS1-1	98.4	8208	12.06	63.5	92.2	28.7	0.078	46.79	0.699	0.014	0.645	7	0.429
140602.006.HS1-1	98.3	9983	12.06	76.1	106.5	30.5	0.073	46.05	0.710	0.015	0.722	6	0.471
140602.008.HS1-1	98.4	12155	12.05	68.7	100.5	31.8	0.070	45.43	0.720	0.016	0.800	5	0.523
140602.026.HS1-1	98.4	14987	12.03	71.7	104.8	33.1	0.067	44.75	0.731	0.017	0.896	4	0.593
140602.010.HS1-1	98.4	17910	12.06	74.5	109.6	35.1	0.063	44.09	0.742	0.019	1.026	4	0.668
140602.012.HS1-1	98.3	20213	12.05	70.4	106.5	36.2	0.062	43.64	0.749	0.020	1.118	3	0.730
140602.016.HS1-1	98.3	22031	12.07	64.3	101.3	37.0	0.060	43.31	0.755	0.021	1.196	3	0.779
140602.014.HS1-1	98.3	25014	12.05	71.5	110.1	38.5	0.058	42.80	0.764	0.022	1.331	3	0.862
140602.018.HS1-1	98.3	27306	12.05	64.3	103.6	39.3	0.057	42.44	0.771	0.023	1.425	2	0.928
140602.020.HS1-1	98.3	30079	12.07	83.2	123.6	40.4	0.055	42.03	0.778	0.025	1.558	2	1.008
140602.023.HS1-1	98.2	32113	12.06	87.3	128.3	41.1	0.054	41.76	0.783	0.026	1.649	2	1.070

From Window to Piston

File Name	T (°C)	P (psig)	Angle (°)	Between Light Ports 2 and 3 Start Time (s)	Stop Time (s)	Dif (s)	Velocity (cm/s)	Internal Cell Volume (mL)	Density (g/cc)	k/l	Viscosity (mPa•s)	Re	Octane Viscosity for Comparison (mPa•s)
140602.029.HS1-1	147.7	5295	12.02	69.9	87.9	18.0	0.124	49.80	0.657	0.013	0.371	17	0.265
140602.031.HS1-1	147.7	8052	12.04	94.8	114.6	19.8	0.112	48.36	0.676	0.014	0.445	13	0.313
140602.034.HS1-1	147.7	10179	12.05	82.8	103.6	20.8	0.107	47.57	0.687	0.015	0.496	12	0.350
140602.052.HS1-1	147.7	11893	12.07	103.5	125.2	21.7	0.103	47.10	0.694	0.016	0.544	10	0.381
140602.037.HS1-1	147.7	14990	12.05	87.4	110.7	23.3	0.095	46.05	0.710	0.017	0.635	8	0.438
140602.040.HS1-1	147.6	17898	12.02	91.8	116.0	24.2	0.092	45.32	0.722	0.019	0.706	7	0.492
140602.054.HS1-1	147.7	19823	12.06	91.6	116.9	25.3	0.088	44.88	0.729	0.020	0.777	7	0.528
140602.042.HS1-1	147.8	21973	11.94	120.9	146.2	25.3	0.088	44.42	0.736	0.021	0.811	6	0.569
140602.044.HS1-1	147.5	24953	12.03	96.9	122.8	26.0	0.086	43.85	0.746	0.022	0.895	6	0.627
140602.048.HS1-1	147.7	27178	12.09	106.6	132.7	26.1	0.085	43.46	0.753	0.023	0.951	5	0.670
140602.050.HS1-1	147.7	30045	11.96	106.7	133.9	27.2	0.082	42.98	0.761	0.025	1.040	5	0.726

From Piston to Window

File Name	T (°C)	P (psig)	Angle (°)	Between Light Ports 3 and 2 Start Time (s)	Stop Time (s)	Dif (s)	Velocity (cm/s)	Internal Cell Volume (mL)	Density (g/cc)	k/l	Viscosity (mPa•s)	Re	Octane Viscosity for Comparison (mPa•s)
140602.030.HS1-1	147.7	5337	12.05	38.7	57.0	18.3	0.122	49.80	0.657	0.013	0.378	17	0.265
140602.032.HS1-1	147.7	8104	12.04	51.3	71.4	20.1	0.111	48.36	0.676	0.014	0.451	13	0.313
140602.035.HS1-1	147.5	10232	12.03	50.2	71.3	21.1	0.105	47.57	0.687	0.015	0.504	11	0.352
140602.053.HS1-1	147.7	11951	12.03	48.6	70.6	22.0	0.101	47.10	0.694	0.016	0.551	10	0.382
140602.039.HS1-1	147.3	15041	12.01	61.8	85.2	23.5	0.095	46.05	0.710	0.017	0.637	8	0.440
140602.041.HS1-1	147.4	17951	12.04	53.9	78.2	24.3	0.092	45.30	0.722	0.019	0.711	7	0.494
140602.055.HS1-1	147.7	19878	12.03	53.2	78.4	25.2	0.088	44.88	0.729	0.020	0.773	7	0.529
140602.043.HS1-1	147.3	22042	12.03	55.4	80.6	25.2	0.088	44.42	0.736	0.021	0.814	6	0.572
140602.046.HS1-1	147.4	25013	12.02	63.2	89.2	26.0	0.086	43.83	0.746	0.022	0.898	6	0.629
140602.049.HS1-1	147.6	27229	12.02	56.7	83.2	26.5	0.084	43.44	0.753	0.023	0.962	5	0.671
140602.051.HS1-1	147.5	30096	12.02	59.1	86.3	27.2	0.082	42.98	0.761	0.025	1.046	5	0.728

From Window to Piston

File Name	T (°C)	P (psig)	Angle (°)	Between Light Ports 2 and 3 Start Time (s)	Stop Time (s)	Dif (s)	Velocity (cm/s)	Internal Cell Volume (mL)	Density (g/cc)	k/l	Viscosity (mPa•s)	Re	Octane Viscosity for Comparison (mPa•s)
140605.002.HS1-1	197.5	7952	11.97	56.4	69.5	13.1	0.170	49.37	0.662	0.014	0.291	31	0.237
140605.004.HS1-1	197.5	9848	11.99	60.5	74.3	13.8	0.161	48.46	0.675	0.015	0.326	26	0.263
140605.006.HS1-1	197.8	12104	11.97	61.1	75.7	14.6	0.152	47.54	0.688	0.016	0.366	23	0.294
140605.009.HS1-1	197.6	14992	12.04	65.4	80.8	15.4	0.145	46.55	0.703	0.017	0.418	19	0.335
140605.019.HS1-1	197.3	17960	12.00	64.9	80.9	15.9	0.140	45.79	0.714	0.019	0.466	17	0.377
140605.011.HS1-1	197.6	20018	12.02	67.6	84.0	16.4	0.136	45.16	0.724	0.020	0.504	15	0.405
140605.013.HS1-1	197.7	22185	12.02	66.7	83.2	16.6	0.134	44.63	0.733	0.021	0.537	14	0.436
140605.021.HS1-1	197.7	24954	12.01	84.3	101.5	17.1	0.130	44.06	0.742	0.022	0.590	13	0.475
140605.015.HS1-1	197.6	27047	12.00	72.0	89.3	17.3	0.129	43.64	0.749	0.023	0.623	12	0.505
140605.017.HS1-1	197.7	30207	11.98	71.2	89.0	17.7	0.125	43.08	0.759	0.025	0.682	11	0.549

From Piston to Window

File Name	T (°C)	P (psig)	Angle (°)	Between Light Ports 3 and 2 Start Time (s)	Stop Time (s)	Dif (s)	Velocity (cm/s)	Internal Cell Volume (mL)	Density (g/cc)	k/l	Viscosity (mPa•s)	Re	Octane Viscosity for Comparison (mPa•s)
140605.003.HS1-1	197.4	7987	11.98	38.1	51.4	13.3	0.168	49.37	0.662	0.014	0.296	30	0.238
140605.005.HS1-1	197.5	9886	11.99	38.3	52.3	14.0	0.159	48.44	0.675	0.015	0.329	26	0.264
140605.007.HS1-1	197.6	12135	12.00	38.5	53.3	14.7	0.151	47.54	0.688	0.016	0.370	22	0.295
140605.010.HS1-1	197.7	15023	11.97	38.9	54.6	15.7	0.142	46.55	0.703	0.017	0.425	19	0.335
140605.020.HS1-1	197.3	18005	11.99	39.5	55.7	16.1	0.138	45.79	0.714	0.019	0.472	17	0.378
140605.012.HS1-1	197.3	20064	11.99	39.8	56.4	16.5	0.134	45.14	0.725	0.020	0.509	15	0.407
140605.014.HS1-1	197.4	22229	11.99	46.7	63.5	16.9	0.132	44.63	0.733	0.021	0.545	14	0.437
140605.022.HS1-1	197.3	24988	11.97	44.8	62.1	17.3	0.129	44.06	0.742	0.022	0.595	13	0.476
140605.016.HS1-1	197.4	27093	11.99	42.4	59.9	17.5	0.127	43.64	0.749	0.023	0.632	12	0.506
140605.018.HS1-1	197.5	30259	11.99	42.8	60.7	17.9	0.124	43.08	0.759	0.025	0.691	11	0.551

Summary of viscosity data for 2.473 wt% 60ML45RS in Octane

d/D = 0.998									
20°C		50°C		100°C		150°C		200°C	
Pressure (Psig)	Viscosity (mPa•s)	Pressure (Psig)	Viscosity (mPa•s)	Pressure (Psig)	Viscosity (mPa•s)	Pressure (Psig)	Viscosity (mPa•s)	Pressure (Psig)	Viscosity (mPa•s)
2442	0.943	2310	0.636	1933	0.426	5316	0.374	7970	0.293
4975	1.102	5408	0.785	5075	0.539	8078	0.448	9867	0.327
8102	1.299	7889	0.918	8192	0.643	10205	0.500	12119	0.368
10037	1.481	10391	1.056	9967	0.721	11922	0.548	15007	0.421
12190	1.647	12191	1.155	12140	0.798	15015	0.636	17983	0.469
15029	1.895	15034	1.327	14970	0.893	17924	0.709	20041	0.506
17972	2.173	18103	1.513	17896	1.022	19851	0.775	22207	0.541
20197	2.422	20049	1.610	20198	1.116	22008	0.812	24971	0.592
21821	2.599	22203	1.770	22017	1.193	24983	0.897	27070	0.627
25212	2.960	24957	1.971	24999	1.327	27203	0.957	30233	0.687
27259	3.192	27344	2.129	27291	1.427	30071	1.043		
30166	3.596	30073	2.336	30066	1.557				

Viscosity of pure octane

d/D = 0.998									
20°C		50°C		100°C		150°C		200°C	
Pressure (Psig)	Viscosity (mPa•s)	Pressure (Psig)	Viscosity (mPa•s)	Pressure (Psig)	Viscosity (mPa•s)	Pressure (Psig)	Viscosity (mPa•s)	Pressure (Psig)	Viscosity (mPa•s)
2442	0.608	2310	0.442	1933	0.293	5316	0.265	7970	0.237
4975	0.718	5408	0.535	5075	0.359	8078	0.313	9867	0.264
8102	0.866	7889	0.616	8192	0.429	10205	0.351	12119	0.295
10037	0.965	10391	0.703	9967	0.470	11922	0.382	15007	0.335
12190	1.083	12191	0.769	12140	0.522	15015	0.439	17983	0.377
15029	1.251	15034	0.879	14970	0.593	17924	0.493	20041	0.406
17972	1.439	18103	1.005	17896	0.668	19851	0.529	22207	0.436
20197	1.596	20049	1.088	20198	0.730	22008	0.570	24971	0.476
21821	1.714	22203	1.186	22017	0.779	24983	0.628	27070	0.505
25212	1.979	24957	1.315	24999	0.862	27203	0.670	30233	0.550
27259	2.149	27344	1.431	27291	0.927	30071	0.727		
30166	2.405	30073	1.571	30066	1.008				

APPENDIX E. Viscometer Assembly Protocol

Cell body
- Check for cleanliness
  - Fitting ports
  - Threads
  - Blow with nitrogen inside as well as ports
- Cell ends
  - Cone seals
  - Interior surfaces
  - Bolt faces
- Visually ensure light transmission through light ports

Start with Bellow Side End Cap
- Check for bellow cleanliness
- Ensure cone is clean
- Bolt to cell
  - Use star pattern for tightening bolts
  - First hand tight all the bolts
  - Tight bolts with stepwise torque
  - 5 to 10 to 15 to 20 to 25 ft•lbs
  - Place pin in L4-R4 ports
  - Place plugs in L4 and R4 ports and hand tight

Ball
- Blow the cell with nitrogen
- Check for ball cleanliness
- Insert gently into cell
- Check for free rolling

Port Fittings
- Check for cleanliness of ports and all fittings
- Place the fittings as listed

side ports

L1 – plug	R1 – Thermocouple
L2 – light window	R2 – light window
L3 – light window	R3 – light window
L4 – plug	R4 – plug

Bottom port
  - B – plug

Top ports

- T1, window side – valve
- T2, bellow side – thermocouple

• Tight all fittings using 25 ft•lbs torque
• Check for light transmission

Window assembly
• Check for cleanliness of window, kapton washer, window cap, and window base
• Place window in the cap and place kapton washer on top of the window
• Screw-in window base and hand tight
• Secure window base in small vise
• Tight the cap using 18 ft•lbs torque

Window side end cap
• Check for cleanliness
• Bolt to cell

- Use star pattern for tightening bolts
- First hand tight all the bolts
- Tight bolts with stepwise torque
- 5 to 10 to 15 to 20 to 25 ft•lbs

Transfer cell to the viscometer table
• Check for ball rolling

RTD mounting
• Place hose clamp between 2nd and 3rd set of ports
• Apply thermal paste to RTD
• Place RTD sensor beneath hose clamp and hand tighten the clamp

LVDT connection
• Connect LVDT rod to the bellow
• Tighten HF6 nut with 25 ft•lbs torque
• Check free-standing LVDT reading

Thermocouples connection
• Connect thermocouples to the respective readouts

Heating tape
• Wrap heating tape around the cell as evenly as possible without overlap

Propane flush
• flush the cell with propane for three times
• check light transmission and ball rolling

Cell loading

• Load the cell with fluid of interest

Final check

• All fittings are double checked @ 25 ft•lbs
• Ensure valve (T1) is closed
• Light transmission is checked
• Ball free rolling is checked

APPENDIX F. Detailed s-PS Chemical Analysis

Both 1H and 13C NMR spectra were taken for the following six samples:

Item No.	Batch No.
PSS-psts45k	psst2081
PSS-psts100k	psst14082
PSS-psts300k	psst13091
PSS-ps33kARM	ps9029n
PSS-ps120kARM	ps10065
15.5 PSARM	15.5 PS

Though all the 1H NMR and 13C NMR appear to be similar for all the samples, 13C NMR data indicate that these polystyrene are mostly atactic polymers. Particularly, Comparison of methylene carbon (B) region (42-47 ppm) and Phenyl C-1 (A-quarternary carbon) region (145-147 ppm) with the literature reported regions clearly indicates that these polystyrenes are atactic (random) polymers.

Also the almost the same 13C NMR spectra for all the samples indicate that the tacticity is the same for all irrespective of the molecular weight.

Since it is hard to observe the end group (styrene olefinic 1H or 13C), it is difficult to estimate the molecular weight of the polymer; This may be due to the higher mwts for all the samples, which broadens the resonances; however, we will try to use the TD (Time – Domain) NMR to determine the mwt of this polymer (hope to observe different T2 depending on the mwt of the polymers)

13C NMR of PS33K, PS120K, PS15.5 (from bottom)
(B-CH2 carbon region)

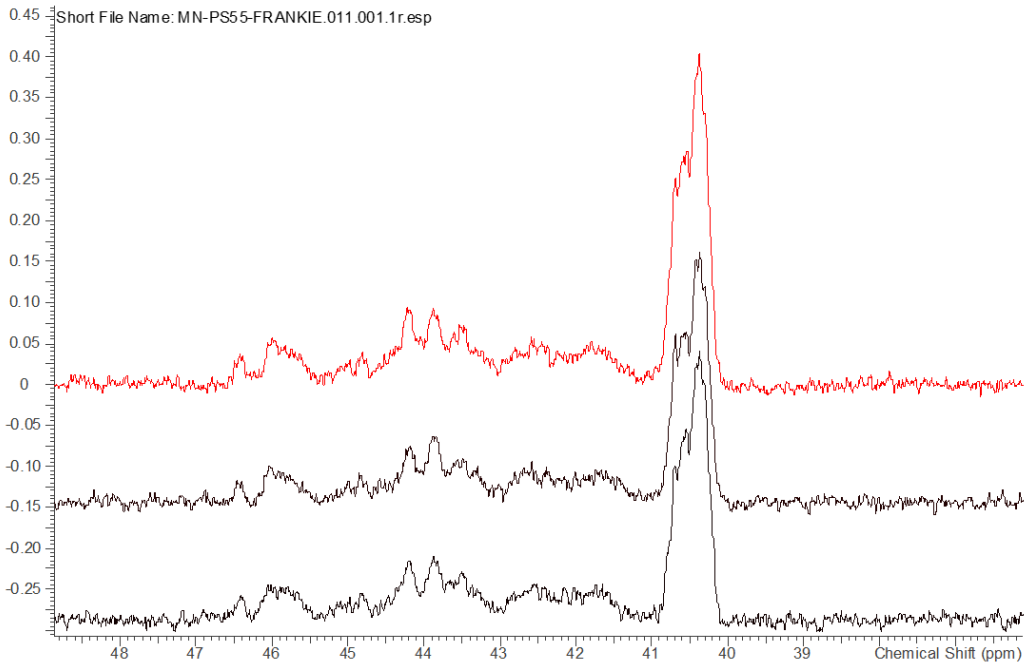

13C NMR of PS33K, PS120K, PS15.5 (from bottom)

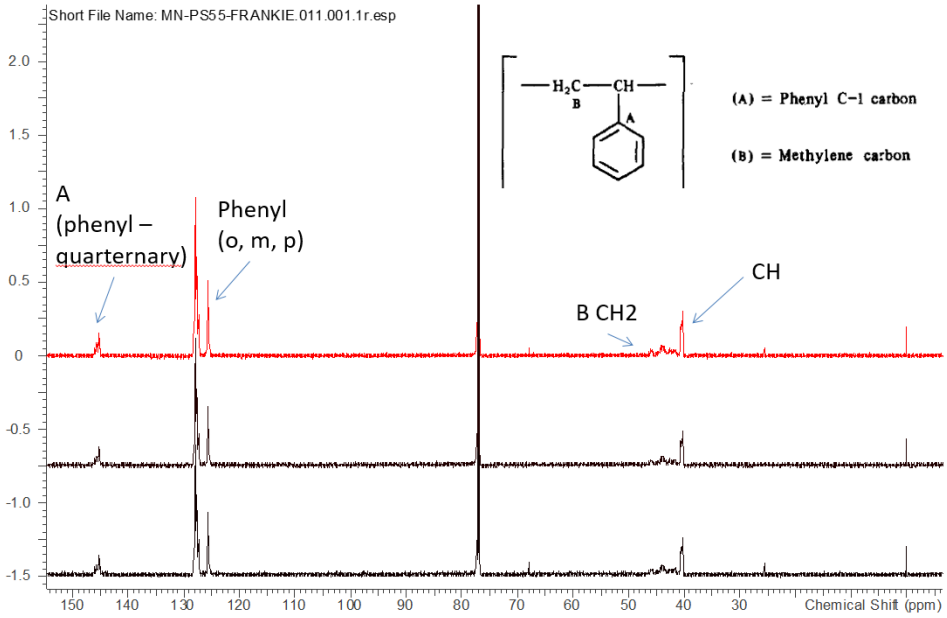

13C NMR of PS33K, PS120K, PS15.5 (from bottom)
(A- Phenyl quaternary carbon region)

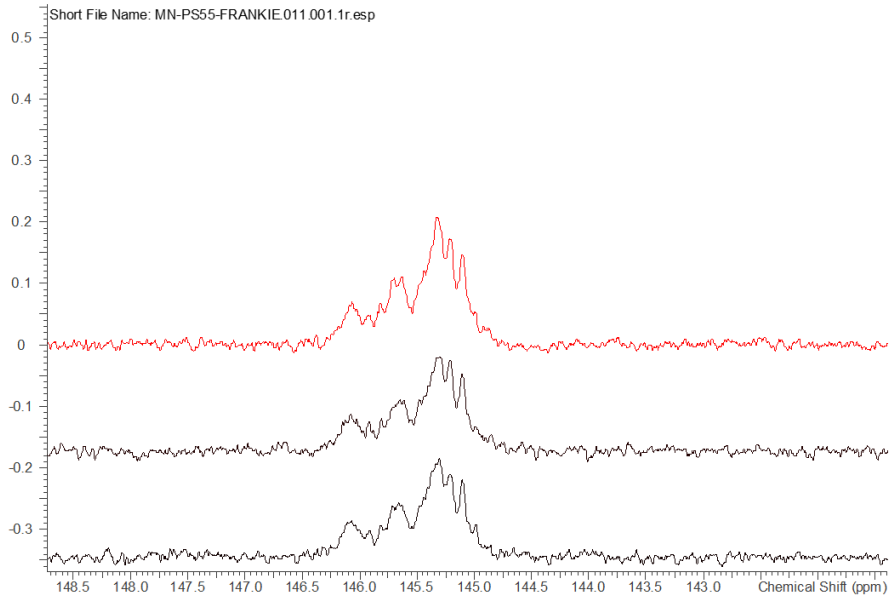

13C NMR of PSTS45K, PSTS100K, PSTS300K (from bottom)

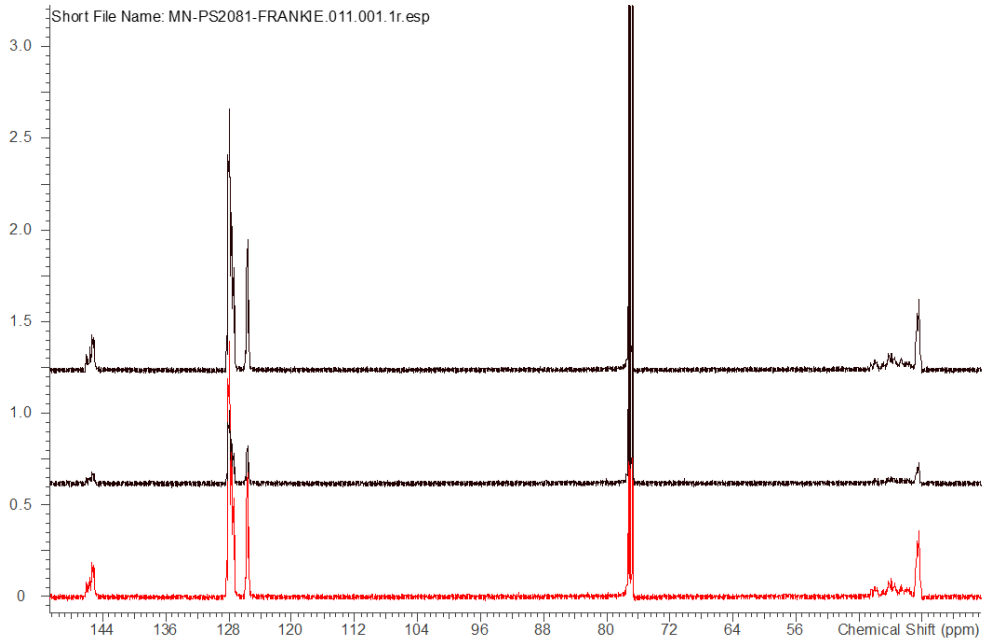

13C NMR of PSTS45K, PSTS100K, PSTS300K (from bottom)
(B-CH2 carbon region)

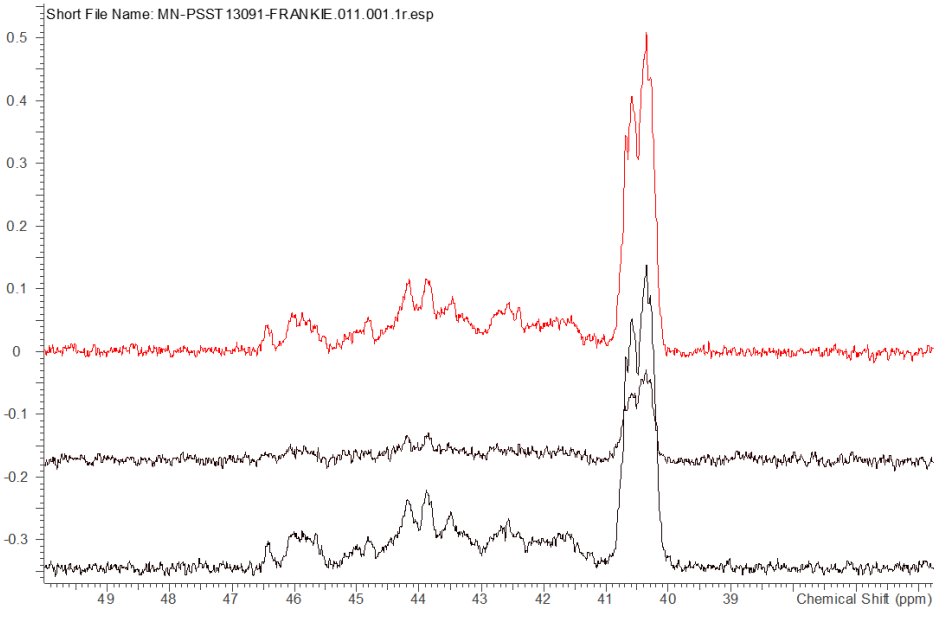

13C NMR of PSTS45K, PSTS100K, PSTS300K (from bottom)
(A- Phenyl quaternary carbon region)

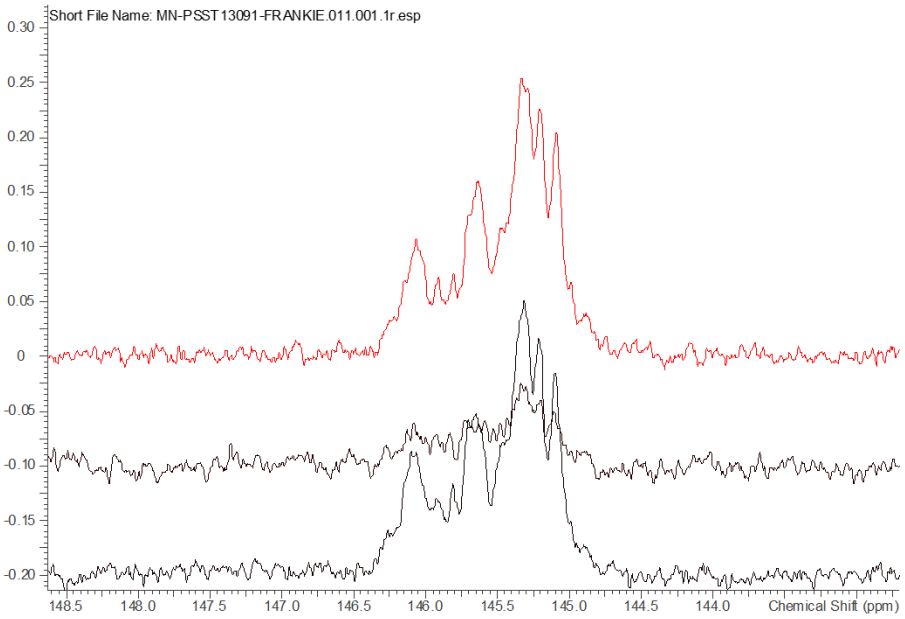

Reference: Int. J. Polymer Analysis & Characterization, 1996, Vol. 2, pp. 439-455
PS samples that are analyzed give more or less the same atactic type polymer spectrum (bottom trace for methylene carbon, 42-47 ppm)

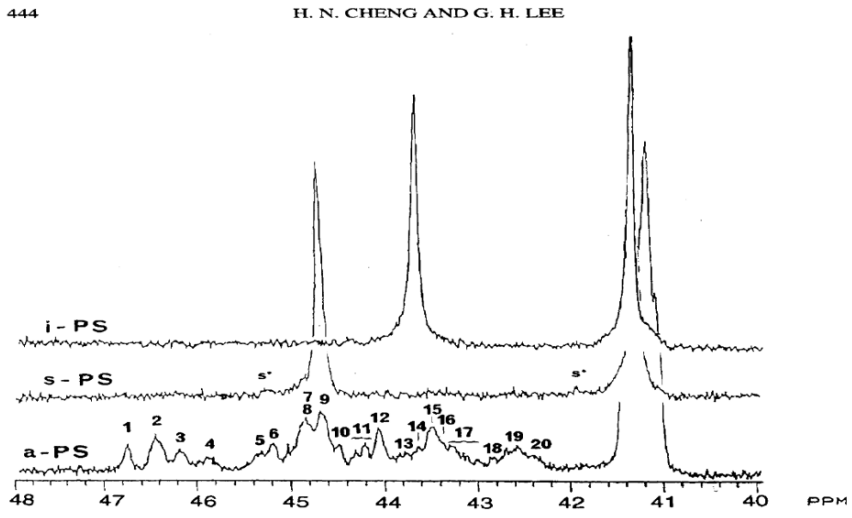

FIGURE 2 ^{13}C NMR spectra of the aliphatic carbons of atactic polystyrene (lower trace), syndiotactic polystyrene (middle trace), and isotactic polystyrene (upper trace), in 1,2,4-trichlorobenzene at ca. 115°C. The notation s* in the middle trace represents spinning side band.

Reference: Int. J. Polymer Analysis & Characterization, 1996, Vol. 2, pp. 439-455
PS samples that are analyzed give more or less the same atactic type polymer spectrum (bottom trace for Phenyl quarternary carbon)

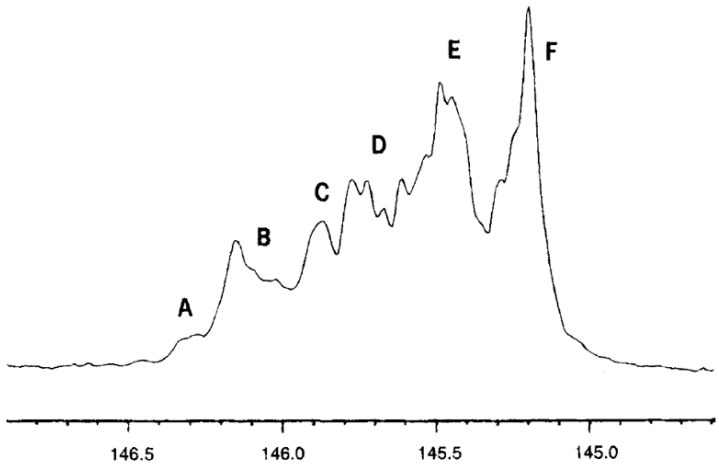

FIGURE 1 ^{13}C NMR spectrum of aromatic C_1 carbon of atactic polystyrene (sample *a*) in 1,2,4-trichlorobenzene at ca. 115°C.

1H NMR of PS33K, PS120K, PS15.5 (from bottom)

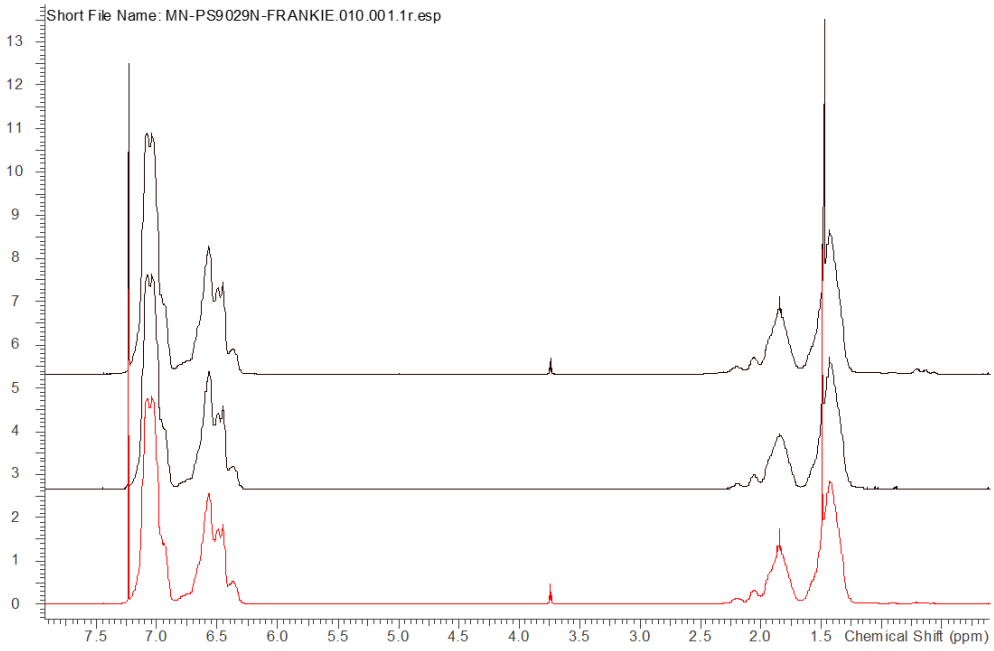

1H NMR of PSTS45K, PSTS100K, PSTS300K (from bottom)

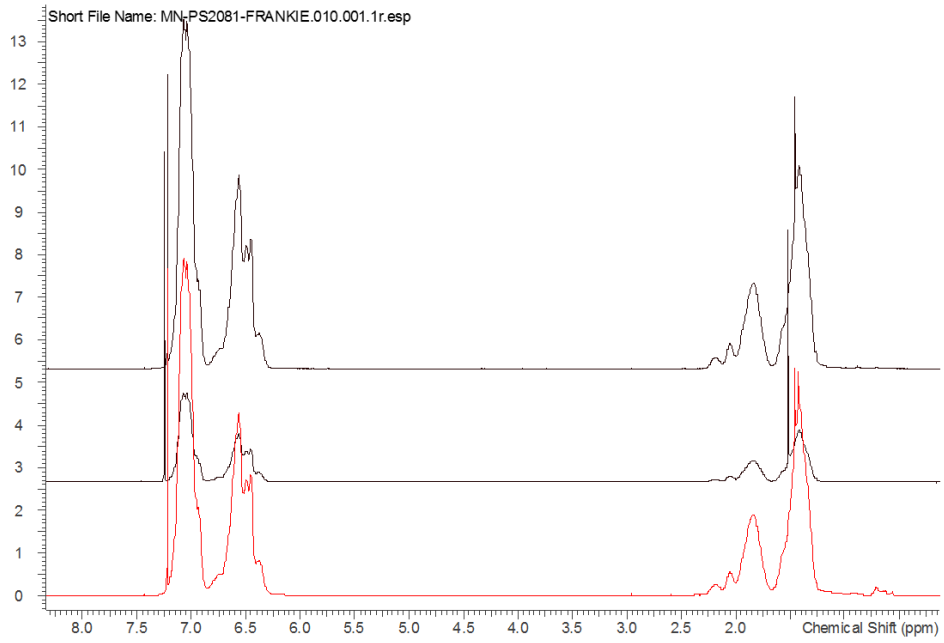

An representative with integration

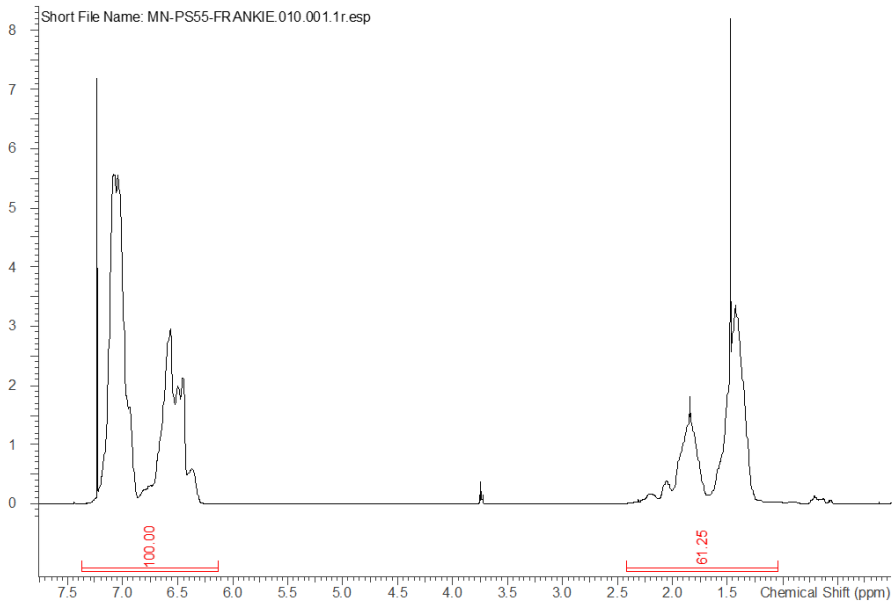

An representative with integration

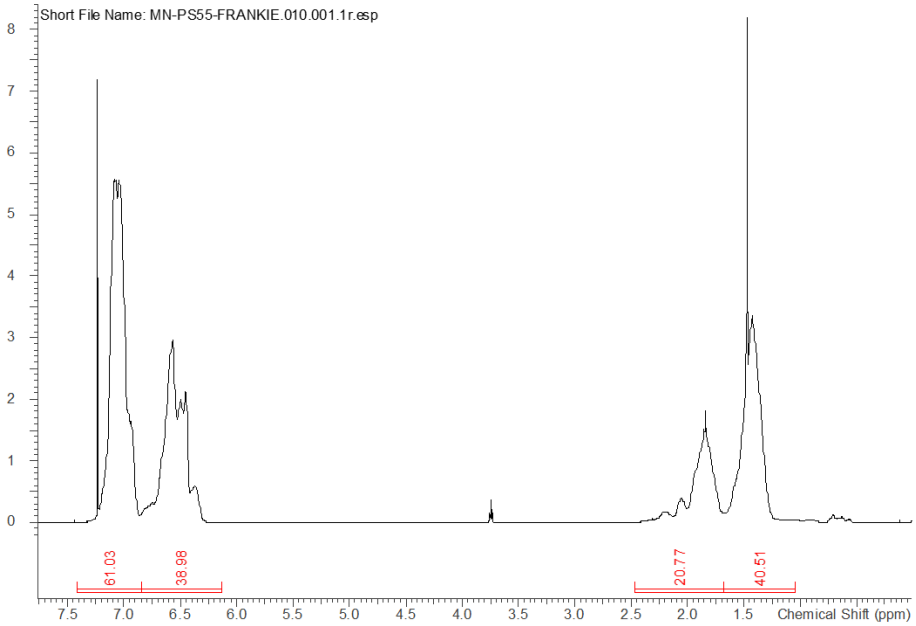

Polymer type: Poly(styrene)
Part No: PSS-ps15k
Lot No: ps1088

Molar Mass Distribution

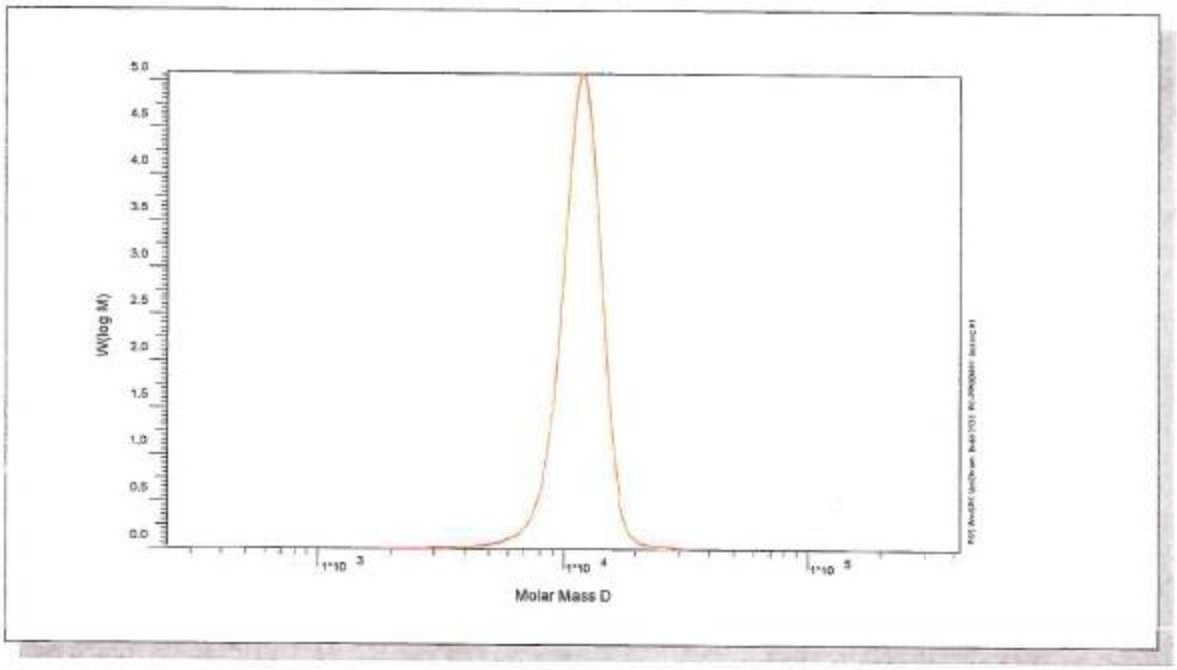

GPC/SEC - Conditions

Sample concentration	1,00 g/l	Inject volume	20 µl
Flow rate	1,00 ml/min	Temperature	23 °C
Solvent	THF		
Precolumn [8 x 50 mm]	PSS SDV 5µm		
Columns [analytical, each 8 x 300 mm]	PSS SDV 5µm 10e3Å / 10e5Å / 10e6Å		
Data Acquisition Software	PSS WinGPC	Operator	S. Fugmann

GPC/SEC - Results

Detector	Mw [Da]	Mn [Da]	Mp [Da]	PDI [Mw/Mn]
Shodex RI 71	15500	14700	15700	1,05

Note:

Mw = Weight average molecular weight
Mn = Number average molecular weight
Mp = Molar mass at the peak maximum
PDI = Polydispersity Index

Polymer type: Poly(styrene)
Part No: PSS-ps33k
Lot No: ps9029n

Molar Mass Distribution

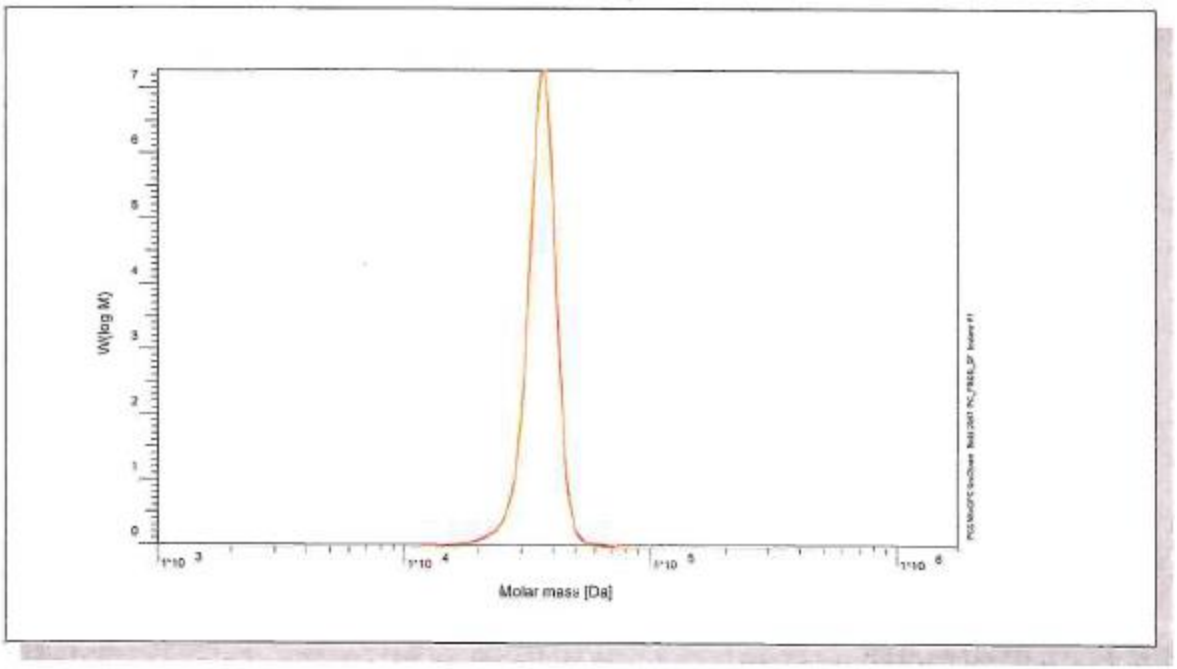

GPC/SEC - Conditions

Sample concentration	1,00 g/l	Inject volume	20 µl
Solvent	Tetrahydrofuran	Flow rate	1,00 ml/min
Precolumn [8 x 50 mm]	PSS SDV 5µm	Temperature	23 °C
Columns [analytical, each 8 x 300 mm]	PSS SDV 5µm 10e3Å / 10e5Å / 10e6Å	Operator	S.Fugmann
Data Acquisition Software	PSS WinGPC		

GPC/SEC - Results

Detector	Mw [Da]	Mn [Da]	Mp [Da]	PDI [Mw/Mn]
Agilent RID	34000	32700	34800	1,04

Note:

Mw = Weight average molecular weight
Mn = Number average molecular weight
Mp = Molar mass at the peak maximum
PDI = Polydispersity Index

Polymer type:	Poly(styrene)
Part No:	PSS-ps120k
Lot No:	ps10065

Molar Mass Distribution

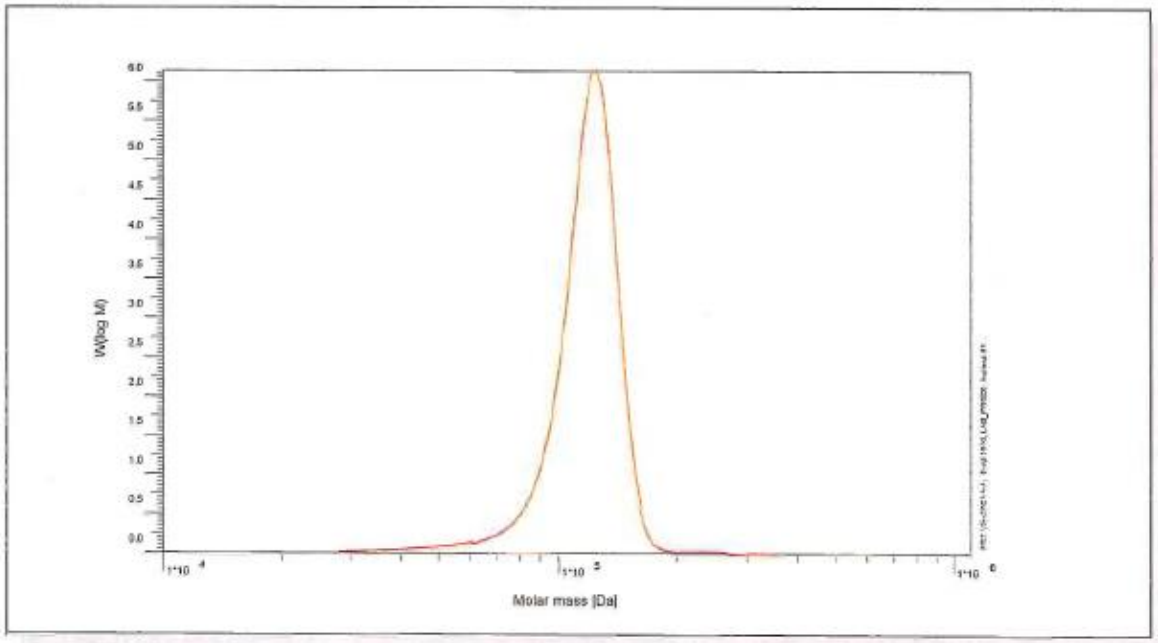

GPC/SEC - Conditions

Sample concentration	1,00 g/l	Inject volume	20 µl
Solvent	THF	Flow rate	1,00 ml/min
Precolumn [8 x 50 mm]	PSS SDV 5µm	Temperature	20,0° C
Columns [analytical, each 8 x 300 mm]	PSS SDV 5µm 10e3Å / 10e5Å / 10e6Å		
Data Acquisition Software	PSS WinGPC	Operator	T.Hofe

GPC/SEC - Results

Detector	Mw (Da)	Mn (Da)	Mp (Da)	PDI (Mw/Mn)
Shodex RI 71	120000	115000	127000	1,05

Note:
Mw = Weight Average Molecular Weight

Polymer type:	Poly(styrene) 3-star
Part No:	PSS-psts45k
Lot No:	psst2081

Molar Mass Distribution

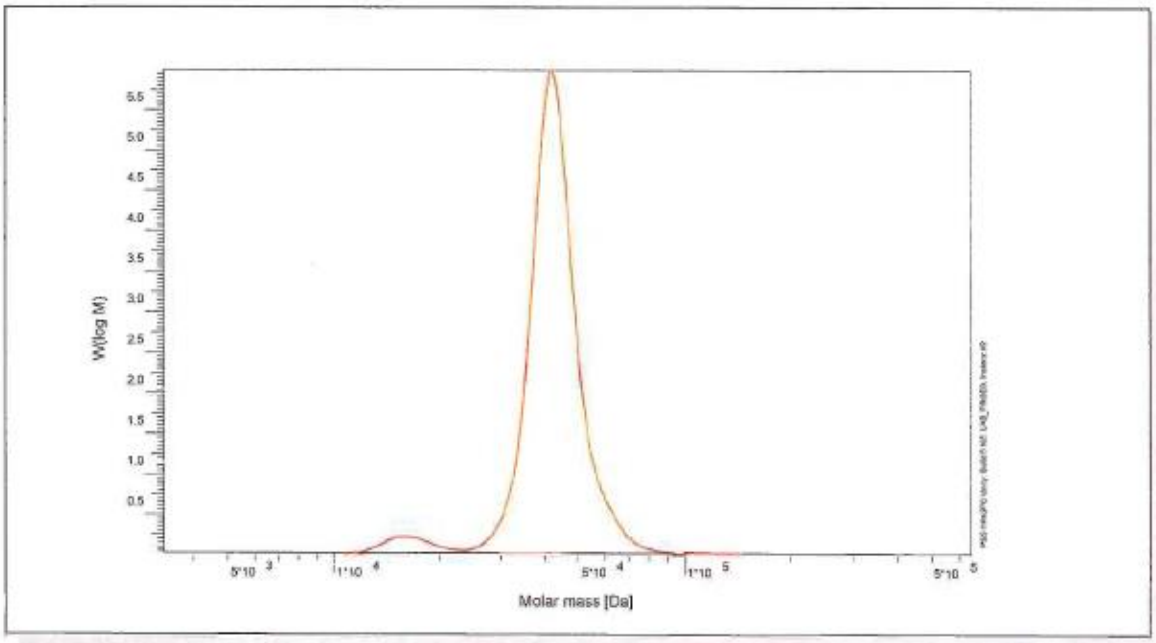

GPC/SEC - Conditions

Sample concentration	1,00 g/l	Inject volume	20 µl
Solvent	THF	Flow rate	1,00 ml/min
Precolumn [8 x 50 mm]	PSS SDV 5µm	Temperature	23,0° C
Columns [analytical, each 8 x 300 mm]	PSS SDV 5µm 10e3Å / 10e5Å / 10e6Å		
Data Acquisition Software	PSS WinGPC	Operator	S. Fugmann

GPC/SEC - Results

Detector	Mw [Da]	Mn [Da]	Mp [Da]	PDI [Mw/Mn]
Shodex RI 71	41200	38100	41300	1,08

GPC/SEC - Results based on Poly(styrene) calibration, one arm Mn [Da] = 15 400

Note:
Mw = Weight average molecular weight

Polymer type:	Poly(styrene) 3-star
Part No:	PSS-psts100k
Lot No:	psst14082

Molar Mass Distribution

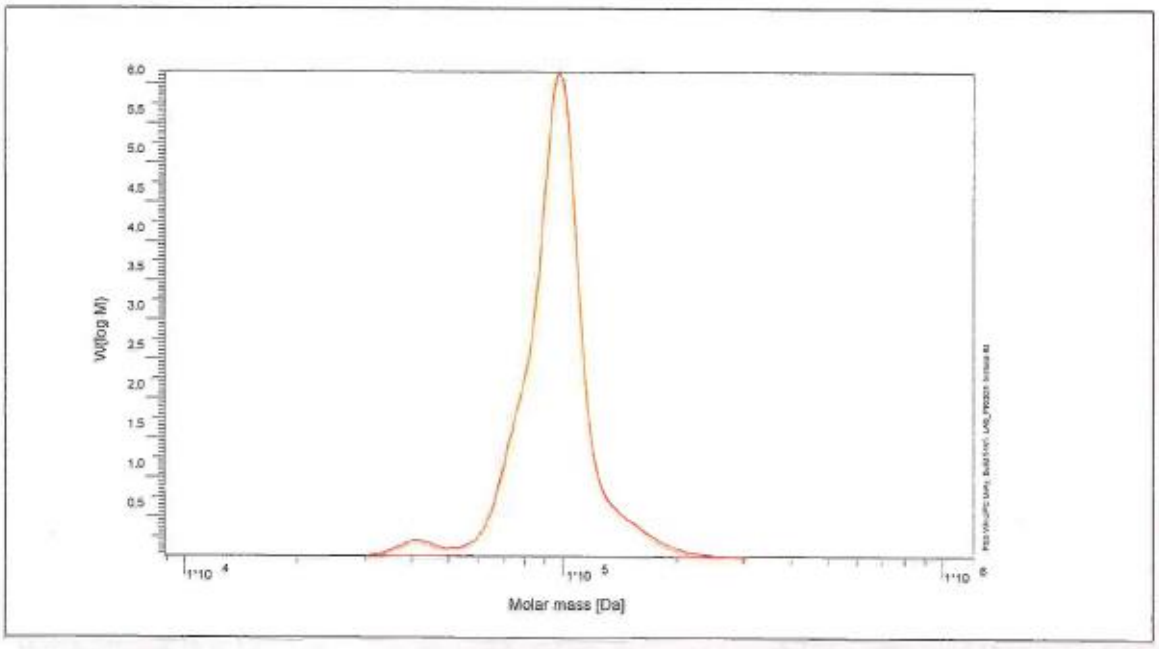

GPC/SEC - Conditions

Sample concentration	1,00 g/l	Inject volume	20 µl
Solvent	THF	Flow rate	1,00 ml/min
Precolumn [8 x 50 mm]	PSS SDV 5µm	Temperature	23,0° C
Columns [analytical, each 8 x 300 mm]	PSS SDV 5µm 10e3Å / 10e5Å / 10e6Å		
Data Acquisition Software	PSS WinGPC	Operator	S. Fugmann

GPC/SEC - Results

Detector	Mw [Da]	Mn [Da]	Mp [Da]	PDI [Mw/Mn]
Shodex RI 71	97600	91300	98000	1,07

GPC/SEC - Results based on Poly(styrene) calibration, one arm Mn [Da] = 36 000

Note:
Mw = Weight average molecular weight

Polymer type:	Poly(styrene) 3-star
Part No:	PSS-psts300k
Lot No:	psst13091

Molar Mass Distribution

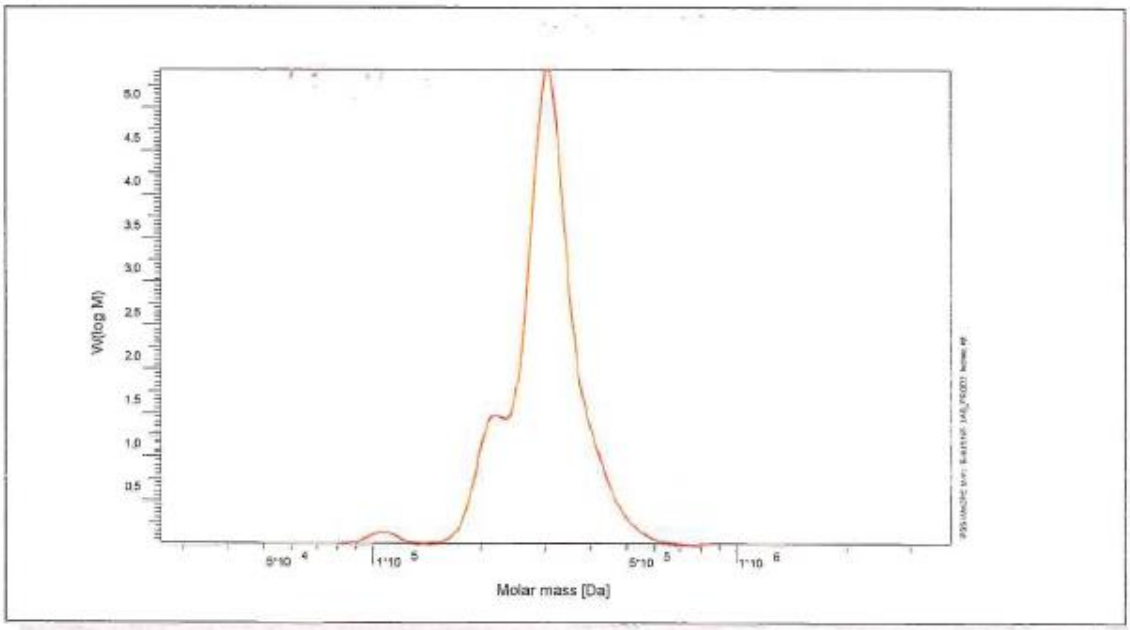

GPC/SEC - Conditions

Sample concentration	1,00 g/l	Inject volume	20 µl
Solvent	THF	Flow rate	1,00 ml/min
Precolumn [8 x 50 mm]	PSS SDV 5µm	Temperature	23,0° C
Columns [analytical, each 8 x 300 mm]	PSS SDV 5µm 10e3Å / 10e5Å / 10e6Å		
Data Acquisition Software	PSS WinGPC	Operator	S. Fugmann

GPC/SEC - Results

Detector	Mw [Da]	Mn [Da]	Mp [Da]	PDI [Mw/Mn]
Shodex RI 71	305000	288000	307000	1,06

GPC/SEC - Results based on Poly(styrene) calibration, one arm Mn [Da] = 108 000

Note:
Mw = Weight average molecular weight

APPENDIX G. Detailed and Summary Data for all s-PS Experiments Conducted

2 wt% 45k star PS in

0.016

BW — **Bellow to Window**

Time	T @ Bellows (°C)	T @ Window (°C)	$P_{combine}$ (psia)	LVDT Reading (T.R.)	Corrected Angle	Roll Time	Calculated K-Value (cm^2/s^2)	Calc Cell Volume (ml)	Density VCU (g/cm^3)	Viscosity VCU (cP)	η_{BW}/η_{WB}	Re	f	Shear Rate	Toluene Density from RefProp [g/cc]	Toluene Viscosity from RefProp [cP]
4:10	106.8	104.7	2046	25.6	6.27	37.52	1.33E-04	46.06	0.8027	0.404	1.000	9.3	668059	26499	0.8003	0.291
4:24	106.6	104.9	605	21.1	6.05	36.59	1.27E-04	46.80	0.7899	0.365	1.002	10.4	624133	27172	0.7883	0.265
4:43	106.6	105.1	3885	30.2	5.97	41.13	1.40E-04	45.28	0.8165	0.445	1.000	7.9	750239	24173	0.8133	0.321
5:17	106.6	104.2	7364	37.5	5.93	45.06	1.55E-04	44.09	0.8385	0.534	1.006	6.1	868355	22065	0.8344	0.376
5:35	106.6	104.2	12139	45.0	6.05	47.64	1.77E-04	42.88	0.8623	0.655	1.000	4.9	959859	20870	0.8573	0.448
5:54	106.6	104.3	7410	37.5	6.00	44.38	1.55E-04	44.09	0.8386	0.532	0.993	6.3	852176	22403	0.8346	0.377
Average											1.000					

Window to WB — **Window to Bellow**

Time	T @ Bellows (°C)	T @ Window (°C)	$P_{combine}$ (psia)	LVDT Reading (T.R.)	Corrected Angle	Roll Time	Calculated K-Value (cm^2/s^2)	Calc Cell Volume (ml)	Density VCU (g/cm^3)	Viscosity VCU (cP)	Re	f	Shear Rate	Toluene Density from RefProp [g/cc]	Toluene Viscosity from RefProp [cP]
4:15	106.7	104.7	2034	25.6	5.98	39.40	1.33E-04	46.06	0.8027	0.404	8.9	701824	25234	0.8002	0.290
4:31	106.6	104.8	587	21.1	6.03	36.71	1.27E-04	46.80	0.790	0.364	10.4	625337	27084	0.7883	0.265
4:54	106.5	104.7	3850	30.3	5.99	41.10	1.40E-04	45.28	0.817	0.445	7.9	750606	24191	0.8133	0.321
5:12	106.6	104.2	7351	37.5	6.15	43.26	1.55E-04	44.09	0.839	0.530	6.4	828886	22983	0.8343	0.376
5:27	106.6	104.1	12132	45.0	6.13	47.09	1.77E-04	42.88	0.862	0.655	4.9	948932	21114	0.8573	0.448
5:43	106.5	104.0	7378	37.5	6.05	44.44	1.55E-04	44.09	0.839	0.536	6.2	860430	22373	0.8346	0.377

2 wt% 45k star PS in

BW **Bellow to Window**

Time	T @ Bellows (°C)	T @ Window (°C)	$P_{combine}$ (psia)	LVDT Reading (T.R.)	Corrected Angle	Roll Time	Calculated K-Value (cm^2/s^2)	Calc Cell Volume (ml)	Density VCU (g/cm^3)	Viscosity VCU (cP)	η_{BW}/η_{WB}	*Re*	*f*	Shear Rate	Toluene Density from RefProp [g/cc]	Toluene Viscosity from RefProp [cP]
12:03	170.6	167.8	6090	19.1	6.02	27.60	1.50E-04	47.26	0.7822	0.322	1.002	15.5	357216	36023	0.7778	0.239
12:12	171.1	168.0	6153	19.1	5.20	31.89	1.50E-04	47.26	0.7822	0.322	1.001	13.4	412178	31177	0.7781	0.240
12:24	171.2	168.0	9114	26.5	5.99	29.84	1.63E-04	46.03	0.8031	0.377	1.015	12.6	403539	33319	0.7983	0.270
12:38	171.2	168.1	15287	38.0	6.11	31.73	1.92E-04	44.16	0.8372	0.480	1.003	9.7	444373	31334	0.8309	0.329
12:53	171.2	168.2	12153	32.7	5.99	31.17	1.77E-04	45.01	0.8213	0.427	1.003	10.9	429505	31897	0.8155	0.300
1:16	171.1	168.4	20307	44.9	5.98	33.93	2.19E-04	43.05	0.8587	0.569	1.007	7.8	483489	29303	0.8518	0.374
1:37	171.0	168.2	3345	10.8	6.06	25.01	1.38E-04	48.67	0.7597	0.272	1.001	19.7	304957	39754	0.7539	0.207
	Average										1.005					

WB **Window to Bellow**

Time	T @ Bellows (°C)	T @ Window (°C)	$P_{combine}$ (psia)	LVDT Reading (T.R.)	Corrected Angle	Roll Time	Calculated K-Value (cm^2/s^2)	Calc Cell Volume (ml)	Density VCU (g/cm^3)	Viscosity VCU (cP)	*Re*	*f*	Shear Rate	Toluene Density from RefProp [g/cc]	Toluene Viscosity from RefProp [cP]
12:08	171.1	167.9	6136	19.1	6.35	26.11	1.50E-04	47.26	0.7822	0.322	16.4	336714	38079	0.7780	0.240
12:18	171.2	167.8	6157	19.1	5.10	32.54	1.50E-04	47.26	0.7822	0.322	13.1	420269	30554	0.7781	0.240
12:29	171.3	167.9	9104	26.5	5.99	29.45	1.63E-04	46.03	0.8032	0.371	12.9	392521	33760	0.7982	0.270
12:44	171.2	168.0	15267	38.0	6.16	31.44	1.92E-04	44.16	0.8372	0.479	9.8	439253	31623	0.8308	0.329
12:58	171.3	168.1	12149	32.7	6.11	30.51	1.77E-04	45.01	0.8213	0.425	11.1	419186	32587	0.8155	0.300
1:22	171.1	168.2	20253	44.9	6.10	33.13	2.18E-04	43.05	0.8587	0.565	8.1	469570	30010	0.8517	0.374
1:41	171.2	168.0	3343	10.8	6.03	25.15	1.38E-04	48.67	0.7596	0.272	19.6	306468	39532	0.7538	0.207

2 wt% 45k star PS in

BW **Bellow to Window**

Time	T @ Bellows (°C)	T @ Window (°C)	$P_{combine}$ (psia)	LVDT Reading (T.R.)	Corrected Angle	Roll Time	Calculated K-Value (cm^2/s^2)	Calc Cell Volume (ml)	Density VCU (g/cm^3)	Viscosity VCU (cP)	η_{BW}/η_{WB}	*Re*	*f*	Shear Rate	Toluene Density from RefProp [g/cc]	Toluene Viscosity from RefProp [cP]
3:32	254.7	249.8	10010	10.8	5.95	19.74	1.67E-04	48.91	0.7559	0.255	0.998	26.4	187556	50367	0.7487	0.189
3:42	254.9	249.4	15164	23.1	5.92	21.67	1.92E-04	46.86	0.7889	0.319	1.007	20.1	214532	45881	0.7825	0.222
3:57	254.8	249.9	19266	31.1	6.15	21.70	2.13E-04	45.54	0.8117	0.367	1.005	18.0	216507	45817	0.8036	0.245
4:08	254.8	250.2	23745	38.2	5.95	23.19	2.38E-04	44.40	0.8326	0.422	1.010	15.0	232599	42873	0.8231	0.270
4:18	254.7	250.5	28264	44.6	6.11	22.97	2.64E-04	43.39	0.8520	0.476	1.009	13.7	228388	43284	0.8401	0.293
4:33	254.5	250.6	15294	25.1	5.95	21.59	1.93E-04	46.53	0.7946	0.320	1.004	20.3	212347	46051	0.7830	0.222
	Average										1.005					

Window to WB **Window to Bellow**

Time	T @ Bellows (°C)	T @ Window (°C)	$P_{combine}$ (psia)	LVDT Reading (T.R.)	Corrected Angle	Roll Time	Calculated K-Value (cm^2/s^2)	Calc Cell Volume (ml)	Density VCU (g/cm^3)	Viscosity VCU (cP)	*Re*	*f*	Shear Rate	Toluene Density from RefProp [g/cc]	Toluene Viscosity from RefProp [cP]
3:29	254.6	249.4	9983	10.8	6.06	19.46	1.67E-04	48.91	0.7559	0.256	26.7	185387	51091	0.7487	0.189
3:39	255.1	249.4	15161	23.1	6.12	20.84	1.92E-04	46.86	0.7889	0.317	21.1	204821	47708	0.7824	0.222
4:00	254.9	249.7	19221	31.1	6.02	22.11	2.13E-04	45.54	0.8118	0.365	17.7	219726	44968	0.8034	0.245
4:11	254.8	250.0	23658	38.3	5.97	22.96	2.37E-04	44.40	0.8327	0.418	15.3	228428	43303	0.8228	0.269
4:22	254.7	250.4	28096	44.7	5.93	23.57	2.63E-04	43.38	0.8522	0.471	13.5	233030	42182	0.8396	0.292
4:37	254.7	250.4	15270	25.1	6.14	20.88	1.92E-04	46.53	0.7946	0.319	21.0	204650	47617	0.7829	0.222

2 wt% 100k star

0.016

BW **Bellow to Window** 0.99

Time	T @ Bellows (°C)	T @ Window (°C)	$P_{combine}$ (psia)	LVDT Reading (T.R.)	Corrected Angle	Roll Time	Calculated K-Value (cm^2/s^2)	Calc Cell Volume (ml)	Density VCU (g/cm^3)	Viscosity VCU (cP)	η_{BW}/η_{WB}	*Re*	*f*	Shear Rate	Toluene Density from RefProp [g/cc]	Toluene Viscosity from RefProp [cP]
12:51	44.5	43.9	2015	30.2	8.98	62.63	1.33E-04	46.89	0.855	0.956	0.998	2.52	2480261	15875	0.8552	0.495
1:17	44.2	43.8	391	26.8	9.07	59.32	1.26E-04	47.40	0.845	0.871	1.002	2.88	2274755	16761	0.8461	0.454
1:37	44.3	43.8	5110	35.7	9.06	67.17	1.45E-04	46.05	0.870	1.131	1.000	2.02	2820560	14802	0.8708	0.577
1:56	44.3	43.8	9653	42.2	9.18	72.40	1.65E-04	45.07	0.889	1.402	0.993	1.54	3240662	13733	0.8899	0.702
2:17	44.2	43.7	9640	42.2	9.13	72.93	1.65E-04	45.06	0.889	1.404	0.992	1.53	3270284	13633	0.8899	0.702
2:37	44.3	43.8	15174	48.5	8.94	81.78	1.92E-04	44.11	0.909	1.784	0.997	1.10	3931717	12157	0.9092	0.870
3:01	44.3	43.8	18975	52.1	9.12	84.59	2.11E-04	43.55	0.920	2.070	0.995	0.93	4229848	11754	0.9208	1.000
3:31	44.2	43.7	9839	42.2	6.02	111.23	1.66E-04	45.06	0.889	1.423	1.001	0.99	5028998	8939	0.8907	0.708
	Average										0.997					

WB **Window to Bellow**

Time	T @ Bellows (°C)	T @ Window (°C)	$P_{combine}$ (psia)	LVDT Reading (T.R.)	Corrected Angle	Roll Time	Calculated K-Value (cm^2/s^2)	Calc Cell Volume (ml)	Density VCU (g/cm^3)	Viscosity VCU (cP)	*Re*	*f*	Shear Rate
1:05	44.5	43.9	1995	30.2	9.13	61.76	1.33E-04	47.36	0.846	0.958	3	2477158	16098
1:25	44.3	43.8	388	26.8	9.00	59.62	1.26E-04	47.89	0.837	0.869	3	2303966	16676
1:46	44.3	43.8	5099	35.8	9.07	67.07	1.45E-04	46.50	0.862	1.131	2	2843929	14824
2:08	44.3	43.8	9642	42.2	9.07	73.75	1.65E-04	45.52	0.880	1.411	1	3357275	13481
2:23	44.2	43.7	9627	42.2	9.17	73.17	1.65E-04	45.52	0.881	1.414	1	3340692	13588
2:47	44.2	43.7	15152	48.4	9.14	80.26	1.92E-04	44.56	0.900	1.789	1	3911757	12388
3:14	44.2	43.7	18934	52.1	9.24	83.97	2.11E-04	43.99	0.911	2.081	1	4265940	11840
3:46	44.2	43.7	9681	42.2	6.17	108.89	1.66E-04	45.52	0.880	1.421	1	4988866	9131

2 wt% 100k star PS in Toluene at 0.016

BW **Bellow to Window**

Time	T @ Bellows (°C)	T @ Window (°C)	$P_{combine}$ (psia)	LVDT Reading (T.R.)	Corrected Angle	Roll Time	Calculated K-Value (cm^2/s^2)	Calc Cell Volume (ml)	Density VCU (g/cm^3)	Viscosity VCU (cP)	η_{BW}/η_{WB}	*Re*	*f*	Shear Rate	Toluene Density from RefProp [g/cc]	Toluene Viscosity from RefProp [cP]
6:19	106.0	104.2	8015	25.7	6.27	55.84	1.58E-04	48.05	0.834	0.712	0.989	4	1418083	17805	0.8381	0.387
6:36	106.0	104.1	3020	16.2	5.89	52.61	1.37E-04	49.52	0.809	0.548	1.003	5	1222861	18898	0.8081	0.308
6:51	106.2	104.2	5058	20.3	5.99	54.21	1.45E-04	48.89	0.820	0.608	0.989	4	1301886	18340	0.8214	0.341
7:08	106.3	104.1	12950	34.0	5.96	63.66	1.81E-04	46.77	0.857	0.881	0.998	3	1700322	15618	0.8609	0.461
7:24	106.2	104.0	19265	42.2	6.15	66.36	2.13E-04	45.52	0.880	1.112	0.991	2	1849391	14982	0.8846	0.559
7:43	106.2	104.0	25476	48.5	6.18	69.91	2.47E-04	44.55	0.900	1.364	0.992	2	2013010	14222	0.9041	0.662
8:03	106.2	103.9	29502	52.1	6.22	71.98	2.71E-04	43.99	0.911	1.548	0.995	1	2117821	13813	0.9152	0.734
8:24	106.0	103.8	13000	34.0	6.00	62.06	1.81E-04	46.77	0.857	0.866	0.995	3	1626725	16021	0.8613	0.463
	Average										0.994					
	St. Dev.															

WB **Window to Bellow**

Time	T @ Bellows (°C)	T @ Window (°C)	$P_{combine}$ (psia)	LVDT Reading (T.R.)	Corrected Angle	Roll Time	Calculated K-Value (cm^2/s^2)		Density VCU (g/cm^3)	Viscosity VCU (cP)		*Re*	*f*	Shear Rate
6:28	106.2	104.1	8018	25.7	6.14	57.70	1.58E-04	48.05	0.834	0.720		4	1480952	17231
6:43	106.2	104.1	3015	16.2	6.07	50.99	1.37E-04	49.52	0.809	0.546		5	1182109	19499
6:59	106.3	104.0	5045	20.3	6.03	54.53	1.45E-04	48.89	0.820	0.615		4	1324309	18233
7:16	106.3	104.0	12916	34.0	6.28	60.69	1.81E-04	46.77	0.857	0.883		3	1625898	16382
7:32	106.2	103.9	19237	42.2	6.06	68.11	2.13E-04	45.52	0.880	1.122		2	1917238	14597
7:54	106.2	103.8	25454	48.5	6.28	69.47	2.47E-04	44.55	0.900	1.375		2	2017127	14312
8:12	106.2	103.7	29460	52.1	6.27	71.94	2.71E-04	43.99	0.911	1.556		1	2129603	13820
8:32	106.2	103.7	12959	34.0	6.08	61.69	1.81E-04	46.77	0.857	0.870		3	1626589	16117

2 wt% 100k star PS in

Δ Angle

BW **Bellow to Window**

Time	T @ Bellows (°C)	T @ Window (°C)	$P_{combine}$ (psia)	LVDT Reading (T.R.)	Corrected Angle	Roll Time	Calculated K-Value (cm^2/s^2)	Calc Cell Volume (ml)	Density VCU (g/cm^3)	Viscosity VCU (cP)	η_{BW}/η_{WB}	*Re*	*f*	Shear Rate	Toluene Density from RefProp [g/cc]	Toluene Viscosity from RefProp [cP]
3:13	193.8	190.7	17684	31.2	5.96	38.65	2.05E-04	47.21	0.831	0.607	0.993	6	648508	25724	0.8286	0.311
3:46	193.5	190.4	13017	23.0	6.01	37.14	1.81E-04	48.47	0.810	0.523	0.992	7	621673	26770	0.8061	0.274
3:59	193.4	190.1	9996	17.5	6.08	34.64	1.67E-04	49.33	0.796	0.455	0.984	9	557800	28702	0.7886	0.249
4:13	193.6	190.4	17586	31.2	6.05	38.93	2.04E-04	47.21	0.831	0.619	0.991	6	667830	25539	0.8283	0.311
	Average										0.990					
	St. Dev.															

WB **Window to Bellow**

Time	T @ Bellows (°C)	T @ Window (°C)	$P_{combine}$ (psia)	LVDT Reading (T.R.)	Corrected Angle	Roll Time	Calculated K-Value (cm^2/s^2)		Density VCU (g/cm^3)	Viscosity VCU (cP)		*Re*	*f*	Shear Rate	Toluene Density from RefProp [g/cc]	Toluene Viscosity from RefProp [cP]
3:20	193.6	190.5	17649	31.2	6.02	38.64	2.05E-04	47.21	0.831	0.612		6	653803	25731	0.8286	0.311
3:41	193.8	190.3	13017	23.0	6.04	37.30	1.81E-04	48.47	0.810	0.527		7	629326	26655	0.8061	0.274
3:55	193.6	189.9	9988	17.5	5.98	35.86	1.67E-04	49.33	0.796	0.463		8	587210	27725	0.7886	0.249
4:09	193.8	190.4	17589	31.2	6.12	38.90	2.04E-04	47.21	0.831	0.625		6	673604	25559	0.8283	0.311

2 wt% 300k star PS in

0.016

BW **Bellow to Window**

Time	T @ Bellows (°C)	T @ Window (°C)	$P_{combine}$ (psia)	LVDT Reading (T.R.)	Corrected Angle	Roll Time	Calculated K-Value (cm^2/s^2)	Calc Cell Volume (ml)	Density VCU (g/cm^3)	Viscosity VCU (cP)	η_{BW}/η_{WB}	*Re*	*f*	Shear Rate	Toluene Density from RefProp [g/cc]	Toluene Viscosity from RefProp [cP]
10:05	42.9	42.3	3308	21.2	9.17	123.26	1.38E-04	46.73	0.860	1.995	1.001	0.62	9738649	8066	0.8634	0.538
10:26	42.9	42.2	378	15.8	9.14	113.04	1.26E-04	47.67	0.843	1.673	1.004	0.79	8346922	8795	0.8474	0.460
10:58	42.9	42.2	7480	27.7	9.10	137.62	1.56E-04	45.64	0.881	2.488	1.002	0.45	11732544	7224	0.8823	0.651
11:32	43.2	42.3	15196	36.9	9.14	158.44	1.92E-04	44.11	0.911	3.533	1.002	0.29	15033999	6275	0.9101	0.884
12:05	43.1	42.3	23004	44.0	9.20	177.67	2.33E-04	42.95	0.936	4.831	0.999	0.19	18463476	5596	0.9328	1.173
12:42	42.7	41.9	11167	32.5	9.08	148.36	1.72E-04	44.84	0.897	2.959	0.998	0.36	13340388	6702	0.8967	0.761
	Average										1.001					

WB **Window to Bellow**

Time	T @ Bellows (°C)	T @ Window (°C)	$P_{combine}$ (psia)	LVDT Reading (T.R.)	Corrected Angle	Roll Time	Calculated K-Value (cm^2/s^2)	Calc Cell Volume (ml)	Density VCU (g/cm^3)	Viscosity VCU (cP)	*Re*	*f*	Shear Rate	Toluene Density from RefProp [g/cc]	Toluene Viscosity from RefProp [cP]
10:13	43.1	42.5	3327	21.2	9.20	122.81	1.38E-04	46.73	0.860	1.994	0.6	9690669	8096	0.8633	0.537
10:42	42.8	42.2	368	15.8	9.17	112.38	1.26E-04	47.67	0.843	1.667	0.8	8269415	8847	0.8474	0.460
11:12	43.3	42.4	7512	27.7	9.15	136.55	1.56E-04	45.64	0.881	2.482	0.5	11604165	7281	0.8822	0.650
11:50	43.4	42.5	15218	36.9	9.21	156.92	1.92E-04	44.11	0.911	3.525	0.3	14846110	6336	0.9101	0.883
12:23	43.2	42.4	23015	44.0	9.32	175.72	2.33E-04	42.95	0.936	4.837	0.2	18278305	5658	0.9328	1.171
12:58	43.2	42.3	11203	32.5	9.21	146.51	1.73E-04	44.84	0.897	2.964	0.4	13183067	6786	0.8966	0.758

2 wt% 300k star PS in

0.016

BW **Bellow to Window**

Time	T @ Bellows (°C)	T @ Window (°C)	$P_{combine}$ (psia)	LVDT Reading (T.R.)	Corrected Angle	Roll Time	Calculated K-Value (cm^2/s^2)	Calc Cell Volume (ml)	Density VCU (g/cm^3)	Viscosity VCU (cP)	η_{BW}/η_{WB}	*Re*	*f*	Shear Rate	Toluene Density from RefProp [g/cc]	Toluene Viscosity from RefProp [cP]
3:41	110.4	108.0	10381	16.9	6.14	117.70	1.69E-04	47.52	0.8460	1.568	1.015	0.8	6073374	8447	0.8469	0.410
4:11	109.9	107.5	10323	16.9	9.11	77.75	1.69E-04	47.52	0.8460	1.531	1.019	1.3	3922351	12788	0.8469	0.411
4:36	109.8	107.4	6611	10.8	9.02	71.06	1.52E-04	48.56	0.8278	1.251	0.999	1.6	3323581	13991	0.8279	0.356
5:00	109.9	107.4	15248	24.3	9.10	82.74	1.92E-04	46.27	0.8689	1.850	1.004	1.0	4306910	12016	0.8679	0.483
5:26	110.2	107.7	20352	30.6	9.12	87.42	2.19E-04	45.23	0.8889	2.224	1.003	0.8	4697148	11373	0.8861	0.559
5:54	110.2	107.8	25419	35.9	9.11	91.95	2.47E-04	44.35	0.9064	2.632	1.006	0.7	5078383	10813	0.9018	0.640
6:17	110.5	108.0	30420	40.5	9.24	93.25	2.77E-04	43.61	0.9219	3.028	1.001	0.6	5196697	10662	0.9155	0.724
	Average										1.007					
	St. Dev.															

WB **Window to Bellow**

Time	T @ Bellows (°C)	T @ Window (°C)	$P_{combine}$ (psia)	LVDT Reading (T.R.)	Corrected Angle	Roll Time	Calculated K-Value (cm^2/s^2)		Density VCU (g/cm^3)	Viscosity VCU (cP)		*Re*	*f*	Shear Rate	Toluene Density from RefProp [g/cc]	Toluene Viscosity from RefProp [cP]
3:57	110.5	107.9	10357	16.9	6.08	117.32	1.69E-04	47.52	0.8460	1.545		0.8	5967925	8475	0.8467	0.410
4:22	109.8	107.2	10273	16.9	9.21	75.68	1.68E-04	47.52	0.846	1.503		1.3	3753440	13137	0.8468	0.411
4:46	109.9	107.3	6587	10.8	9.07	70.82	1.52E-04	48.56	0.828	1.252		1.6	3316404	14039	0.8277	0.356
5:11	109.7	107.2	15192	24.3	9.10	82.63	1.92E-04	46.27	0.869	1.844		1.0	4291691	12032	0.8679	0.483
5:38	110.3	107.8	20336	30.6	9.24	86.14	2.19E-04	45.23	0.889	2.217		0.8	4616124	11542	0.8859	0.558
6:05	110.2	107.7	25353	35.9	9.15	91.25	2.47E-04	44.35	0.906	2.617		0.7	5018352	10896	0.9016	0.639
6:28	110.4	107.8	30377	40.5	9.23	93.41	2.77E-04	43.61	0.922	3.024		0.6	5204441	10644	0.9155	0.724

2 wt% 300k star PS in

BW — **Bellow to Window**

Time	T @ Bellows (°C)	T @ Window (°C)	$P_{combine}$ (psia)	LVDT Reading (T.R.)	Corrected Angle	Roll Time	Calculated K-Value (cm^2/s^2)	Calc Cell Volume (ml)	Density VCU (g/cm^3)	Viscosity VCU (cP)	η_{BW}/η_{WB}	*Re*	*f*	Shear Rate	Toluene Density from RefProp [g/cc]	Toluene Viscosity from RefProp [cP]
2:37	173.2	169.6	20401	20.6	9.20	52.60	2.19E-04	47.01	0.8552	1.357	1.004	2.1	1791001	18902	0.8513	0.372
2:56	173.1	169.3	13013	10.0	9.08	48.41	1.81E-04	48.81	0.8237	1.025	0.998	2.9	1561347	20538	0.8190	0.306
3:16	173.4	169.3	16769	15.5	9.22	50.63	2.00E-04	47.87	0.8397	1.198	1.007	2.4	1697093	19637	0.8365	0.339
3:31	173.7	169.3	20397	20.6	9.16	52.74	2.19E-04	47.01	0.8552	1.355	1.002	2.1	1792726	18852	0.8513	0.372
3:53	173.6	169.3	24429	25.8	9.18	54.54	2.41E-04	46.16	0.8710	1.544	0.999	1.8	1882526	18229	0.8658	0.408
4:04	173.6	169.6	28400	30.1	9.18	56.01	2.65E-04	45.44	0.8848	1.736	1.005	1.6	1950754	17751	0.8786	0.443
	Average										1.003					

WB — **Window to Bellow**

Time	T @ Bellows (°C)	T @ Window (°C)	$P_{combine}$ (psia)	LVDT Reading (T.R.)	Corrected Angle	Roll Time	Calculated K-Value (cm^2/s^2)	Calc Cell Volume (ml)	Density VCU (g/cm^3)	Viscosity VCU (cP)	*Re*	*f*	Shear Rate	Toluene Density from RefProp [g/cc]	Toluene Viscosity from RefProp [cP]
2:46	173.7	169.6	20435	20.6	9.28	51.93	2.19E-04	47.01	0.8552	1.352	2.1	1759227	19146	0.8513	0.372
3:03	173.4	169.1	13004	10.0	9.04	48.76	1.81E-04	48.81	0.8237	1.027	2.9	1575772	20390	0.8189	0.305
3:23	173.6	169.2	16761	15.5	9.13	50.83	2.00E-04	47.87	0.8397	1.190	2.4	1692511	19560	0.8365	0.339
3:37	173.8	169.2	20368	20.6	9.06	53.28	2.19E-04	47.01	0.8552	1.352	2.1	1808245	18661	0.8511	0.371
3:59	173.6	169.1	24398	25.7	9.11	55.08	2.41E-04	46.16	0.8710	1.545	1.8	1903889	18051	0.8658	0.407
4:15	173.6	169.7	28378	30.1	9.22	55.58	2.65E-04	45.44	0.8848	1.727	1.6	1927475	17888	0.8785	0.443

HTHP density and viscosity of 2 wt% 45k star-PS in Toluene

Density and viscosity of Toluene calculated using REFPROP

T [°C]	P [psia]	Solution Density [g/cc]	Solution Viscosity [cP]	Toleuene Density [g/cc]	Toluene Viscosity [cP]
38.2	2458	0.8643	0.788	0.8633	0.543
	1286	0.8580	0.732	0.8572	0.511
	361	0.8527	0.695	0.8520	0.486
	2452	0.8643	0.782		
	1287	0.8581	0.735		
	369	0.8526	0.690		
106.8	2046	0.8027	0.404	0.8003	0.291
	605	0.7899	0.365	0.7883	0.265
	3885	0.8165	0.445	0.8133	0.321
	7364	0.8385	0.534	0.8344	0.376
	12139	0.8623	0.655	0.8573	0.448
	7410	0.8386	0.532	0.8346	0.377
	2034	0.8027	0.404		
	587	0.7899	0.364		
	3850	0.8165	0.445		
	7351	0.8385	0.530		
	12132	0.8623	0.655		
	7378	0.8386	0.536		
171.2	6090	0.7822	0.322	0.7778	0.239
	6153	0.7822	0.322	0.7781	0.240
	9114	0.8031	0.377	0.7983	0.270
	15287	0.8372	0.480	0.8309	0.329
	12153	0.8213	0.427	0.8155	0.300
	20307	0.8587	0.569	0.8518	0.374
	3345	0.7597	0.272	0.7539	0.207
	6136	0.7822	0.322		
	6157	0.7822	0.322		
	9104	0.8032	0.371		
	15267	0.8372	0.479		
	12149	0.8213	0.425		
	20253	0.8587	0.565		
	3343	0.7596	0.272		
254.6	10010	0.7559	0.255	0.7487	0.189
	15164	0.7889	0.319	0.7825	0.222
	19266	0.8117	0.367	0.8036	0.245
	23745	0.8326	0.422	0.8231	0.270
	28264	0.8520	0.476	0.8401	0.293
	15294	0.7946	0.320	0.7830	0.222
	9983	0.7559	0.256		
	15161	0.7889	0.317		
	19221	0.8118	0.365		
	23658	0.8327	0.418		
	28096	0.8522	0.471		
	15270	0.7946	0.319		

HTHP density and viscosity of 2 wt% 100k PS star in Toluene				Density and viscosity of Toluene calculated using REFPROP	
T [˚C]	P [psia]	Solution Density [g/cc]	Solution Viscosity [cP]	Toleuene Density [g/cc]	Toluene Viscosity [cP]
44.7	391	0.8455	0.871	0.8461	0.454
	2015	0.8548	0.956	0.8552	0.495
	5110	0.8704	1.131	0.8708	0.577
	9640	0.8894	1.404	0.8899	0.702
	9653	0.8894	1.402	0.8899	0.702
	9839	0.8894	1.423	0.8907	0.708
	15174	0.9087	1.784	0.9092	0.870
	18975	0.9202	2.070	0.9208	1.000
	388	0.8370	0.869		
	1995	0.8463	0.958		
	5099	0.8619	1.131		
	9627	0.8805	1.414		
	9642	0.8805	1.411		
	9681	0.8805	1.421		
	15152	0.8995	1.789		
	18934	0.9112	2.081		
106.3	3020	0.8094	0.548	0.8081	0.308
	5058	0.8197	0.608	0.8214	0.341
	8015	0.8341	0.712	0.8381	0.387
	12950	0.8569	0.881	0.8609	0.461
	13000	0.8569	0.866	0.8613	0.463
	19265	0.8804	1.112	0.8846	0.559
	25476	0.8997	1.364	0.9041	0.662
	29502	0.9110	1.548	0.9152	0.734
	3015	0.8094	0.546		
	5045	0.8197	0.615		
	8018	0.8341	0.720		
	12916	0.8569	0.883		
	12959	0.8569	0.870		
	19237	0.8805	1.122		
	25454	0.8998	1.375		
	29460	0.9111	1.556		
193.9	9996	0.7955	0.455	0.7886	0.249
	13017	0.8096	0.523	0.8061	0.274
	17586	0.8311	0.619	0.8283	0.311
	17684	0.8311	0.607	0.8286	0.311
	9988	0.7955	0.463		
	13017	0.8096	0.527		
	17589	0.8311	0.625		
	17649	0.8311	0.612		

HTHP density and viscosity of 2 wt% 300k PS star in Toluene				Density and viscosity of Toluene calculated using REFPROP	
T [°C]	P [psia]	Solution Density [g/cc]	Solution Viscosity [cP]	Toleuene Density [g/cc]	Toluene Viscosity [cP]
43.2	378	0.8434	1.673	0.8474	0.460
	3308	0.8603	1.995	0.8634	0.538
	7480	0.8809	2.488	0.8823	0.651
	11167	0.8965	2.959	0.8967	0.761
	15196	0.9114	3.533	0.9101	0.884
	23004	0.9361	4.831	0.9328	1.173
	368	0.8434	1.667		
	3327	0.8603	1.994		
	7512	0.8809	2.482		
	11203	0.8965	2.964		
	15218	0.9114	3.525		
	23015	0.9361	4.837		
110.1	6611	0.8278	1.251	0.8279	0.356
	10323	0.8460	1.531	0.8469	0.410
	10381	0.8460	1.568	0.8469	0.411
	15248	0.8689	1.850	0.8679	0.483
	20352	0.8889	2.224	0.8861	0.559
	25419	0.9064	2.632	0.9018	0.640
	30420	0.9219	3.028	0.9155	0.724
	6587	0.8278	1.252		
	10273	0.8460	1.503		
	10357	0.8460	1.545		
	15192	0.8689	1.844		
	20336	0.8889	2.217		
	25353	0.9064	2.617		
	30377	0.9219	3.024		
173.0	13013	0.8237	1.025	0.8190	0.306
	16769	0.8397	1.198	0.8365	0.339
	20397	0.8552	1.355	0.8513	0.372
	20401	0.8552	1.357	0.8513	0.372
	24429	0.8710	1.544	0.8658	
	28400	0.8848	1.736	0.8786	0.443
	13004	0.8237	1.027		
	16761	0.8397	1.190		
	20368	0.8552	1.352		
	20435	0.8552	1.352		
	24398	0.8710	1.545		
	28378	0.8848	1.727		

Vita

Matthew Newkirk was born in Chicago, Illinois, on November 7, 1964. He has been employed by Afton Chemical Corporation, a worldwide manufacturer and marketer of petroleum additives and specialty chemicals, for almost 20 years since July 1998 where he currently serves as Worldwide Director, Global R&D Technology Support, Analytical, and Quality Systems. His previous positions at Afton have included R&D senior management and leadership roles in Mechanical Testing, Fuels Customer Technical Service, and Transmission Fluid Product Development and OEM Support. As a member of Afton's R&D Leadership Team, his management, technical, and administrative responsibilities currently include oversight, strategic planning, and operation of Afton's R&D facilities in China, Japan, United Kingdom, and Richmond, Virginia.

Prior to joining Afton, Mr. Newkirk was employed for 11 years from June 1987 through June 1998 at Southwest Research Institute's Department of Emissions Research in San Antonio, Texas, where he managed a variety of multi-million dollar research projects for industry and governmental agencies. His areas of technical expertise include polymer engineering; polymer structural effects on physical properties and function; viscosity behavior of polymer solvent systems at ultra-high pressures and temperatures; light- and heavy-duty vehicle and engine emission testing; fuel, lubricant, and additive effects on exhaust emissions and fuel economy; chemical characterization of mobile and stationary source regulated and unregulated exhaust and evaporative emissions; ambient and atmospheric modelling of ozone forming potential of vehicle exhaust emissions; and effects of fuel and lubricant additives on gasoline-, diesel-, and alternative-led engines and exhaust aftertreatment systems. He is a licensed professional engineer and has authored more than 30 peer-reviewed technical papers and journal articles, and holds several U.S.

patents and Afton Trade Secrets. He has been an active member of Society of Automotive Engineers for 25+ years during which time he has regularly organized and chaired technical conference sessions and panel discussions, served as an invited speaker, and received several awards including the Forest R. McFarland award for key contributions to the Fuels & Lubricants Activity during his tenure as Vice-Chair of Fuels. He has also served as past Chairman of the SAE Powertrain, Fuels, and Lubricants Activity, and member of the Engineering Meetings Board. He received his Bachelor's degree from The University of Texas at Austin, in 1987; a Master's Degree in Engineering from The University of Texas at San Antonio, in 1993; and is a licensed Professional Engineer in the State of Texas.